REPORT NO. SRS-440

Contract NObs-78572
BuShips Subproject 013 02 01
Task 1709

LONGITUDINAL STABILITY AND CONTROL OF CANARD HYDROFOIL CRAFT

by
Gilbert Chuck
and
Richard K. C. Luke

June 1961

AEROSPACE GROUP
HUGHES
HUGHES AIRCRAFT COMPANY
CULVER CITY, CALIFORNIA

June 1961 SRS-440

LONGITUDINAL STABILITY AND CONTROL OF CANARD HYDROFOIL CRAFT

by
Gilbert Chuck
and
Richard K. C. Luke

approved by:

H. V. Nuttall
Head, Control System Section

J. A. Mitchell
Manager, Control Systems Department

Prepared Under
Bureau of Ships
Contract NObs-78572
Subproject 013 02 01
Task 1709

GUIDANCE AND CONTROLS
DIVISION
AEROSPACE GROUP

HUGHES

HUGHES AIRCRAFT CO.
CULVER CITY,
CALIFORNIA

ABSTRACT

A study of longitudinal stability and control of canard hydrofoil-supported craft of the 110-long-ton weight class, in both calm and disturbed seas, is presented. Configurations involve craft with all foils fully submerged, all foils surface-piercing, and foils of hybrid arrangement (submerged forward, surface-piercing aft and vice versa). As a design aid, effects of variations of major parameters such as speed, c.g. location, foil spacing, dihedral angle, etc. are illustrated. It is shown that autopilot stabilization of the submerged-foil reference craft is required in waves. Although the surface-piercing-foil reference craft is inherently stable in both smooth water and disturbed seas, its capabilities in waves are more limited than those for the submerged-foil vehicle.

Also presented is a comparison of canard and conventional configurations in calm and disturbed seas.

FOREWARD

This report was prepared by the Hughes Aircraft Company, Culver City, California, under Contract NObs-78572. The work was accomplished under the direction of Mr. Sam M. Lum of the Bureau of Ships, Code 421.

The major portion of the work was performed by Messrs. G. Chuck and R.K.C. Luke. Mr. M. A. Sloan, Jr. assisted in developing procedures necessary to allow automatic computation of the data and suggested methods for simulating random seas. Technical editing of the report was provided by Mr. W. N. Turner. All personnel are with the Control Systems Section, Guidance and Controls Division, Aerospace Group.

TABLE OF CONTENTS

TABLE OF CONTENTS

INTRODUCTION

This study of longitudinal stability and control of hydrofoil craft with canard configurations forms a continuation of Reference 1, which was primarily concerned with conventional configurations. Inherent craft stability in calm seas and dynamic performance in regular sinusoidal seas are presented herein. Comparisons between the canard craft of this report and the conventional vehicles of Reference 1 are given.

Canard craft, with the main supporting foil aft of the center of gravity, in the weight/size class approximated by figures of 110 long tons gross weight and 110 ft. overall length are considered. Four basic types of vehicles, each characterized by its foil operating mode, are treated; the foil modes are: (1) both foils fully submerged, (2) both foils surface-piercing, (3) forward foil submerged, aft foil surface-piercing, and (4) forward foil surface-piercing, aft foil submerged.

Parametric variations, such as speed, center of gravity location, foil spacing, etc., are made on the four canard configurations to study inherent craft stability. Locus-of-root analysis of the vehicle as a dynamic system is the primary tool for analysis.

Dynamic performance in regular sinusoidal seas of the submerged-foil and surface-piercing-foil reference craft is obtained by analog simulation. The former vehicle is investigated with an autopilot while the latter craft is unaugmented. A non-linear model is used in disturbed sea simulations. Root-loci analyses are also made for the submerged-foil craft with autopilot.

LIMITATIONS OF THE STUDY

In order to contain the study effort within reasonable bounds, it is necessary to adopt a number of simplifying ground rules. Data and conclusions must, therefore, be qualified to the extent that these rules are significant. This section briefly discusses the primary factors involved.

Vehicle Size

Only one size and weight class is considered. This is not, however, considered a severe limitation, as the general results are applicable to vehicles somewhat above or below the reference craft in weight and dimensions.

Vehicle Structure

It was necessary to ignore the effects of structural flexibility. It is unlikely that this will appreciably influence the primary results here. No hydrofoil craft, however, will be absolutely rigid. The presence of fundamental structural modes on the order of two cycles per second will require serious consideration during the design of a specific vehicle to prevent adverse forcing of these modes in disturbed seas.

Hydrodynamic Data

Because specific hydrodynamic test data on the many configurations studied are not available, theoretical data were developed in the interests of consistency. The best available information was always used for this purpose, with empirical substantiation whenever possible. Any differences which may be found to exist between the theory and actual test data are expected to be easily compensated by small adjustments in the basic craft or autopilot parameters.

Foil Operating Mode

Only foil-borne operation is considered, with restrictions to subcavitating, non-ventilated foil conditions. To this end the maximum speed is limited to 50 knots.

Equations of Motion

For the analysis of stability in smooth water, linearization of the equations of motion about the operating point is valid and is employed. To insure validity of results for the studies of behavior in waves, however, significant non-linearities, such as the curvature of lift-curve slope with depth, and the exponential variation of orbital-velocity magnitude with depth, are taken into account. The mathematical models should not, then, introduce any significant limitations.

Sea Types

Regular wave trains of various heights and wave lengths are simulated, rather than disturbed seas requiring statistical description, as a matter of expediency. This is a perfectly valid approach here, as the most severe condition to be encountered is represented by a regular wave train forcing the motion at a sensitive frequency. A sinusoidal rather than a trochoidal wave form is used, but the approximation is very close for the wave steepness ratios of interest.

Propeller Effects

Effects of propeller slipstream and power derivatives are, of necessity, ignored. When these are established for a particular design, interpretation in terms of equivalent foil or strut variations will allow an estimate of their effects.

Interference Effects

Similarly, effects of foil-strut or foil-nacelle interference are not determined.

Aerodynamic Forces

The neglect of aerodynamic forces on hull and struts introduces no limitations because these forces normally represent only a fractional percent of the total.

Autopilot

Only rudimentary autopilot functions are considered, as these are sufficient for stabilization. Ultimate performance available by special control techniques is not determined. Perfect instrumentation is assumed. Flaps are driven by an actuator with a .1 sec first-order lag and rate limited at 20 deg/sec.

INHERENT CRAFT STABILITY IN SMOOTH WATER

In this portion of the study on the inherent craft stability of canard hydrofoil craft in smooth water, four reference craft are selected, one for each of the foil operating modes. Variations of physical parameters are made about the reference craft values, and inherent stability, as determined by the characteristic roots of the linear model, is presented in locus-of-root type plots. Some analyses of the loci and inherent stability are given.

The basic hydrodynamic data, equations of motion, and stability derivative forms used in the computation of longitudinal characteristic roots are taken from Reference 1. A product of this computation is the component hydrodynamic coefficients, which are used (internally in digital computer programs) to compute dimensional stability derivatives. These coefficients for the reference craft and parametric variations are listed in Appendix A. It should be noted that the data apply also to the conventional-layout craft of Reference 1 if the appropriate forward and aft components are interchanged.

Reference Craft

Physical Characteristics

Four reference craft are selected, one for each of the foil

operating modes. Sub-cavitating, non-ventilated foils are used: two fully-submerged and two V-type, surface-piercing foils. The four canard reference craft, according to their foil operating modes, incorporate:

1. submerged foils forward and aft.
2. surface-piercing foils forward and aft.
3. hybrid foils: surface-piercing aft, submerged forward.
4. hybrid foils: submerged aft, surface-piercing forward.

Craft physical data, based on a fixed beam of 30 ft. (at water line for surface-piercing foils) and 110 ft. between perpendiculars, are shown in Figure 1.

The basic craft configuration selected has a 40/60 load distribution in percent gross weight on forward/aft foils, and foil loadings of 1000 psf. For a craft weight of 250,000 lbs, the resulting horizontal projected foil areas are 100 $ft.^2$ and 150 $ft.^2$ for the forward and aft foils respectively. All foils considered are rectangular; that is, taper ratio of 1 and unswept quarter-chord lines. Reference craft foil aspect ratios are arbitrarily set at 6 (at the water line for surface-piercing foils). The fully-submerged foils are flat ($\Gamma = 0$), and the V-type surface-piercing foils have a 20 deg. dihedral. With the above values of area, aspect

ratio, and taper ratio, the foil spans (at the water line for surface-piercing foils) are 24.5 ft. and 30 ft. for the forward and aft foils respectively; and the mean chords, 4.08 ft. and 5.0 ft. respectively. The overall spans for surface-piercing foils (measured at the base line) are 52 ft. and 57.4 ft. for the forward and aft foils respectively.

Struts are used with submerged foils only. A single strut, placed at mid-span, is used to support the forward (or secondary) foil. Two struts, placed symmetrically at quarter-spans, are used to support the aft (or main) foil.

Only two nacelles (bodies of revolution) are used on each craft and are located on the main foil. The two nacelles are located at the foil-strut intersection of the submerged aft foils. On the aft surface-piercing foils the nacelles are located symmetrically at quarter-spans. Nacelles are included on surface-piercing foils to permit a more direct comparison. The practical aspects of power shafts to these nacelles are not considered.

The vertical distance from the craft center of gravity (c.g.) to the base line is 9 ft. The vertical distance between base line and flying water line is 5 ft. The mean-depth-to-mean-chord ratio for submerged foils is referenced at 1; and for surface-piercing foils, at 0.55.

With the 40/60 load distribution and 88 ft. between foil quarter-chord lines, the c.g. is located 52.8 ft. from the forward foil and 35.2 ft. from the aft foil. The c.g. also coincides with the craft area centroid. The craft area centroid is defined as the point at which the foil horizontal projected area moments are equal. Area moment is the product of individual foil area and the distance between the craft area centroid and the individual foil area centroid. The individual (pseudo) foil area centroids are assumed to be located on the quarter-chord ($\bar{c}/4$) line rather than on the more conventional half-chord ($\bar{c}/2$) line in order to allow for the normal type of chordwise load distribution on the foils. Hereafter the horizontal c.g. location is expressed relative to the craft area centroid as a fraction of the distance between foils, ℓ; i.e. $(x_{c.g.} - x_{a.c.})/\ell$ or $\Delta x/\ell$. For the reference craft $\Delta x/\ell = 0$.

Hydrodynamic Data

Reference craft component hydrodynamic coefficients are listed in Table A-1. Strut coefficient, used with submerged foils only, are based on the associated foil depth; e.g. forward strut coefficients are based on forward foil depth. Struts on surface-piercing foils are clear of the water and so do not contribute any hydrodynamic forces. There are only two non-zero nacelle coefficients, and these are constant throughout the study.

Characteristic Roots

The linear model of hydrodoil craft used herein has five longitudinal characteristic roots. The roots for all four reference craft are shown in Figure 2. The real part of the root, a, is plotted on the abscissa, and the imaginary part, $j\omega$, on the ordinate. Only half of the complex plane is shown. Since complex roots occur in conjugate pairs, the other half of the complex plane is symmetric about the real axis.

The submerged-foil canard reference craft is stable (Fig. 2a). It has two large negative real roots, one about -24, and the other about -11. The other three roots are small: one negative real at about -.2 and a complex pair with negative real parts of -.05 and imaginary part of .07. The dominant modes are governed by the three small roots, where the real root is an exponential decay with about a 5-sec time constant, and the complex pair is a damped oscillation with a frequency of about .08 rad/sec, and damping ratio of about 0.6.

The surface-piercing-foil canard reference craft is stable (Fig. 2b). It has one large negative real root in the order of -16, an intermediate negative real root at about -5, a complex pair with negative real parts about -4 and imaginary part of 4, and one small negative real root on the order of -.02. The dominant mode is

a long time constant (about 50 sec) exponential decay due to the small negative real root. The oscillation and exponential decay from the three roots near -5 may also be important modes.

The hybrid surface-piercing-aft-foil canard reference craft (Fig. 2c) is unstable. It has one large negative real root in the order of -22, a complex pair with real part of about -6 and imaginary part of about 4, a small negative real root at approximately -.07, and a positive real root at about +.66. The positive real root contributes a divergent exponential mode whose time to double amplitude is slightly less than one second.

The hybrid submerged-aft-foil canard reference craft (Fig. 2d) is stable. It has all negative real roots located at -20, -7.5, -3, -2, -.06. The dominant mode is a 16 sec time constant exponential decay. There is some contribution from the .5 sec and .3 sec exponential decays.

Craft Comparison

The inherent stability of the submerged-foil reference craft appears to be much weaker than for the surface-piercing-foil reference craft, as indicated by its three small roots (near the origin) compared with one for the surface-piercing-foil craft. Except for the positive root, the root pattern for the hybrid surface-piercing-

main-foil reference craft is similar to the craft with both foils surface-piercing. The root pattern of the hybrid submerged-main-foil reference craft bears more resemblance to the surface-piercing-foil craft than the submerged-foil craft, although the characteristic of each are noticeable.

Parametric Variations

Configuration variations made for study of craft inherent stability are listed in Table 1 for each of the four types of craft. There are 125 configurations including the reference configurations. The same variations in speed, c.g. location, and foil spacing are made for all four craft.

There are no dihedral angle variations for submerged foils. Dihedral angles on the craft with both foils surface-piercing are increased simultaneously.

Foil depth variations are not made for surface-piercing foils; the mean-depth-to-mean chord ratio ($h/\bar{c}$) for these foils is referenced at 0.55. Submerged-foil $h/\bar{c}$ variations of 1, 1.5, and 2 are made. The craft with both foils submerged had combinations of these $h/\bar{c}$'s. The combinations are such that each foil is independently submerged deeper relative to the other, or both foils are submerged simultaneously.

There are eleven combinations of foil areas for the craft with both foils surface-piercing and nine for the other three craft. Forward foil areas used are 50, 75, 100, 113, and 150 $ft.^2$; aft foil areas are 75, 100, and 150 ft^2.

Longitudinal characteristic roots for each of these variations are presented in locus-of-root type plots.

Speed Variation

Physical Data: Equilibrium speed of all four reference craft is varied. The speeds considered are 30, 40, and 50 knots. No physical craft parameters are changed to accommodate this speed variation.

Hydrodynamic Data: Hydrodynamic coefficients, however, are functions of speed. Foil coefficients for 40 and 30 knots are listed in Table A-2; those for 50 knots are given in Table A-1. Strut and nacelle coefficients are the same for all speeds and are given in Table A-1.

Characteristic Roots: The longitudinal characteristic roots of all reference craft at equilibrium speed of 30, 40 and 50 knots are shown in Figure 3. At these speeds the hybrid surface-piercing-aft-foil canard vehicle is unstable; the other three craft are stable. However, with increasing speed the unstable craft becomes less

unstable (i.e. the magnitude of the positive real root decreases), while the other three craft become more stable (i.e. the magnitude of the smallest negative real root or the real part of the complex roots increases).

At the lower speeds the submerged-foil canard craft (Fig. 3a) has only exponential decay modes (all negative real roots); the surface-piercing-foil canard craft (Fig. 3b) has an additional higher frequency mode (complex roots) formed by the two large negative real roots; and each hybrid craft has only one oscillatory mode (Figs. 3c and 3b). For the three craft that have oscillatory modes at the lower speeds, the damping ratio decreases and the oscillation frequency increases as speed is reduced.

Dimensionless Roots: In an attempt to determine if any of the longitudinal characteristic roots are dependent on equilibrium speed, the roots are non-dimensionalized by a parameter τ, defined as the ratio of the distance between foils, ℓ, to the equilibrium speed, V_o (i.e. $\tau = \ell/V_o$.). Dimensionless roots for the speed variation are shown in Figure 4. The submerged-foil canard craft shows that the two large negative real roots are almost proportional to V_o (Fig. 4a). The three small roots of this craft do not show any dependence on equilibrium speed.

The surface-piercing-foil canard craft shows that its smallest real negative real root is proportional to V_o since the dimensionless roots all have the same value (See Fig. 4b). The dimensionless complex roots appear to move primarily parallel to the imaginary axis. This indicates that the negative real part of the complex roots may be proportional to V_o. In other words, the damping (or the exponential decay) of the oscillatory modes is proportional to V_o.

The positive real root of the hybrid surface-piercing-aft-foil canard craft appears to be somewhat dependent on speed (See Fig. 4c). This seems to indicate, in the light of the surface-piercing-foil craft, that the instability of this hybrid craft may be due to a speed divergence mode. The dimensionless real part of the complex roots changes slightly with speed indicating a weaker speed dependence than the craft with both foils surface-piercing.

In the speed variation the craft responses based on dimensionless or dimensional roots of the hybrid submerged-main-foil canard craft seem to be somewhat similar to those for the surface-piercing-foil canard craft. However, the negative real root around -2 (Fig. 4d) is the speed sensitive mode for the hybrid craft rather than the real root near the origin as noted earlier for the surface-piercing-foil craft (Fig. 4b).

Craft Comparison: Cruise speed does not appear to be a significant factor in determining the inherent stability of canard hydrofoil craft. With increasing equilbrium speed the hybrid surface-piercing-aft-foil craft becomes more unstable. The effect of increasing speed on the inherent stability of the other three craft is not clear, although inherent stability appears to be increasing.

Horizontal C.G. Location

Physical Data: In this variation only load distribution between the foils is varied to accomplish a c.g. change. All other physical characteristics of the reference craft remain the same. The load distributions considered are: 50/50, 40/60, 30/70, 20/80, and 10/90 in percent of gross weight on forward/aft foils. Relative to the craft area centroid these load distributions correspond to c.g. locations of +.1,0, -.1, -.2, and -.3 of the distance between foils, ℓ. Because of the fixed foil areas, forward foil unit loading decreases while aft foil unit loading increases as the c.g. is moved aft. Table 2 lists some of the physical parameters of this variation.

Hydrodynamic Data: With varying loads on each foil the lift coefficient and other hydrodynamic coefficients vary. These coefficients are tabulated in Table A-3. Reference craft ($\Delta x/\ell = 0$) coefficients are given in Table A-1. Strut and nacelle coefficients are the same in all cases as for the reference craft.

Characteristic Roots: Longitudinal characteristic roots for horizontal c.g. variation are shown in Figure 5. In general, it appears that moving the c.g. forward is more favorable for stability.

Aft c.g. movement on the submerged-foil canard craft is destabilizing (Fig. 5a). For $\Delta x/\ell = -.1$ the craft has an oscillatory divergence. When the c.g. is moved farther aft to -.2 and -.3, the craft has an exponential divergence. Thus, aft c.g. movement drives the original oscillatory mode to instability. Forward c.g. movement increases the oscillation frequency and moves the small negative real root closer to the origin. It appears that the craft will remain stable for extreme forward c.g. locations.

The surface-piercing-foil canard craft is stable throughout the range of c.g. variations (Fig. 5b). The most significant root movement appears to be the intermediate real root, which moves towards the origin with aft c.g. shift. At the most aft c.g. location considered this root combines with the smallest negative real root to form a low-frequency oscillatory mode. Forward c.g. movement of +.1 has less effect on the roots than -.1 aft movement.

The unstable hybrid surface-piercing-aft-foil canard craft becomes more unstable with aft c.g. movement, as evidenced by the increasing positive real root (Fig. 5c). As the positive real root increases the time to double amplitude decreases. Aft c.g. movement

also increases the craft's oscillation frequency and reduces its damping ratio, although the undamped natural frequency remains relatively constant.

Although the hybrid submerged-aft-foil canard craft is stable within the given range of c.g. locations, there is a possibility that it may become unstable outside of this range, particularly for forward c.g. locations (Fig. 5d). Within the given range, the aft c.g. locations produce a low-frequency oscillatory mode, which may go unstable with further aft c.g. movement. However, the most aft position considered is already near the practical aft limit; and the oscillatory mode does not seem to be moving very fast with c.g. movement. At the most forward c.g. position considered a higher frequency oscillatory mode is formed and the smallest negative real root has moved towards the origin. Thus, it is conceivable that at some more forward c.g. location this small root may move into the right-half plane to create an exponential divergent mode.

Craft Comparison: The surface-piercing-foil canard craft can tolerate large horizontal c.g. changes and still remain stable. The hybrid submerged-aft-foil canard craft, although stable within the given c.g. range, may be more susceptible to instability outside the considered range. The submerged-foil canard craft is unstable for aft c.g. movement; and it appears that this craft has a limited

c.g. range for stability. Although forward c.g. movement reduces the instability of the hybrid surface-piercing-aft-foil canard craft, it appears that extreme forward location would not result in a satisfactory level of stability.

Vertical C.G. Location

Physical Data: A variation of ± 43% of the reference distance from c.g. to flying water line is made. The reference distance, $h_{c.g._{ref}}$ is 14 ft., which includes the 5 ft. from base line to flying water line. The ± 43% is equivalent to ± 6 ft., where the positive increment is for the c.g. higher than the reference position.

Hydrodynamic Data: Hydrodynamic coefficients for this variation are the same as those of the reference craft (Table A-1).

Characteristic Roots and Craft Comparisons: This rather large variation of vertical c.g. location has a relatively minor effect on the longitudinal characteristic roots (see Fig. 6). In other words, longitudinal stability is essentially unaffected by craft vertical c.g. location.

Lateral stability, however, is strongly influenced by vertical c.g. location. Figure 7 shows the real part of the significant root (or real root) as a function of c.g. height above the flying water line ($h_{c.g.}$). Figure 7 shows that craft with submerged-main-foils

become less unstable laterally as the c.g. moves nearer the flying water line. Extrapolation of the curves for these two craft indicates, however, that they will not be laterally stable for any reasonable vertical c.g. location. Craft with V-type, surface-piercing-main-foils are inherently stable laterally for the c.g. below some critical height, and these craft become more stable as the c.g. is moved nearer the flying water line.

Foil Spacing

Physical Data: The distance between foil quarter-chords is reduced from 1.0 to .75, .50, and .25 of the reference value (ℓ_{ref} = 88 ft.). In this variation the load on each foil is held constant since the ratio of foil distances from the c.g. is maintained constant. Table 3 lists some of the physical parameters for this variation, which is made on all four reference craft.

Hydrodynamic Data: Hydrodynamic coefficients for foil spacing variation are constant and are the same as those listed for the reference craft in Table A-1. Dimensional derivatives, however, are not constant, since they depend upon other parameters such as the distances from c.g. to foils (x_f and x_a of Table 3). Thus, the characteristic roots are changed according to these derivatives.

Characteristic Roots: Longitudinal characteristic roots for foil spacing variation are shown in Figure 8. In general, the effect of reducing foil spacing is to reduce longitudinal stability.

At a foil spacing of half the reference value the oscillatory mode of the submerged-foil canard craft is essentially neutrally stable (Fig. 8a). When foil spacing is reduced further to a quarter, the oscillatory mode deteriates into a pair of exponential divergent roots. Thus, this craft can tolerate only a limited reduction in foil spacing.

Figure 8b for the surface-piercing-foil canard craft shows that a higher frequency oscillatory mode is formed for ℓ/ℓ_{ref} of .75 or less. The damping ratios of both oscillatory modes are reduced as foil spacing is decreased. Although the craft is stable throughout this variation, its stability level, as indicated by the oscillatory modes, is reduced for the closer foil spacings.

The hybrid surface-piercing-aft-foil canard craft is unstable at the reference foil spacing and becomes more unstable as foil spacing is reduced (Fig. 8c). The damping ratio of the oscillatory mode is also reduced for the closer foil spacings.

An oscillatory mode exists at $\ell/\ell_{ref} = .75$ or less for the hybrid submerged-aft-foil canard craft (Fig. 8d). Like all the above

craft, the damping ratio of this mode also decreases for reduced foil spacing. At a quarter of the reference foil spacing, this oscillatory mode is divergent, and the craft becomes unstable.

Craft Comparison: As foil spacing is reduced the damping ratio of oscillatory modes decreases. On craft with submerged-main-foils it is the oscillatory mode that goes unstable with reduced foil spacing. However, the hybrid submerged-main-foil craft can tolerate a larger reduction in foil spacing than craft with both foils submerged before instability occurs. On craft with surface-piercing-main-foils the oscillatory mode (or modes) is stable throughout this variation. However, the hybrid surface-piercing-main-foil craft has an exponential divergent mode to begin with, and the rate of divergence of this mode increases with reduced foil spacing; whereas the craft with both foils surface-piercing is stable for all foil spacing considered.

The hybrid submerged-main-foil craft is similar to craft with surface-piercing-main-foil in that the smallest negative real root is essentially unaffected by foil spacing, while this is not so for the craft with both foils submerged. Thus, it appears that this small negative real root is governed, to some extent, by surface-piercing-foil characteristics.

Another observation that may be made from the data for this variation is that, if the foil spacing is reduced to zero, (that is, a craft with only one large foil located directly under the c.g.) the craft would be longitudinally unstable. This intuitively obvious conclusion is confirmed by the trend of the loci of roots.

Dihedral Angle

Fully-submerged foils used in this study are flat; that is, the dihedral angle Γ is always zero and no Γ variation is made for these foils. Hence, only three craft are involved in this variation. Dihedral angle on V-type surface-piercing foils is varied from 20 degs. (the reference value) to 50 deg. in 10-deg. increments. On the craft with both foils surface-piercing the dihedral angles are varied simultaneously in 10-deg. increments.

Physical Data: For rectangular planform, V-type surface-piercing foils (i.e. no taper and no sweep) the dihedral angle Γ, aspect ratio (measured at the water line) AR, horizontal projected area A, and foil mean depth h (mean depth is half apex depth) are all related by the following expression:

$$(AR)(A) = 16\, h^2/\tan^2\Gamma \tag{1}$$

It can be seen that for fixed values of $\mathcal{R}$ and A, (say, at the reference values) as Γ is varied h must also change, as prescribed by the above expression. Thus, dihedral angle variation is accompanied by a mean-depth variation. Also, the wetted plan area S, is varied according to the expression:

(2) $$S = A/\cos\Gamma$$

The mean-depth-to-mean-chord ratio $h/\bar{c}$ varies with dihedral angle because $\bar{c}$ is constant in this variation.

The three foil parameters that change with dihedral angle are listed in Table 4. All these parameters increase with larger dihedral angle.

Hydrodynamic Data: The coefficients for the forward and aft surface-piercing-foil dihedral variations are shown in Table A-4. Nacelle hydrodynamic coefficients are the same as those for the reference craft listed in Table A-1.

Characteristic Roots: Increasing dihedral angle simultaneously on both surface-piercing foils appears to affect, primarily, the oscillatory mode (Fig. 9a); the oscillation frequency is reduced while damping ratio is increased slightly. However, the stability

of the mode is reduced since the real part of the complex roots is reduced. Although the negative real roots are moved around, these movements do not appear to significantly alter the inherent stability of the craft.

Increasing the dihedral angle of the hybrid surface-piercing-main-foil canard craft also affects, primarily, the oscillatory mode (Fig. 9b). In this case the oscillatory mode forms two exponential decay modes with larger dihedral angles. However, the craft is unstable throughout this variation, although the divergence rate of the unstable exponential mode is reduced. The remaining roots do not seem to be appreciably affected.

The effect of increasing the dihedral angle on the forward (secondary) surface-piercing foil of the hybrid submerged-aft-foil canard craft is to form a low-frequency mode (Fig. 9c). Although the oscillation frequency and damping ratio are decreased with increasing dihedral angle, the craft is stable for all dihedral angles considered.

Craft Comparison: In general, increasing dihedral angle on the main (aft) foil tends to eliminate the oscillatory mode, while increasing dihedral angle on the secondary (forward) foil tends to generate a low-frequency oscillatory mode. These two trends are

shown individually in the loci-of-roots for the two hybrid craft and collectively in the locus-of-roots for the canard craft with both foils surface-piercing.

Aspect Ratio

Physical Data: Foil aspect ratios of 4, 6, and 8 are used. The following foil quantities are kept constant while aspect ratio (AR) is varied: horizontal projected area, dihedral angle, and taper ratio. This means that foil chord and span are altered to obtain the desired aspect ratio. Mean-depth of surface-piercing foils, as stated earlier, is allowed to vary. Submerged foil depth is also allowed to vary so as to keep $h/\bar{c}$ constant at unity. Physical data for this aspect ratio variation are tabulated in Table 5.

Hydrodynamic Data: Foil hydrodynamic coefficients for aspect ratios of 4 and 8 are shown in Table A-5. Coefficients for aspect ratio of 6, which is the reference value, are given in Table A-1. Two strut coefficients, listed in Table A-5 and used for submerged foils, differ from the reference values because of foil depth, which is varied to maintain $h/\bar{c} = 1$.

Characteristic Roots: Seven combinations of aspect ratios are considered. These combinations are chosen to vary each foil aspect ratio while the other remains at the reference value, and both foil

aspect ratios simultaneously by the same increment. Longitudinal characteristic roots for these variations are shown in Figure 10.

Aspect ratio changes affect, primarily, the three small roots of the submerged-foil canard craft (Fig. 10a). Increasing forward foil aspect ratio alone increases the oscillation frequency; whereas increasing aft foil aspect ratio alone decreases the frequency. Increasing both foil aspect ratios tends to increase the damping ratio with slight changes in frequency. In these variations the small negative real root tends to move towards the origin.

Small forward foil aspect ratio on the surface-piercing-foil canard craft produces an additional oscillatory mode (Fig. 10b). Small aspect ratio, on either or both foils, increases the frequency of the original oscillatory mode, while large aspect ratio tends to reduce the frequency. The smallest negative real root of this craft tends to move towards the origin whenever aspect ratio is increased.

The oscillatory mode of the hybrid surface-piercing-aft-foil canard craft is controlled by aspect ratio (Fig. 10c). The small aft aspect ratio ($AR_a = 4$) increases the oscillation frequency while the large value ($AR_a = 8$) produces a pair of negative real roots. Forward foil aspect ratio variation results in an almost negligible change in the oscillatory mode. The smallest negative real root and positive

real root are affected slightly by all these combinations of aspect ratio, and it appears that these roots are moving towards the origin for the larger aspect ratios.

Forward foil aspect ratio is more effective in changing the longitudinal characteristic roots of the hybrid submerged-aft-foil canard craft (Fig. 10d). Small forward aspect ratio ($AR_f = 4$) produces a relatively high-frequency oscillatory mode, while large forward foil aspect ratio ($AR_f = 8$) produces a relatively low-frequency oscillatory mode. Aft foil aspect ratio variation apparently did not influence the characteristic roots much. The smallest negative real root is essentially unaffected by foil aspect ratio.

Craft Comparison: Summarizing the foil aspect ratio variation it appears that: (1) both foil aspect ratios are important to the inherent stability of the submerged-foil canard craft; (2) the surface-piercing-foil aspect ratio has more influence on longitudinal characteristic roots of the two hybrid craft than their submerged foils. In general, small aspect ratio surface-piercingfoil tends to increase an oscillatory mode's frequency; while large aspect ratio tends to reduce the frequency.

Foil Depth

Physical Data: Foil depth variation is made for fully-submerged flat foils only. V-type surface-piercing foil depth cannot be changed independent of other foil parameters. Thus, only three craft have this variation.

Actually, submerged foil depth-to-chord ratio $h/\bar{c}$, is also varied, since the chord remains constant at the reference value. Values of $h/\bar{c}$ considered are 1 (reference value), 1.5, and 2. For the submerged-foil canard craft seven of the nine possible combinations of these $h/\bar{c}$'s are made. These combinations may be viewed as submerging: (1) the forward foil deeper than the aft, (2) the aft foil deeper than the forward, and (3) both foils deeper simultaneously. For the two hybrid craft the submerged foil is lowered while the surface-piercing foil is maintained at the reference depth.

Hydrodynamic Data: Hydrodynamic coefficients for the submerged foils and their associated struts are listed in Table A-6. Coefficients for $h/\bar{c} = 1$ are the same as for the reference craft (see Table A-1).

Characteristic Roots and Craft Comparison: Submerged-foil canard craft characteristic roots for foil depth variation are shown in Figure 11a. The craft is stable for the reference foil depths and for

aft foil submerged deeper than the forward foil. The craft is unstable for all other combinations of foil depths.

When the forward foil is submerged deeper than the aft foil, the craft is exponentially divergent, and the rate of divergence increases with deeper forward foil depth. When the aft foil is submerged deeper than the forward foil, the craft remains stable, although the oscillation frequency is increased and the damping ratio is reduced. When both foils are submerged deeper simultaneously, the craft is first oscillatory divergent and then exponentially divergent with increasing foil depths. Note that in this last variation only the oscillatory mode is affected while the small negative real root is essentially undisturbed. In all these variations the two large negative real roots are negligibly affected.

Variations of the depth-to-chord ratio of the submerged foil on the two hybrid craft have a negligible effect on the longitudinal characteristic roots (Figs. 11b and 11c). This results from the strong depth dependence of surface-piercing-foil forces in comparison to those of submerged foils.

Foil Area

Flat submerged-foil area is varied while maintaining foil aspect ratio and depth-to-chord ratio at the reference values. This requires changing foil span and chord to obtain the desired area. Changing chord requires altering foil depth to maintain constant depth-to-

chord ratio.

V-type surface-piercing-foil horizontal projected area is varied while maintaining foil aspect ratio and dihedral angle at their reference values. Foil span, chord, and mean-depth are then dependent on the selection of area and the reference values of aspect ratio and dihedral angle. The mean-depth-to-mean-chord ratio, however, is kept constant for area variation since this ratio is dependent only on aspect ratio and dihedral angle.

Physical Data: Five foil areas considered are: 50, 75, 100, 113, and 150 ft^2. Combinations of these areas used are shown in Figure 12. There are 11 combinations for the surface-piercing-foil craft and 9 for the other three craft. Figure 12 also shows lines of constant (horizontal projected) area ratios A_f/A_a, and lines of constant craft foil loading W/A_T, defined as craft gross weight divided by total horizontal projected foil area. Individual foil loadings are also noted on the axes of this figure. Center of gravity position is constant at 60% ℓ_{ref}.

Four obvious ways of considering foil area variations are: (1) varying forward foil area for fixed aft area, (2) varying aft area for fixed forward area, (3) varying foil area ratio, and (4) varying craft foil loading. Unfortunately all of the variations are

interrelated such that changing one foil area automatically changes some of the other parameters. (see Fig. 12). For example, decreasing forward foil area also means increasing both forward foil loading and craft foil loading, and decreasing area ratio. In the following examination of characteristic root patterns, the most meaningful variations are considered for each craft.

Hydrodynamic Data: Hydrodynamic data for the 12 submerged and surface-piercing foils (excluding the reference) are listed in Table A-7.

Characteristic Roots: The submerged-foil craft's characteristic roots for area variation are shown in Figure 13a. Area ratios of 1 and 3/2 result in longitudinally unstable craft with an exponential divergent mode. The divergence rate appears to be strongly dependent on area ratio. Area ratios of 2/3 and 1/2 result in stable craft with an oscillatory mode, whose oscillation frequency is increased with higher craft foil loading. Individual foil area variations do not appear to be particularly significant.

The surface-piercing-foil canard craft is stable for each of the 11 foil area combinations (Fig. 13b). Area ratio and total craft foil loading do not appear to be the meaningful control parameters. Rather, it is the individual foil area (and individual foil loading)

that seem to be more directly related to the resulting root patterns. For forward foil areas of 50 and 75 ft.^{2} an additional oscillatory mode is formed whose frequency increases with higher aft foil loading. With forward foil area of 50 ft.^{2}, the original oscillatory mode's frequency is relatively constant for varying aft foil area. For forward foil areas of 75, 100, and 150 ft.^{2}, however, the original oscillatory mode's frequency increases with smaller aft foil area. The negative real roots appear to be governed by forward foil area, except the one nearest the origin, which appears to be somewhat independent of foil area.

The hybrid surface-piercing-main-foil canard craft is unstable for all the combinations of foil areas as shown by the positive real root in Figure 13c. The degree of instability is apparently not a strong function of foil area. The other four roots, however, are affected by foil area. The oscillatory mode is governed almost entirely by aft foil area. In particular, the oscillation frequency is increased and damping ratio decreases when aft foil loading is increased. The largest negative real root tends to be positioned by forward foil area; the root is moved towards the origin when forward foil loading is increased. The smallest negative real root, however, tends to be related to total craft foil loading; this root is moved towards the origin with increasing total craft foil loading.

The characteristic roots of the hybrid submerged-main-foil craft show it to be stable for the foil area variation (Fig. 13d) concerned. The formation of an oscillatory mode (there is none for the reference craft) is apparently determined by the magnitude of the forward foil area. A relatively low-frequency oscillatory mode is formed when forward foil area is 150 $ft.^2$ or 113 $ft.^2$, exponential decay modes exist when forward foil area is 100 $ft.^2$; and a relatively higher frequency oscillatory mode is formed when forward foil area is 75 $ft.^2$ or 50 $ft.^2$. The frequency of the latter oscillatory mode is increased with decreasing forward foil area. Like the other hybrid craft the smallest negative real root tends to move towards the origin with increasing total craft foil loading. No apparent trend is noted for the larger negative real roots.

Craft Comparison: Stability of the submerged-foil craft is determined by area ratio. The craft is stable for area ratio of 2/3 or less. The surface-piercing-foil and hybrid submerged-main-foil craft are both stable while the other hybrid craft is unstable throughout the area variation.

The frequency of the oscillatory mode of stable submerged-foil craft is controlled by area ratio and craft foil loading. Individual foil area appears to govern the oscillatory mode(s) of the surface-piercing-foil craft; whereas it is the area of the surface-piercing

foil that appears to dominate the oscillatory modes of both hybrid craft. The smallest negative real root of both hybrid craft tends to move towards the origin with increasing total craft loading.

Summary of Results For Parametric Variations

Speed: In general, with increasing equilibrium speed the basically stable craft becomes slightly more stable. However, the degree of stability or instability change is not considered significant.

Horizontal C.G. Location: Both surface-piercing-foil and hybrid submerged-aft-foil canard craft are stable for the range of c.g. locations considered. It appears, however, that the former craft has much wider stable c.g. range. The submerged-foil canard craft has a more limited stable c.g. range than the above hybrid craft. The hybrid surface-piercing-aft-foil craft is unstable for the given c.g. range and appears to have an even wider unstable c.g. range.

Vertical C.G. Location: This parameter has essentially negligible effect on longitudinal stability of all four types of craft.

Foil Spacing: Closer foil spacing is destabilizing. The surface-piercing-foil canard craft can tolerate a close foil spacing and remain stable. The hybrid submerged-aft-foil canard craft has a smaller minimum stable foil spacing than the craft with both foils submerged. The hybrid surface-piercing-aft-foil canard craft becomes

more unstable with closer foil spacing.

Dihedral: The effect of (V-type surface-piercing foil) dihedral angle on inherent craft stability is not clear. However, it is shown that dihedral angle influences the oscillatory mode.

Aspect Ratio: This parameter affects craft dynamic modes significantly. Its effect on craft inherent stability is not self evident (although inherent stability is undoubtly affected) because the combinations of aspect ratios investigated did not destabilize the otherwise stable craft nor stabilize the one unstable hybrid craft.

Foil Depth: Relative foil depth is important to the inherent stability for the canard craft with both foils submerged. In genral, aft foil submerged deeper than the forward foil in chords is desirable from a stability standpoint. Depth of submerged foils is inconsequential to longitudinal stability of the two hybrid craft.

Foil Area: Area ratio appears to govern the stability of the submerged-foil canard craft. Individual foil areas determine the dynamics of the surface-piercing-foil canard craft, which is stable for all combinations of areas considered. The surface-piercing-foil area controls the oscillatory mode of both hybrid craft, while craft foil loading influences the exponential decay mode nearest the origin. However, the hybrid surface-piercing-aft-foil craft is unstable and

the hybrid submerged-aft-foil craft is stable throughout the combinations of foil areas concerned.

Craft Comparison: Since the canard craft with both foils surface-piercing is inherently stable for a wide range of parametric variations, this type is probably easiest to design with assurance of a stable craft.

The hybrid submerged-aft-foil canard craft is stable for all parametric variations except the closest foil spacing. However, its region of inherent stability appears to be smaller than that for the surface-piercing-foil craft.

A much limited inherently stable region is seen for the submerged-foil canard craft. In particular, the directions from the reference craft for stability appear to be: (1) more forward horizontal c.g. position, (2) larger aft depth-to-chord ratio than forward, and (3) smaller area ratio and/or higher forward foil loading.

The hybrid surface-piercing-aft-foil canard craft is unstable for all parametric variations. It appears that this craft is inherently unstable for almost all possible but reasonable combinations of parameters.

DYNAMIC PERFORMANCE IN WAVES

The longitudinal dynamic performance for both the fully-submerged- foil and surface-piercing-foil reference craft in regular sinusoidal seaways was studied on an analog simulator. This section presents the data obtained and discusses the equations and standard techniques used in the analog simulation. Typical analog time histories are included to help illustrate the behavior of these craft in a calm sea and in waves. A discussion of an autopilot for stabilization and control of the longitudinal modes of the submerged-foil reference craft is also included. Cruise speeds of 50 knots are used to subject the vehicles to the higher frequencies of encountering waves. All wave heights mentioned are crest-to-trough (double amplitude).

Analog Simulation Equations and Techniques

A set of non-linear longitudinal equations of motion is used in the analog simulation to determine vehicle performance in waves. Some of these non-linearities occur in the hydrodynamic force coefficients. The equations of motion, auxiliary equations, methods for generating wave trains, and other data necessary for simulating the vehicle in waves are presented herein.

The subscript convention adopted denotes the combined contributions due to the forward foil and forward strut by $(\ )_f$ and combined contributions due to the aft foil, aft struts, and nacelles by $(\ )_a$. Whenever equations are applicable to both forward and aft arrangements (combination of foil, strut, nacelle, etc.), the subscripts are omitted.

Longitudinal Equations of Motion

Mathematical representation of the craft used in the simulation consists basically of four equations. These are:

(3) $$\dot{u} = \frac{F_x}{m} - g\theta$$

(4) $$\dot{w} = \frac{F_z}{m} + g + V_o\dot{\theta}$$

(5) $$\ddot{\theta} = \frac{M}{I_y}$$

(6) $$\dot{h} = -\dot{h}_{c.g.} - x\dot{\theta}$$

These equations involve the usual small-angle approximations of letting the sine equal the argument and cosine equal unity.

Auxiliary Equations

To simulate the above equations of motion, certain auxiliary equations are necessary. These are given below.

Total craft forces along the x and z axes are represented by the lift and drag of the forward and aft foil systems with small-angle approximations:

(7) $$F_x = (-D_f + L_f \alpha_f) + (L_a \alpha_a - D_a)$$

(8) $$F_z = (-L_f - D_f \alpha_f) + (-D_a \alpha_a - L_a)$$

The total craft pitching moment is expressed as products of foil forces and distances:

(9) $$M = (-D_f + L_f \alpha_f) z_f + (-D_a + L_a \alpha_a) z_a - (-L_f - D_f \alpha_f) x_f - (-D_a \alpha_a - L_a) x_a$$

The drag and lift expressions are, respectively:

(10) $$D = \tfrac{1}{2} \rho V^2 S C_D$$

(11) $$L = \tfrac{1}{2} \rho V^2 A C_L$$

where one-half the wetted area (S) is used in drag computation and the horizontal projected area (A) is used in lift computation. For the rectangular planforms considered, these areas are expressed as:

(12) $$S = \bar{c}\, b$$ for fully-submerged foils

and

(13) $$S = \frac{4\bar{c}\,h}{\tan\Gamma}$$ for surface-piercing foils

where

(14) $$A = S \cos\Gamma$$

The relative velocity is:

(15) $$V = V_o + u - u_{sea}$$

and the square of velocity is approximated by:

(16) $$V^2 = V_o^2 + 2V_o(u - u_{sea})$$

The component lift and drag coefficients are given in the Hydrodynamic Data section of Reference 1. However, for simulation

purposes coefficient forms are modified. The drag coefficient used for fully-submerged-foil systems is:

(17) $$C_D = C'_{D_o} + C_{D_h} h + K_D C_L^2$$

and for surface-piercing-foil systems is:

(18) $$C_D = C'_{D_o} + K_D C_L^2$$

where C'_{D_0} is the sum of the constant drag coefficients, C_{D_h} is the strut drag due to depth changes (no strut hydrodynamic forces in surface-piercing-foil systems), and K_D is the sum of the induced and wave drag coefficients which can be expressed as:

(19) $$K_D = \frac{K_E (1+\sigma)(1+\delta)}{\pi AR} + \frac{g \bar{c}}{2V^2 e^{\lambda}},$$

For submerged foils K_D is approximated by a constant, evaluated with initial conditions (e.g. $V = V_0$ and $h = h_0$). For surface-piercing foils K_D is made a function of depth (h) only. Considering V-type, rectangular foils only, the aspect ratio as a function of depth is:

(20) $$AR = \frac{4h}{\bar{c} \tan\Gamma}$$

and the planform correction factor (ζ) is approximated by (see Figure A-2 in Reference 1 for ζ as a function of AR):

(21) $$\zeta = .0087 AR - .005$$

The approximation for K_D is then:

(22) $$K_D = \frac{K_E(1+\sigma)\bar{c}\tan\Gamma}{4\pi}\left[\frac{(1+\zeta_0)}{h} + \zeta_1\right] + \frac{g\bar{c}}{2V_0^2 e^{(2gh_0/V_0^2)}}$$

where:

(23) $$\zeta_1 = \frac{4(.0087)}{\bar{c}\tan\Gamma}$$

and

(24) $$\zeta_0 = -.005$$

The lift coefficient can be expressed as:

(25) $$C_L = C_{L_\alpha}(\alpha + \alpha_\delta \delta)$$

The lift-curve slope expression is a complicated equation which is evaluated for a given foil as a function of submergence. The lift-

curve slope characteristics (C_{L_α} vs. h) are approximated on function generators using five-straight-line segments and are shown in Figures 14 and 15 respectively for the submerged-foil and surface-piercing-foil reference craft. For simplicity the first straight-line segment, $C_{L_\alpha} = 0$ when $h < 0$, has been omitted from these figures.

The angle of attack at a foil is approximated by:

$$\alpha = \frac{w + w_{sea} - x\dot{\theta}}{V_o} \tag{26}$$

where x is the longitudinal distance from the craft c.g. to the foil (positive for the forward foil and negative for the aft foil), w is the c.g. velocity along the z-axis, and w_{sea} is the wave velocity at the foil parallel to the z-axis.

To compute the depth or height at any point on the craft (e.g. the foil depth) Equation (6) is used. The vertical c.g. velocity is approximated by:

$$\dot{h}_{c.g.} = V_o\theta - w \tag{27}$$

Generation of Disturbed Seas

Several approaches may be taken in developing a mathematical representation of a seaway for simulation purposes. Basically, two

general classes of seas are of interest: (1) randomly disturbed and (2) regular periodic. Combinations of these types are, of course, commonly encountered in nature.

The mathematical representation of any sea state requires some sort of specification or pertinent information concerning the sea conditions. The Neumann spectrum (Ref. 2 and 3) provides an accepted description of a fully random sea. In brief, the Neumann spectrum hypothesizes that random seaways are made up of an infinite number of wave systems varying in frequency, direction of travel, and phase. Random sea representations are then developed based on power spectral concepts applied to measurements of the sea surface at a fixed point, assuming a fully developed sea and constant wind velocity.

Representation of regular periodic seas, on the other hand, is much simpler, requiring only specifications of direction of travel, wave length, height, and shape. Although the true surface wave form is trochoidal, a sinusoidal approximation very closely represents the actual conditions and is more readily generated.

The simulation of hydrofoil vehicles in disturbed seas is complicated by the requirement to provide for the difference in time of wave arrival at the individual foils. Actual time delays are necessary for random sea simulations, while a simple phase shift is sufficient for

sinusoidal seas. Consideration of the details involved in each type of simulation follows.

Random Sea States: A means of developing random sea inputs of height and local velocity at each foil for an analog simulation is shown in Figure 16. White noise is passed through a filter designed from data based on the Neumann Spectrum. The output of the filter can then be passed directly to a time delay device or recorded permanently on magnetic tape. The two devices most readily available for getting accurate time delays of long duration are: (1) magnetic tape recorders and (2) digital computers. In the former delay technique, the tape recorder accepts information from the filter output (either directly or from pre-recorded tape) and provides the desired delay between output channels to account for the time differences in wave arrival at the foils. The latter delay method involves a digital computer with an analog-to-digital-to-analog converter. Analog inputs are fed into the digital computer from the filter (directly or pre-recorded), the computer provides the desired delays, and the appropriate analog outputs are fed to the sea state mechanizer, which transforms the inputs into a submergence and local disturbance velocity (properly correlated) at each foil. Outputs of the sea state mechanizer can then be used in an analog computer to obtain dynamic craft responses to waves.

Regular Sinusoidal Sea States: The alternative method for studying craft behavior in waves is to assume operation in seaways that are regular and sinusoidal in nature. This is a conservative approach, as the most severe condition to be encountered is represented by a regular wave train forcing the motion at a sensitive frequency. This approach has been used throughout this study as a matter of expediency.

Equations used to describe regular sinusoidal waves are derived from Reference 4 and are:

(28) $$h_{sea} = H_{sea} \sin\left[\frac{2\pi}{\lambda_{sea}}(V_{sea}t + x)\right]$$

(29) $$u_{sea} = V_{orb.} e^{(-2\pi h/\lambda_{sea})} \sin\left[\frac{2\pi}{\lambda_{sea}}(V_{sea}t + x)\right]$$

(30) $$w_{sea} = V_{orb.} e^{(-2\pi h/\lambda_{sea})} \cos\left[\frac{2\pi}{\lambda_{sea}}(V_{sea}t + x)\right]$$

(31) $$V_{orb.} = \left(\frac{2\pi H_{sea}}{\lambda_{sea}}\right) V_{sea}$$

(32) $$V_{sea} = \sqrt{\frac{g\lambda_{sea}}{2\pi}} = 2.26\sqrt{\lambda_{sea}}$$

Frequency of Wave Encounter: The frequency of wave encounter is expressed as:

(33) $$f = \frac{V_{sea} \pm V_o}{\lambda_{sea}} \quad \text{in cps}$$

The sign convention is to denote head seas by the upper sign and following seas by the lower sign. The frequency of (wave) encounter is the effective frequency of the forcing functions acting on the vehicle and is due to the interactions between the craft and wave velocities. Hence all performance data in waves will be discussed in terms of frequency of encounter.

Range of Sea States Simulated: The sea states in the simulation are chosen in accordance with Reference 5, which specifies, briefly, head and following seas with wave steepness ratios of 20, 30, 40, and 50. Figure 17 summarizes the range of sea states considered. Basically two wave heights, 4 and 10 ft., with steepness ratios of about 5 to 88 (corresponding to wave lengths of 44 to 352 ft.) are examined for the fully-submerged-foil craft. For the surface-piercing-foil vehicle, wave heights of 2 and 4 ft., with steepness ratios of about 11 to 176 (corresponding to wave lengths of 44 to 352 ft.) are studied. This more than covers the specified range.

Flap Actuators and Rate Limiting

Actuator lags of .1 sec (corresponding to a break frequency of 10 rad/sec) are assumed for all flaps whenever used in the simulation. In addition all flaps are rate limited to 20 deg/sec; rate limiting seems to decrease the useful gain margin before craft instability occurs. These arbitrarily selected values appear consistent with current "state-of-the art".

Simulation Block Diagram

A simplified functional block diagram summarizing the simulation procedure is shown in Figure 18.

Limitations of the Simulation

The effect of increased vehicle drag in conditions where hull-slamming occurs is not included in any of the analog simulation. To the extent that this effect is significant, a lower degree of accuracy in the data must be inferred.

Fully-Submerged-Foil Craft

The fully-submerged-foil reference craft is investigated in regular seaways with a rudimentary autopilot sufficient for longitudinal stabilization and control of the vehicle in all sea states concerned. The autopilot design and its basic functions are discussed. Performance data in sea states, summarized from extensive analog

computer studies, are presented. Parameters used to simulate the craft are tabulated in Appendix C.

Basic Craft Stability

Figure 19 shows that the submerged-foil reference craft has a natural tendency to recover from a positive initial disturbance of one-half ft. in c.g. height, but plunges into the sea when the disturbance is increased to one ft. Although the vehicle is inherently stable in a calm sea and for small disturbances, it becomes exponentially divergent when the perturbations become too large or violent. The divergence rate, measured as the time to double amplitude, is found to be about 8-15 sec. This basic instability is considered too severe for long-term manual control. Hence, an autopilot is necessary for stabilization and control of the vehicle.

It is of interest to note that instability always occurs in the same manner. An instability cycle can be initiated by a slight increase in submergence of the foils. The associated increase in strut wetted-area causes an increase in vehicle drag which produces a pitching-down moment and a decrease in forward speed and lift. The overall effects induce the foils to sink even deeper and the craft to pitch downward even more. The cycle continues until the craft finally "crashes" or plunges bow first into the sea.

Autopilot Design

Only rudimentary autopilot functions are considered herein, as these are sufficient for longitudinal stabilization and control of the submerged-foil reference craft. Ultimate performance available by special control techniques is not determined. A composite functional block diagram of the autopilot design is shown in Figure 20. For ease in discussing autopilot functions, however, each control loop is shown individually in Figure 21.

As can be seen, the autopilot control system is composed of three loops: (1) pitch stabilization, (2) vertical stabilization, and (3) acceleration. The pitch and vertical stabilization loops are considered the primary longitudinal stabilization and control loops, for both loops must be closed to assure complete stabilization of the craft in the whole range of sea states considered.* The acceleration loop alone is unable to provide complete vehicle stabilization in all sea states examined. Hence this loop is viewed as a supplementary or secondary loop whose chief function is to induce better ride characteristics, especially in reduced on-board accelerations.

---

* It should be noted that for some sea states examined either the pitch or vertical stabilization loops was sufficient for stabilization, but other seaways required closure of both loops.

Pitch Stabilization Loop: The pitch stabilization loop (Fig. 21a) provides, as the name implies, pitch stabilization for the craft and steady-state control of pitch attitude during cruise by operating the forward and aft flaps asymmetrically, i.e. positive deflection of the forward flap and negative deflection of the aft flap or vice versa. The control signal is obtained by comparing a pitch trim command ($\hat{\theta}$) to a signal from a vertical gyro (θ). Integration of the pitch error signal (K_{θ_p}) is also employed to assure steady-state accuracy. The form of the control law is:

(34) $$\hat{\delta} = \left[\frac{K_{\theta_p}}{s} + K_\theta\right](\hat{\theta} - \theta)$$

where:

$\hat{\delta}$ = flap command

K_θ = pitch error gain

K_{θ_p} = pitch error integral gain

$\hat{\theta}$ = pitch trim command

θ = pitch signal measured by vertical gyro

Vertical Stabilization Loop: The vertical stabilization loop (Fig. 21b) provides height stabilization of the craft and steady-state control of average forward foil depth during cruise by operating the forward flap. The control signal is obtained by comparing the

height command signal ($\hat{h}$) to a signal from a height sensor (h_{sensor}) located over the forward foil. Integral height error signal (K_p) is also employed to assure steady-state accuracy. A height error filter (consisting of a first-order lag) controls, to some extent, the transition frequency between wave contouring and level flight. The form of the control law is:

(35) $$\hat{\delta}_f = \left[\frac{K_p}{s} + \frac{K_h}{\tau_1 s+1}\right](\hat{h} - h_{sensor})$$

where:

$\hat{\delta}_f$ = forward flap command

K_p = height error integral gain

K_h = height error gain

τ_1 = height error filter time constant

$\hat{h}$ = height command

h_{sensor} = height as measured by height sensor

Acceleration Loop: The acceleration loop (Fig. 21c) provides a means for attenuating on-board normal accelerations by operating the forward and aft flaps symmetrically. The control signal is obtained by comparing a normal acceleration command ($\hat{a}_z$) to a signal from an accelerometer (a_z) located over the c.g. A simple high-pass filter offers some control over the transition frequency between wave contouring and level flight. The form of the control law is:

(36) $$\hat{\delta} = \left[K_{a_z} \left\{ \frac{\tau_2 s}{\tau_3 s + 1} \right\} \right] (\hat{a}_z - a_z)$$

where:

$\hat{\delta}$ = flap command

K_{a_z} = normal acceleration error gain

τ_2 and τ_3 = normal acceleration error filter time constants

$\hat{a}_z$ = normal acceleration command

a_z = normal acceleration measured by accelerometer

Parameter Settings: Analog simulation shows that only a small amount of integral height error gain and integral pitch error gain are necessary for steady-state accuracy. Hence the ratio K_p/K_h and K_{θ_p}/K_θ are maintained constant at .01 for all ensuing work.. These low ratios are also beneficial in maintaining maximum gain margins for K_h and K_θ.

The choice of suitable height and normal acceleration error filter time constants (τ_1, τ_2, and τ_3) influences the transition frequency between wave contouring and level flight. The design objective is to contour waves of longer wave lengths and to maintain level flight or "plow" through the shorter ones. At the same time

a large amount of height feedback and small amount of acceleration feedback are required for wave contouring and the opposite for level flight. This can be obtained, to some extent, by using a high-pass filter on the normal acceleration error signal and a low-pass filter on the height error signal, and adjusting the filter time constants appropriately. Suitable results are attainable in all succeeding work by fixing these time constants at .65 sec. ($\tau_1 = \tau_2 = \tau_3 = .65$) which places the transition or break frequency between contouring and level flight at about 1.54 rad/sec or .25 cps.*

The autopilot parameters K_θ, K_h, and K_{a_z} are considered adjustable in sea states. The objectives in adjusting these parameters in waves are: (1) to restrict the vertical maneuvering of the foils to a region that prevents foil broaching or hull-slamming and (2) to minimize adverse dynamic responses in pitch angle and on-board normal accelerations. The former objective is regarded as being more important than the latter and, therefore, is given prime consideration when both objectives cannot be satisfied simultaneously. Further discussions on adjustable autopilot parameter settings can be found later.

---

* Choice of this particular transition frequency is an educated guess based on work done earlier in Reference 1. Performance data for the conventional fully-submerged-foil reference craft, appearing on pp. 79-83 of that report, seem to indicate that a transition frequency of .25 cps is an appropriate value.

Augmented Craft in Calm Sea

Root loci plots showing behavior of the augmented craft (using a linear model) at 50 knots, are summarized in Figures 22 through 25. Additional data and tabulation of critical open-loop poles and zeros appear in Appendix C. Since complex poles and/or zeros always appear as conjugate pairs, only one member of the pair is shown in these figures. None of the autopilot loops examined individually, as noted earlier, can fully stabilize the craft in sea states. However, it is still worthwhile, for ease in demonstrating individual loop effectiveness and functions, to investigate these autopilot loops separately in a calm sea.

Pitch Stabilization Loop Closed: Figure 22 shows the effect on the pitch angle (θ) to pitch command ($\hat{\theta}$) transfer function when the pitch stabilization loop is closed. The root locus has 7 open-loop poles and 4 open-loop zeros. The most important effect of the loop is to move the low-frequency complex pair of poles away from the vicinity of the origin and to relocate the complex poles in a region which provides better overall craft pitch angle stability. As pitch error gain is increased substantially ($K_\theta > 2$), the pitch angle to pitch trim command ($\theta/\hat{\theta}$) transfer function for the augmented craft can be approximated by a third-order system consisting of a complex conjugate pair of poles and a negative real pole far away from the

origin. Therefore the complex closed-loop poles are the dominant poles in determining pitch angle transient time response.

Vertical Stabilization Loop Closed: Figure 23 shows the effect on the cruise height above the water surface at the forward foil (h) to height command ($\hat{h}$) transfer function when the vertical stabilization loop is closed. The root locus has 8 open-loop poles and 4 open-loop zeros. Primary effect of this loop is to increase the oscillation frequency of the low-frequency pair near the origin and to produce an additional oscillatory mode. If height error gain (K_h) is greater than .01 the forward height to height command ($h/\hat{h}$) transfer function for the augmented craft can be approximated by a fifth-order denominator and first-order numerator. The dominant poles for forward height transient time response, however, are the complex pair closer to the origin.

Acceleration Loop Closed: Figure 24 shows the effect on the normal c.g. acceleration (a_z) to normal acceleration command ($\hat{a}_z$) transfer function when the acceleration loop is closed. The root locus has 7 open-loop poles and 6 open-loop zeros. Although this loop may not appear to be of much help in improving craft stability in calm sea, its effectiveness in helping to reduce normal accelerations in waves is invaluable. Hence, further mention of this loop is deferred to a later section where its worth in sea states can

be more easily demonstrated.

Both Pitch and Vertical Stabilization Loops Closed: Figure 25 is a family of root loci plots, showing only complex closed-loop characteristic poles for the augmented craft, with both the pitch and vertical stabilization loops closed. Solid lines show the effect of maintaining K_θ constant and varying K_h while broken lines show the result of maintaining K_h constant and varying K_θ. A comparison of Figures 22, 23, and 25 reveals that the outcome of closing both stabilization loops is two oscillatory modes located in an intermediate region, bounded by the closed-loop complex poles that resulted earlier when each stabilization loop was closed separately and independently of the other. For reasonable fixed values of K_h between .02 and .32, K_θ seems to have its primary affect on the complex poles further from the origin; this is characterized by an increasing oscillation frequency and decreasing damping ratio for increasing K_θ. In contrast, fixing K_θ causes K_h to have most affect on the complex poles closer to the origin; the tendency is an increasing oscillation frequency and decreasing damping ratio for increasing K_h.

Analog studies have verified that these two pairs of complex closed-loop poles are the dominant poles for determining craft time responses. The complex pair of poles nearer the origin is the dominant

set for determining height time response to height commands while the other complex pair is the dominant set for determining pitch angle time response to pitch commands. Therefore, Figure 25 is a useful tool for selecting appropriate combinations of K_h and K_θ for desirable craft responses to either height or pitch trim commands. The procedure for each mode consists basically of 2 steps: (1) select the damping ratio and damped oscillation frequency desired and (2) then by using the appropriate portion of Figure 25 predict the values of K_h and K_θ that correspond to the previously chosen damping ratio and frequency.* Actually, the final choice of K_h and K_θ values involves a compromise; adequate damping must be attained for both pitch and height responses to assure good craft performance in waves.

As an example consider the cases where it is desirable to have: (1) damping ratio of .44 and oscillation frequency of 1.9 rad/sec for c.g. height time response to c.g. height command, and (2) damping ratio of .30 and oscillation frequency of 8.4 rad/sec for pitch angle time response to pitch angle command. The K_θ and K_h values predicted from Figure 25 and those finally used in the analog simulation are tabulated below for both cases. Time histories showed that using

---

* For those unfamiliar with the methods for determining damping ratios see John C. Truxal's "Control System Synthesis", Section 1.4.

the predicted gain values in the simulation did not result in the previously indicated damping ratios and oscillation frequencies; to this end, some readjustments in gain values become necessary. Differences can be attributed to the incorporation of primary non-linearities in the analog simulation. The fact that the adjusted simulation values are identical in both cases is a coincidence. Figure 26 shows time responses for the adjusted values given. In addition, Figure 26 also shows time response when the acceleration loop is closed. The acceleration loop does not seem to affect height or pitch time responses much.

Tabulation of Comparison Data

Quantity	Actual Values (Adj. for Analog Simul.)		Predicted Values (From Fig. 25)	
	Case 1	Case 2	Case 1	Case 2
K_θ	8	8	4-8	7.8
K_h	.1	.1	.06	.12

Figure 27 establishes stable and unstable regions for various combinations of K_θ and K_h. Also illustrated in this figure is the region of K_θ and K_h combinations used later in sea state simulations.

Augmented Craft in Sinusoidal Seas

Effects and Methods of Selecting Variable Autopilot Parameter Settings: As mentioned previously, autopilot parameter settings of K_θ, K_h, and K_{a_z} are considered variable. In general each sea state requires different gain settings for optimum dynamic performance. Figures 28 and 29 present the effects of varying autopilot parameter settings in a typical sea state (4-ft head sea of steepness ratio 22) and demonstrate the type of graphical plots that can be made and used in selecting suitable autopilot parameter values. Solid lines illustrate the effect of varying K_h for three different values of K_θ; broken lines show the effect of the acceleration loop (varying K_{a_z}) with just barely enough stabilization to maintain stable flight (only vertical stabilization is necessary in this particular sea).

Peak-to-peak c.g. height response decreases with increasing K_θ. Provided that K_θ is sufficiently large, c.g. height response decreases with increasing K_h.

Peak-to-peak pitch angle response decreases with increasing K_θ. For sufficient amounts of pitch error feedback (K_θ), pitch response reaches a definite minimum for a certain value of K_h.

Peak-to-peak c.g. normal acceleration increases with increasing K_θ but decreases with increasing K_h.

The acceleration loop is seen to effectively reduce peak-to-peak c.g. normal acceleration, for this sea, 3 to 4 times with no objectionable c.g. height or pitch angle responses.

Thus the selection of final values of K_θ, K_h, and K_{a_z} involves compromises and trade-offs to achieve the most desirable craft responses in sea states. For this particular sea state, values of $K_\theta = 8$, $K_h = .1$, and $K_{a_z} = .009$ seem suitable (see Figures 30 and 31 for additional justification).

For purposes of expediency, however, it is not practical in this study to determine parameter settings for each particular sea state by the detailed graphical means presented in Figures 28 and 29. Therefore, parameter settings for other sea states examined are determined experimentally by simultaneously watching analog time histories like those shown in Figures 30 and 31 and adjusting variable autopilot parameters. The exact procedure followed in each case is to: (1) first adjust K_θ and K_h to provide good overall transient and steady-state responses irrespective of normal acceleration levels, and then (2) adjust K_{a_z} to provide a suitable reduction in acceleration level without introducing objectionable pitch angle and height steady-

state responses when possible. Adjustable autopilot parameters used are tabulated in Appendix C.

Time Responses: Typical time histories of the augmented vehicle in a 4-ft. high, steepness ratio 22, head sea appear in Figures 30 and 31. Figure 30 is for the craft with only pitch and vertical stabilization loops closed and Figure 31 has the acceleration loop closed too. Comparison of Figures 30 and 31 clearly demonstrates the effectiveness of the acceleration loop in reducing on-board accelerations in sea states. Before the acceleration loop is closed the peak-to-peak incremental normal acceleration at the c.g. is about .5g (Fig. 30). In Figure 31 when the acceleration loop is also closed, the peak-to-peak normal acceleration has been reduced to about .16g.

With all three control loops closed the craft responses to step pitch trim commands of 3 degrees and -3 degrees are shown in Figures 32 and 33 respectively. The pitch trim command is applied while the craft is moving in a sinusoidal sea. These two pitch trim commands happen to be the limits attainable in the particular sea; the vehicle seems quite capable of "riding out" all transient effects. In actual flight, however, it is recommended that pitch trim commands ($\hat{\theta}$) be gradually increased to the desired value.

Steady-State Responses: Steady-state peak-to-peak values of some craft response variables are shown in Figures 34 through 37. These values are measured from time histories similar to those shown in Figure 31.

Incremental normal acceleration at the c.g. (Fig. 34) has a tendency in most cases to increase with higher frequencies of wave encounter. For a fixed frequency of encounter, acceleration levels are higher for following seas than head seas. Normal acceleration also increases as the wave amplitude increases.

Craft pitch angle response, shown in Figure 35, becomes more pronounced for larger wave heights. In addition there seems to be a tendency in most cases for pitch angle response to be slightly more severe in following seas than head seas.

Depth of submergence of forward and aft foils are given respectively in Figures 36 and 37. As expected, forward foil depth seems to follow a more regular pattern than the aft foil depth. The reason for this, of course, is that height feedback is applied only to the forward foil. Peak-to-peak response of the forward foil depth increases with larger wave amplitudes and becomes more pronounced in following

seas than head seas. The vehicle operates quite easily through 4-ft. waves with no evidence of foil broaching and/or hull-slamming. In 10-ft. waves, however, the forward foil will broach in following seas much shorter than 88 ft.* There is also a tendency for hull-slamming to occur in 10-ft. waves. Based on the above data it appears the vehicle can traverse sea states up to about 8-ft. in height without foil broaching or hull-slamming.

Surface-Piercing-Foil Craft

The unaugmented surface-piercing-foil reference craft is examined in regular sinusoidal seaways and longitudinal dynamic performance data are summarized from extensive analog computer studies. Typical analog time histories are included to illustrate typical behavior of the craft in waves. Parameters used to simulate the craft are tabulated in Appendix C.

Basic Craft Stability

Analog time histories of the uncontrolled craft indicate that it is stable while flying at 50 knots in a calm sea. For example, Figure 38 shows typical time histories of the vehicle when the forward foil depth of submergence is briefly reduced to zero. As can be seen the craft is inherently stable and requires no autopilot.

---

*Waves 10-ft. high and less than 88 ft. long have steepness ratios less than 8.8. Waves with steepness ratios less than 7 are generally regarded as being unstable and uncommon.

Unaugmented Craft in Sinusoidal Seas

Steady-State Responses: The objective of the study is to examine the uncontrolled craft in a variety of sea states and to determine the degree of incremental pitching, vertical movement at the foils, and incremental normal acceleration at the c.g. These steady-state responses are summarized from analog time histories similiar to those shown in Figure 39 for a 2-ft., steepness ratio 44, head sea.

Incremental c.g. normal acceleration (Fig. 40) has an overall tendency to increase with frequency of wave encounter. Generally, for a given frequency, higher levels of normal acceleration are experienced in a following sea than in a head sea. Normal acceleration also increases as wave amplitude increases.

Craft pitch angle response is presented in Figure 41. As would be expected, a minimum occurs at frequencies corresponding to waves whose length is equal to the foil spacing.

The depth of submergence of both forward and aft foils follow the same trends (Fig. 42 and 43). Incremental changes in foil depth are greater for: (1) larger wave height and (2) following seas than head seas. Foil broaching does not occur for any of the sea conditons examined, but 4-ft. waves will contact the vehicle hull.

Pitch Trim Capabilities in Flight: Pitch trim control of the vehicle in calm to moderate (2-ft.) sea states is attainable by deflecting an aft flap. Trim capabilities in 2-ft. seas, however, are restricted to a region bounded by -.8 to + 1.2 degrees before the water touches the hull or the aft foil broaches. Pitch trim responses to -.8 and +1.2 degree commands in a 2-ft. head sea of steepness ratio 44 are shown in Figures 44 and 45 respectively.

Comparison of Canard Craft Performances in Waves

Comparison of sea state performance is made between the canard fully-submerged-foil reference craft stabilized longitudinally with an autopilot and the unaugmented canard surface-piercing-foil reference craft.

Basic Craft Stability in Waves

Although the fully-submerged-foil reference craft is inherently stable in a calm sea, it becomes unstable in waves. A large pitch-down moment due to increases in foil-strut drag with submergence and a loss in foil lift as this drag slows the craft are the prominent destabilizing factors. Consequently, the submerged-foil craft requires an autopilot for stabilization and control of its longitudinal modes. The surface-piercing-foil reference craft, on the other hand, is stable both in a calm sea and in waves and, thus, needs no stability

augmentation. Henceforth all comparisons made are for the former craft with augmentation and the latter craft without augmentation.

Performance In Sea States

Wave Contouring: One significant consideration in comparing hydrofoil performance in seaways is the manner in which the vehicles tend to track (contour) the waves. This is important from the standpoint of keeping the foil submerged and/or the hull from slamming during foil-borne operation. Both the surface-piercing-foil and submerged-foil reference craft contour waves to some degree. Contouring is achieved to a greater degree in head than following seas in both types of craft. The submerged-foil craft can traverse waves of greater wave heights before foil broaching and/or hull-slamming occurs. This fact alone limits the surface-piercing-foil craft to lower sea states than the submerged-foil craft.

From the data available it appears that the submerged-foil craft can partially contour waves up to about 8-ft. in height without incurring foil broaching and/or hull-slamming. This, of course, prohibits foil-borne operation in seas which have wave heights greater than the craft keel-to-foil distance (except for swells with very long wave lengths) and limits the operational capability of the vehicle to a sea

state just below State 5 (wave heights 10 to 12 ft.). Also in light of the results obtained for the surface-piercing-foil craft, no attempt should be made to operate in seas having wave heights over 2 to 3 ft.

Vertical Acceleration: Another important consideration in comparing hydrofoil performance in sea states is incremental vertical acceleration. Minimization of vertical acceleration along the hull of the craft is essential to insure that design stresses and crew physiological tolerances are not exceeded.

Incremental normal accelerations can become excessive even in moderate sea states. The acceleration has a general tendency in both types of craft to: (1) increase for higher frequencies of encounter in most cases, (2) be often greater in following seas than head seas, and (3) increase for larger wave amplitudes.

For a given wave, the surface-piercing-foil craft gives a much rougher ride with higher accelerations than the fully-submerged-foil vehicle. The principal reasons for this are: (1) the submerged-foil craft has a feedback loop to help reduce accelerations, and (2) each change in wave profile or water surface is transmitted directly to the surface-piercing-foil vehicle by virtue of the area stabilization feature, whereas only the orbital velocity effects act on the fully-submerged foils.

Pitch Response: For a given wave height the surface-piercing-foil craft is more susceptible to pitching than the submerged-foil craft. However, in all sea conditions examined for either vehicle, craft pitch angle response did not exceed 4 degrees peak-to-peak.

COMPARISON OF CONVENTIONAL AND CANARD CONFIGURATIONS

The main differences between conventional and canard configurations are the foil and nacelle locations and horizontal c.g. position. Conventional craft have the main foil forward and secondary foil aft. These foils and their associated struts when used are reversed on the canard craft. The horizontal c.g. position is also reversed in these two configurations. The c.g. is as far forward of the mid-point between foils on the conventional configuration as it is aft on the canard configuration. Nacelles are always located on the main foil. All other physical parameters are identical on both configurations.

The hydrodynamic coefficients for main and secondary foils are identical on both configurations under the same conditions.

Inherent Craft Stability In Smooth Water

Inherent stability of the conventional and canard reference craft, as determined by the characteristic roots, is compared below. Data for the conventional configuration were obtained from Reference 1, which considered only 3 types of craft; the hybrid submerged-main

(forward) -foil craft was not considered. Longitudinal characteristic roots for the reference craft of both configurations are shown in Figure 46.

Submerged-Foil Craft

In the overall evaluation of the inherent stability, in smooth water, of conventional and canard configurations of submerged-foil craft there are no apparent outstanding merits or deficiencies to favor one over the other. Both configurations exhibited the same trends in the parametric variations with the exception of equilibrium speed changes, where increasing speed tends to be destabilizing for the conventional and stabilizing for the canard configuration. The canard reference craft is stable and remains stable over reasonable ranges of the parametric variations. The conventional reference craft is mildly unstable and remains unstable during many of the parametric variations. However, if an inherently stable conventional configuration is selected, it appears possible and reasonable to expect that this craft would exhibit the same degree of stability tolerance to the parameter changes as the canard reference craft.

It is evident that inherent stability of hydrofoil craft with both foils submerged is sensitive to many parameters. Absolute stability or instability cannot be precisely predicted. Regardless of configuration, the inherent stability of these craft, according

to the linear model used, is undoubtedly weak. It is uncertain that, given an inherently stable submerged-foil craft, the degree of stability is sufficient to operate successfully in sea states. Thus, stability augmentation of some form (damper or autopilot) is desirable and probably necessary for any physically realizable craft intended for service in seas.

Surface-Piercing-Foil Craft

Conventional and canard configuration of surface-piercing-foil craft are inherently stable (except the conventional configurations with large dihedral angles) and showed the same trends for all parametric variations. Design of these craft from a longitudinal stability viewpoint is relatively simple since almost any reasonable combination of parameters will probably result in an inherently stable craft.

Hybrid Foil Craft

Of the hybrid surface-piercing-main-foil craft investigated, the conventional configuration is inherently stable for all reasonable parametric variations, and the canard configuration is inherently unstable. It should be noted that the hybrid submerged-main-foil canard craft, however, is inherently stable for all reasonable parametric variations. Thus, it appears that hybrid craft with forward

surface-piercing foil and aft submerged foil, regardless of nominal configuration, are superior in inherent stability to hybrid craft with these foil types reversed.

It is also apparent from the parametric variations made that the much stronger lift dependence on depth of forward surface-piercing foils compared to forward submerged foils is the dominant contribution to craft inherent stability. In fact, it is apparent from the autopilot study of Reference 1, and preceding sections of this study, that a strong lift dependence on depth forward of the c.g. is sufficient, in many cases, to stabilize all craft configurations for operation in sea states. This lift dependence on depth for submerged forward foils is usually obtained by deflecting a forward foil flap as a function of measured submergence.

Dynamic Performance In Sea States

The longitudinal dynamic performance of conventional and canard submerged-foil and surface-piercing-foil reference craft in sinusoidal sea states are compared herein. Cruise speed is 50 knots in all cases and data for conventional craft are from Reference 1. Surface-piercing-foil reference craft are unaugmented. Submerged-foil reference craft include stability augmentation, although not the same augmentation for

both configurations. Some comparison data are shown in Figures 47, 48, and 49. These data are the responses obtained in 4-ft following seas for surface-piercing-foil craft and 10-ft following seas for submerged-foil craft (minimum acceleration cases only).

Submerged-Foil Craft

Height feedback to the forward flap is sufficient to stabilize the conventional submerged-foil reference craft in seaways, whereas height feedback to the forward flap and pitch feedback to both forward and aft flaps are required for stabilization of the canard submerged-foil reference craft. Acceleration feedback is used in both configurations to help reduce on-board accelerations.

Incremental c.g. normal acceleration responses to 10-ft waves for both configurations are shown in Figure 47. It is seen that acceleration increases with higher frequencies of encounter. However, the conventional configuration has greater acceleration increases than the canard configuration as indicated by the overall slope of the curves.

As shown in Figure 48, the conventional configuration has much higher incremental pitch angles at the lower frequencies of encounter than the canard configuration, but exhibits a sharp decrease in pitch

angle to levels comparable with those of the canard configuration as the frequency of encounter increases.

Forward foil depths for both configurations appear to have approximately the same trend and magnitude with increasing frequency of encounter (Fig. 49). Aft foil depth excursions are comparable in magnitude though more erratic in pattern.

Surface-Piercing-Foil Craft

This type of reference craft operates in waves without stability augmentation. However, operation is limited to waves of 4-ft. or less. Hence, the comparison data shown are for 4-ft. waves.

Incremental c.g. normal accelerations of surface-piercing-foil craft are shown in Figure 47. Except for the first peak for the conventional craft, the acceleration responses for both configurations tend to follow a similiar trend especially at the higher frequencies of encounter. The overall trend is to higher acceleration with increasing frequency.

The pitch angle response for the canard configuration is lower than for the conventional configuration at all frequencies of encounter except the highest (see Fig. 48).

V-type surface-piercing foil depth is measured from the water surface to foil apex. Forward foil depths of both configurations of surface-piercing-foil craft are comparable as a function of frequency of encounter (Fig. 49). There is a slight difference in minimum foil depths at the higher frequencies of encounter in which the forward foil of the canard craft is closer to the water surface. Aft foil depth excursions of the conventional craft are more erratic with frequency of encounter than those of the canard craft, with a greater tendency to broach.

Concluding Remarks

Craft response to sea states do not seem to differ enough to justify the selection of canard vehicles as being superior to conventional craft or vice versa. However, submerged-foil craft definitely have the advantages of lower incremental accelerations, craft pitching, and foil depth responses to waves of a given amplitude than surface-piercing-foil craft; hence, the former type of craft can operate in much higher sea states than the latter type.

RECOMMENDATIONS

Based on the foregoing study the following design and study recommendations are made for craft of canard configurations:

1. The design of fully-submerged-foil and hybrid surface-piercing-aft-foil craft should include stability augmentation due to the inherent weak stability or actual instability of such vehicles.

2. In the design of hybrid foil craft from a stability standpoint, a surface-piercing forward foil is recommended.

3. The incorporation of autopilots (and/or other devices) on surface-piercing-foil and hybrid submerged-aft-foil craft should be investigated as means of extending their capabilities in waves.

4. A study of the ultimate performance capabilities of various autopilot philosophies (non-interacting, adaptive, etc.) would be valuable, particularly as regards to suitability over extreme speed ranges and in the transition regions of take-off, landing, and the development and subsidence of cavitation and ventillation.

5. Hydrofoil craft dynamic performance in random seas should be examined and compared with results obtained for regular sinusoidal seas.

6. A detailed investigation of the coupling of structural modes with oscillatory forcing functions arising from sea turbulence should be undertaken.

7. Methods for alleviation of acceleration on board hydrofoil vehicles should be studied more extensively in order to extend the range of sea states in which foil-borne operation is possible, extend the basic structural fatigue life, and ensure that crew physiological tolerance does not prematurely restrict extended operation in seaways.

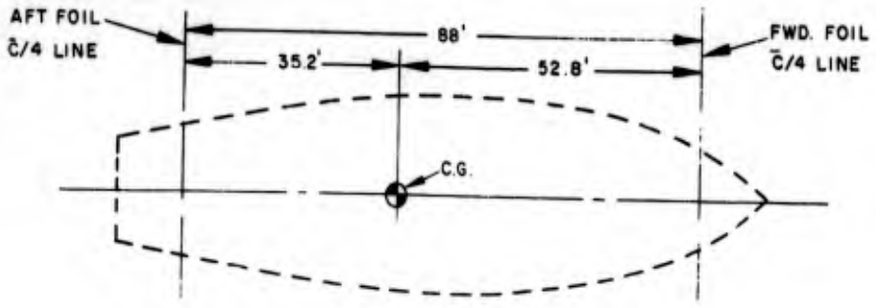

AFT. FOIL	CRAFT	FWD. FOIL
A = 150 FT.^{2}	W = 250,000 LBS.	A = 100 FT.^{2}
AR = 6	V = 50 KTS.	AR = 6
$\bar{c}$ = 5 FT.	I_x = 0.9 X 10^6 SLUG - FT.^{2}	$\bar{c}$ = 4.08 FT.
TR = 1	I_y = 6.4 X 10^6 SLUG - FT.^{2}	TR = 1
Λ = 0	I_z = 6.4 X 10^6 SLUG - FT^2	Λ = 0
i = 0	I_{xz} = 0	i = 0

FULLY-SUBMERGED FOILS
STRUTS : NACA 16-012
FOILS : NACA 16-009

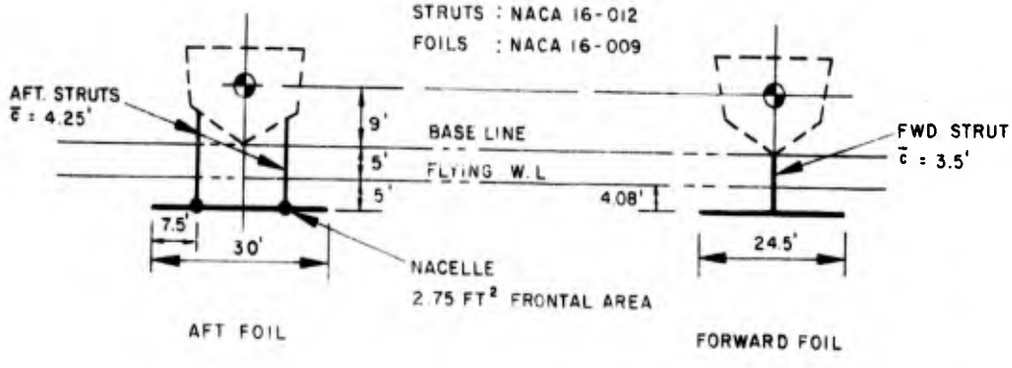

SURFACE-PIERCING, V-TYPE FOILS
FOILS : NACA 16-009

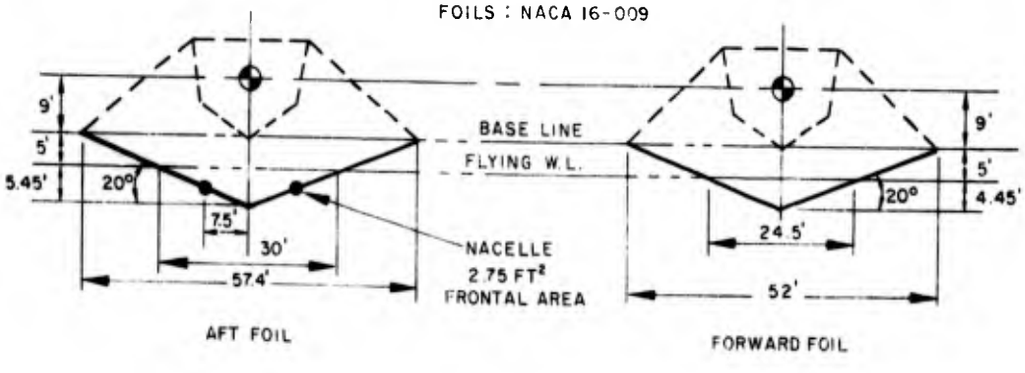

FIGURE I. REFERENCE CRAFT PHYSICAL DATA

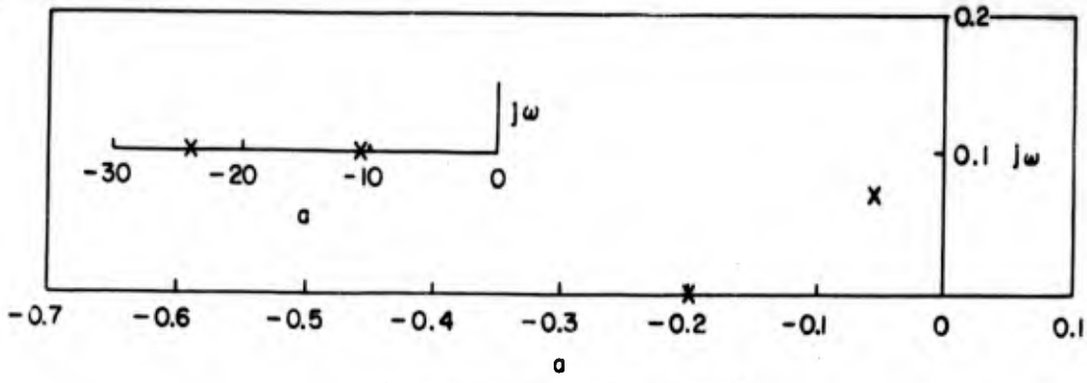

(a) SUBMERGED FOILS CANARD

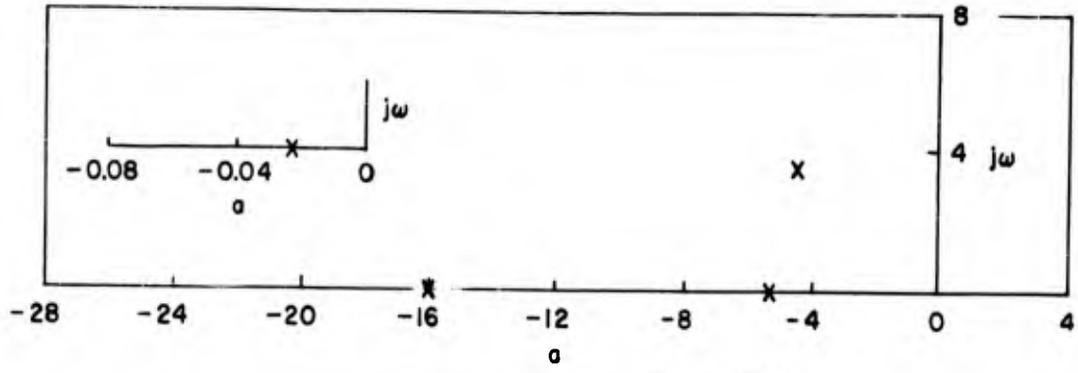

(b) SURFACE-PIERCING FOILS CANARD

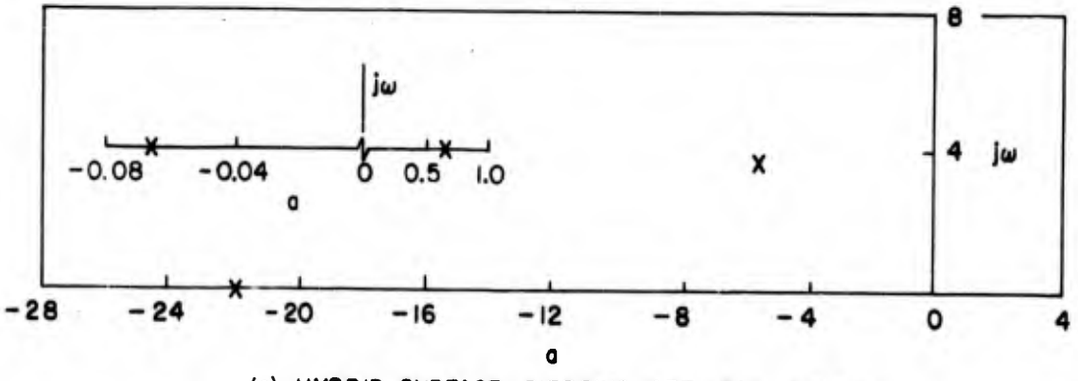

(c) HYBRID SURFACE-PIERCING-AFT-FOIL CANARD

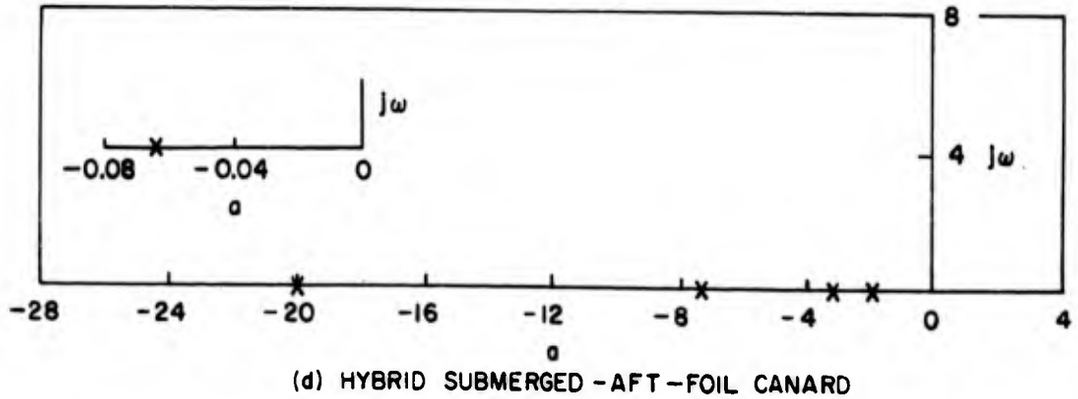

(d) HYBRID SUBMERGED-AFT-FOIL CANARD

FIGURE 2 LONGITUDINAL CHARACTERISTIC ROOTS REFERENCE CRAFT

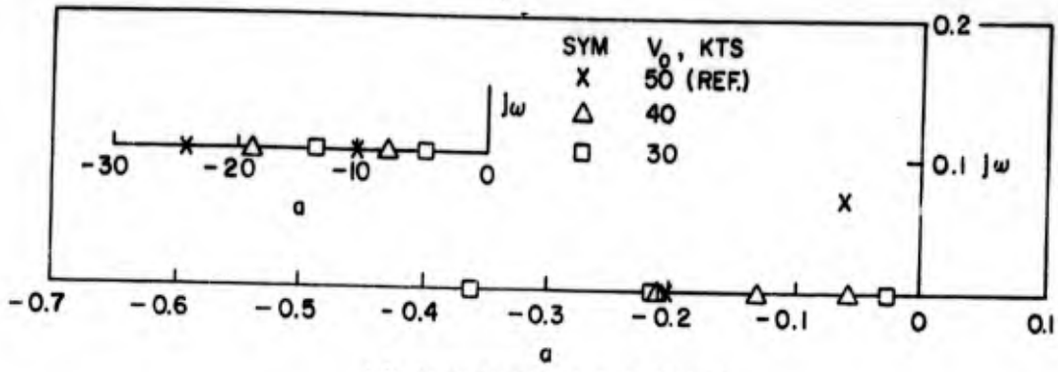

(a) SUBMERGED FOILS CANARD

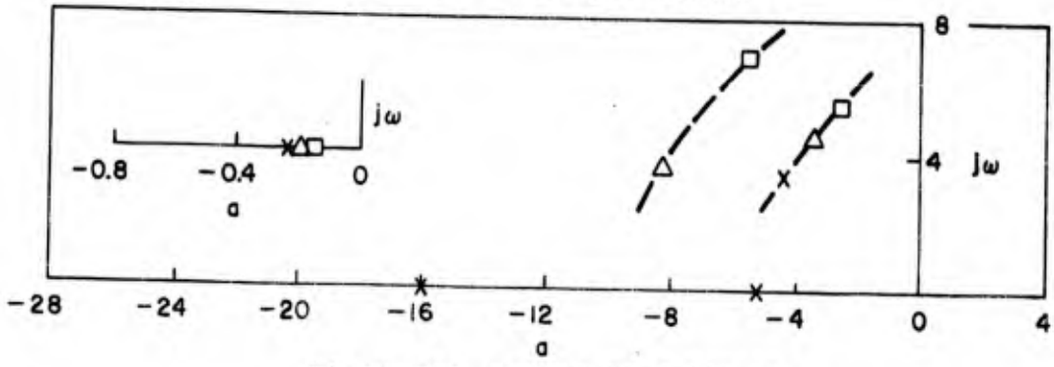

(b) SURFACE-PIERCING FOILS CANARD

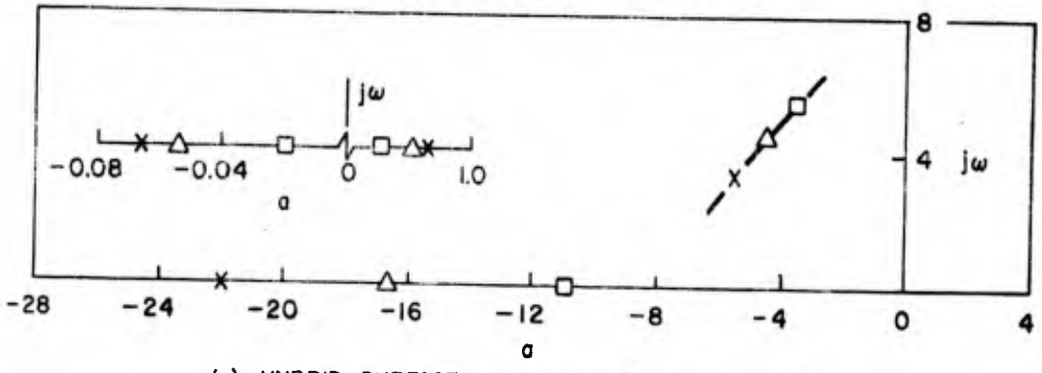

(c) HYBRID SURFACE-PIERCING-AFT-FOIL CANARD

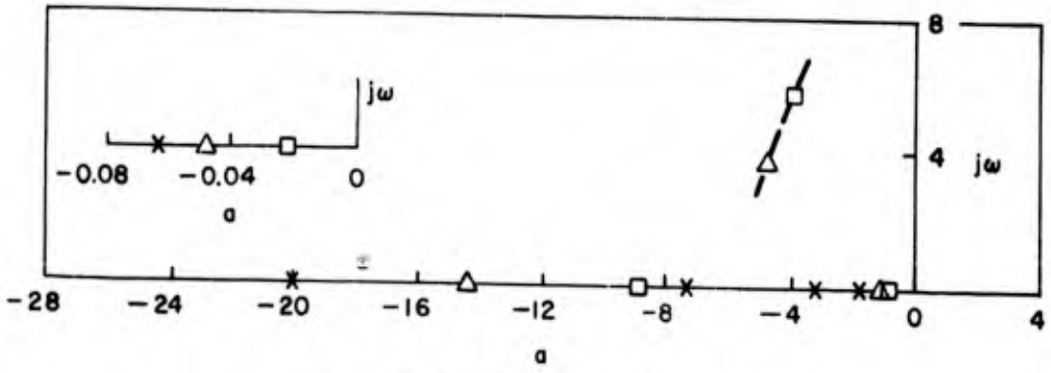

(d) HYBRID SUBMERGED-AFT-FOIL CANARD

FIGURE 3 LONGITUDINAL CHARACTERISTIC ROOTS SPEED VARIATION

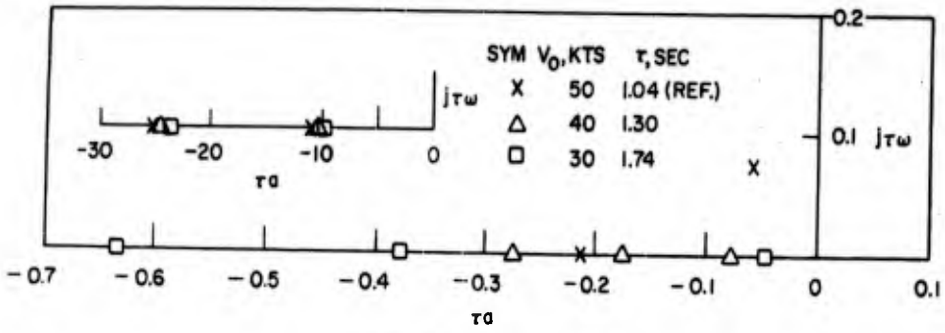

(a) SUBMERGED FOILS CANARD

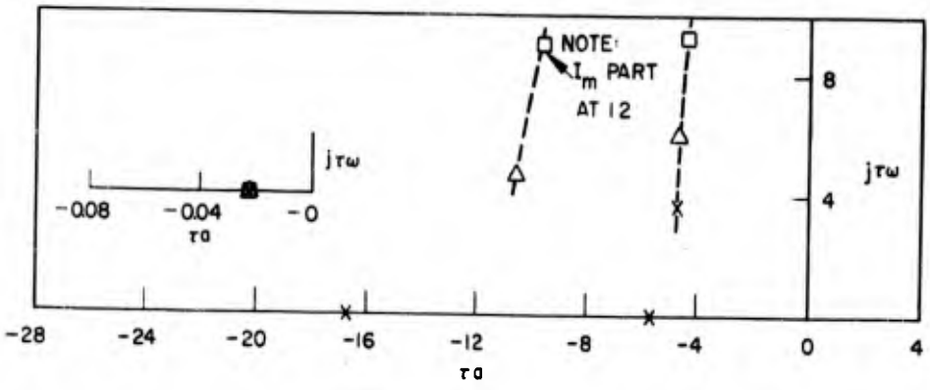

(b) SURFACE-PIERCING FOILS CANARD

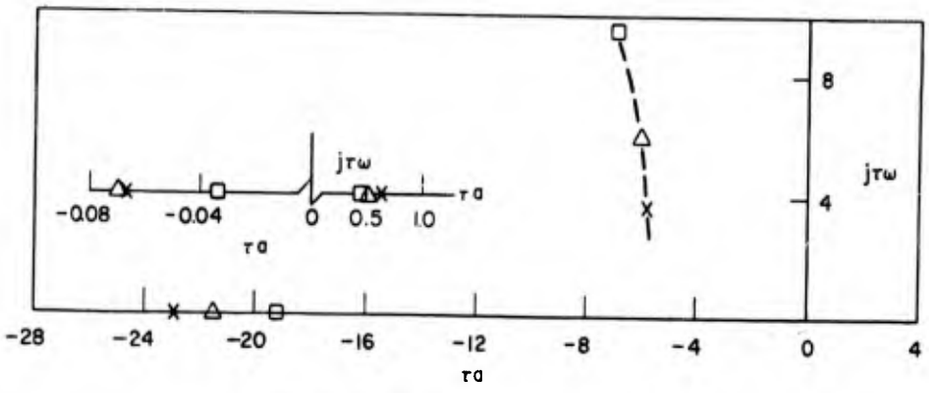

(c) HYBRID SURFACE-PIERCING-AFT-FOIL CANARD

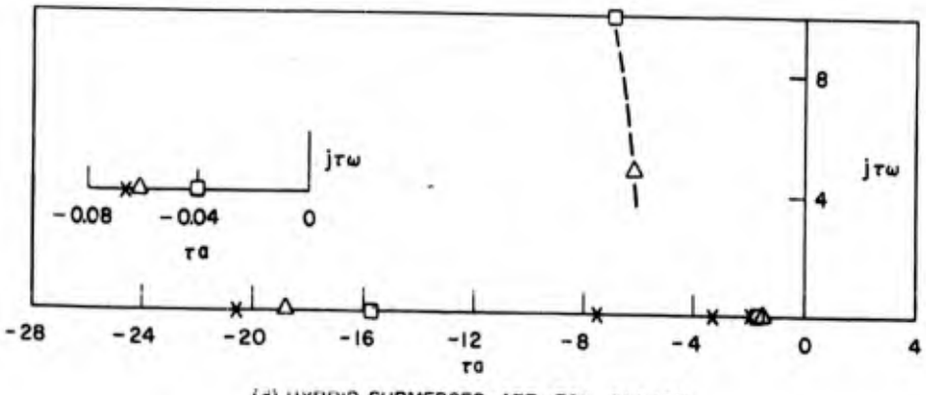

(d) HYBRID SUBMERGED-AFT-FOIL CANARD

FIGURE 4 DIMENSIONLESS LONGITUDINAL CHARACTERISTIC ROOTS SPEED VARIATION

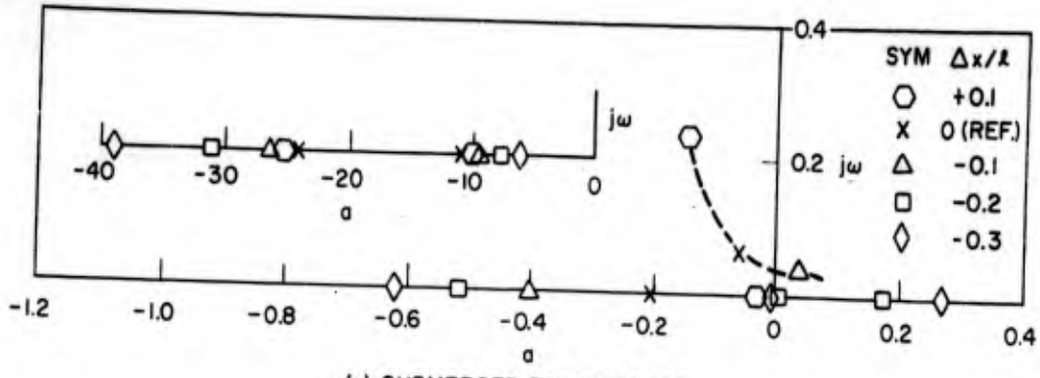

(a) SUBMERGED FOILS CANARD

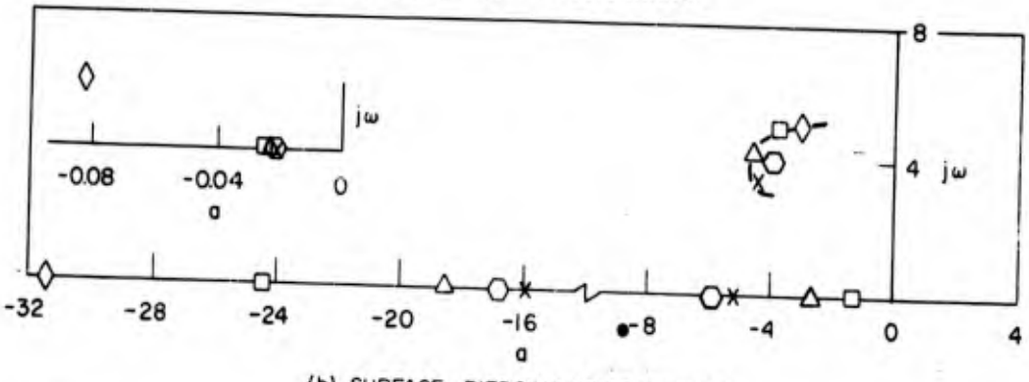

(b) SURFACE-PIERCING FOILS CANARD

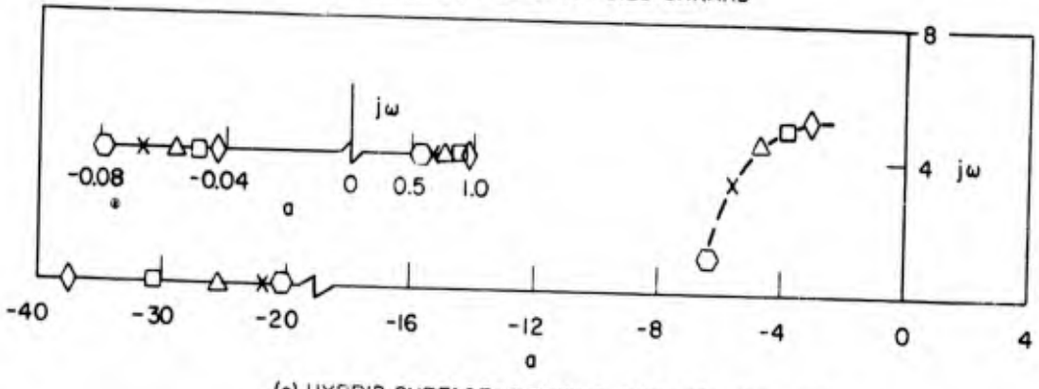

(c) HYBRID SURFACE-PIERCING-AFT-FOIL CANARD

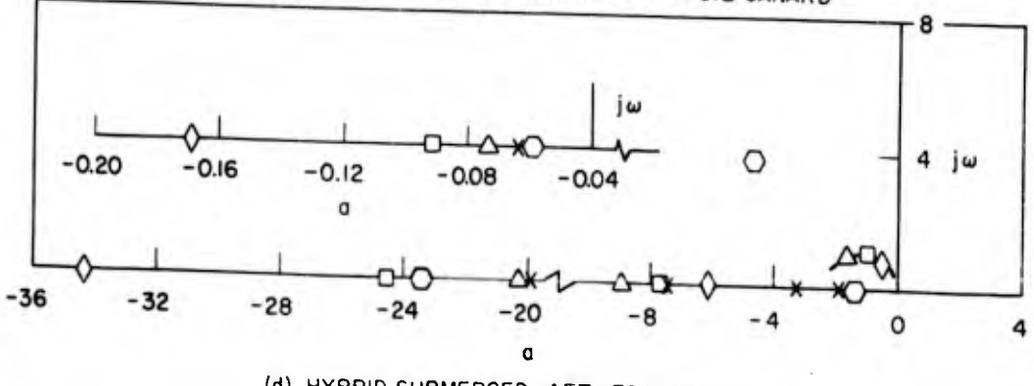

(d) HYBRID SUBMERGED-AFT-FOIL CANARD

FIGURE 5 LONGITUDINAL CHARACTERISTIC ROOTS HORIZONTAL C.G. LOCATION

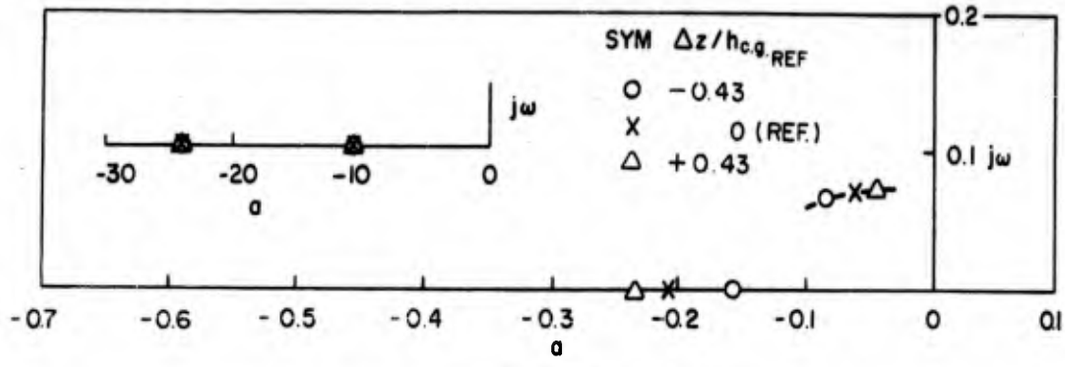

(a) SUBMERGED FOILS CANARD

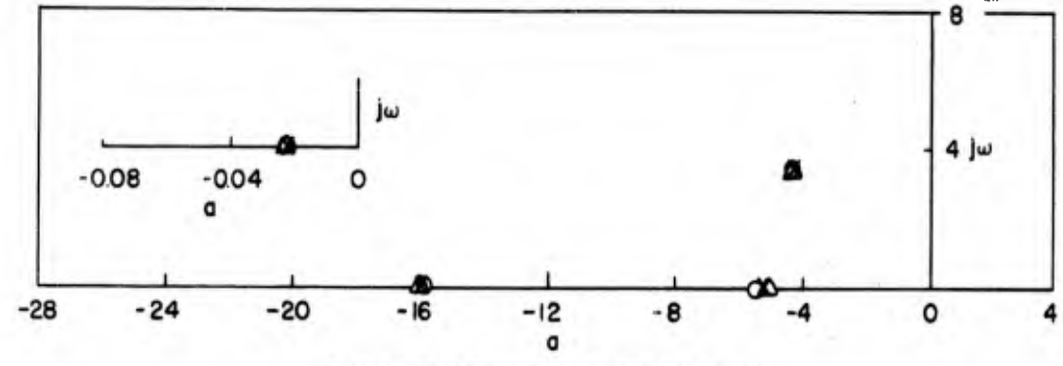

(b) SURFACE – PIERCING FOILS CANARD

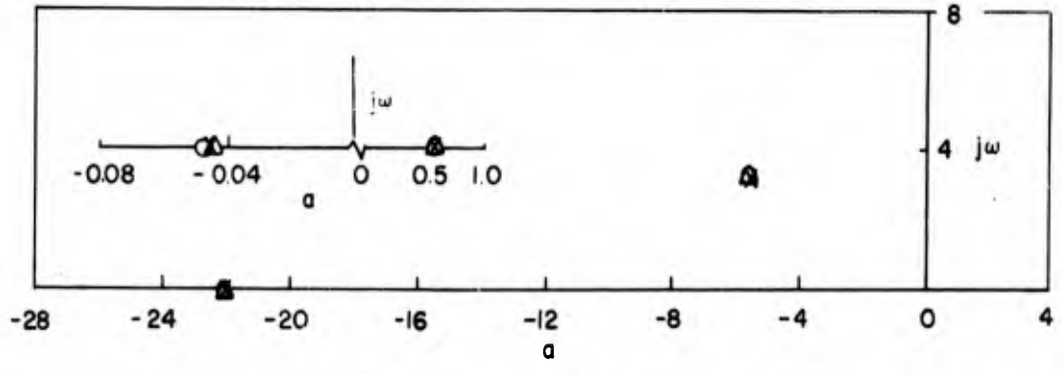

(c) HYBRID SURFACE – PIERCING - AFT – FOIL CANARD

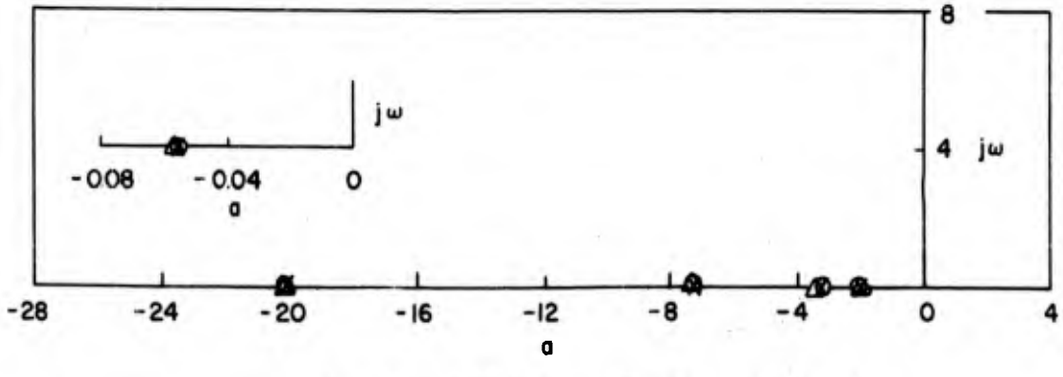

(d) HYBRID SUBMERGED – AFT - FOIL CANARD

FIGURE 6 LONGITUDINAL CHARACTERISTIC ROOTS VERTICAL C.G. LOCATION

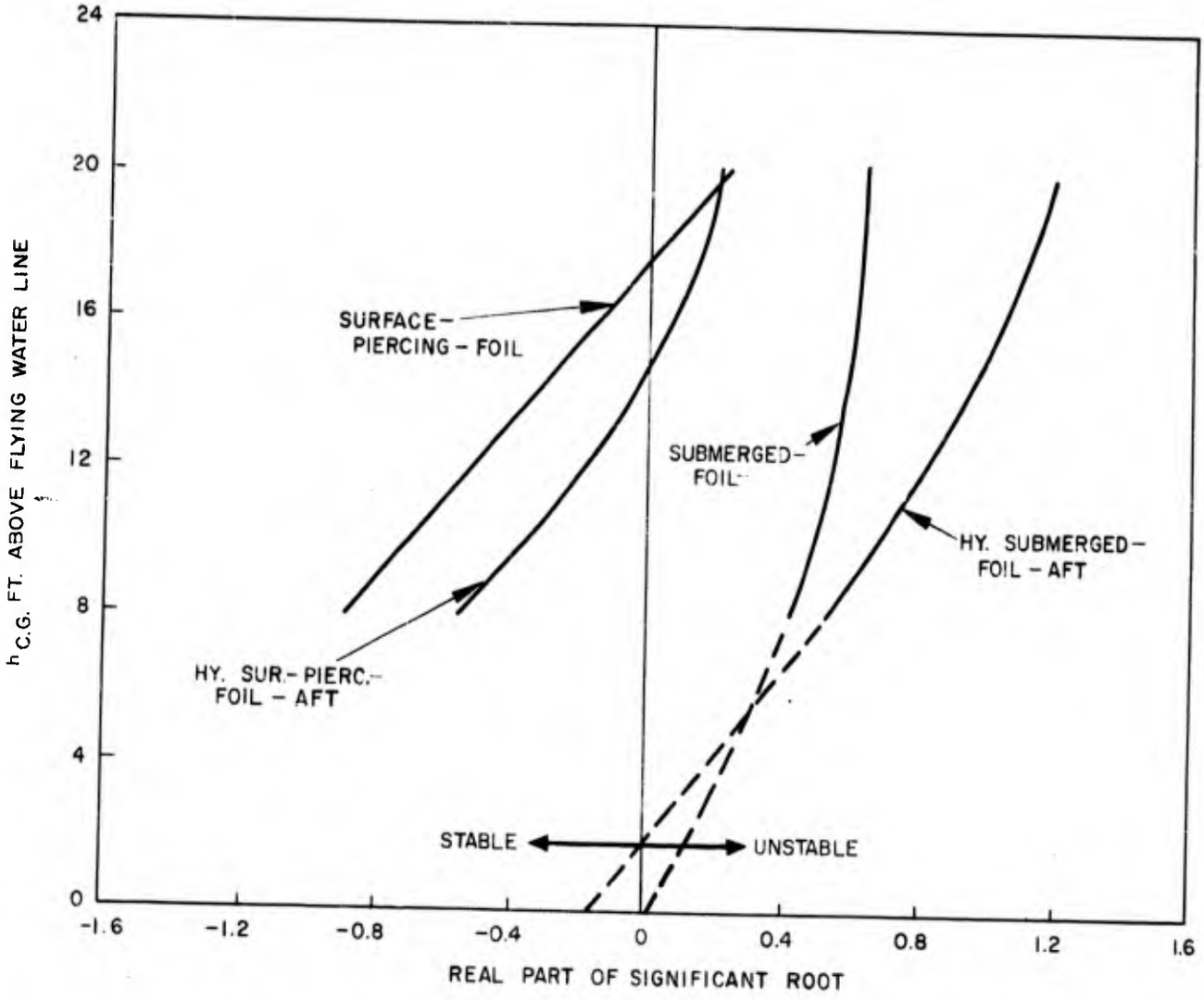

FIGURE 7 EFFECT OF VERTICAL C. G. LOCATION ON LATERAL STABILITY

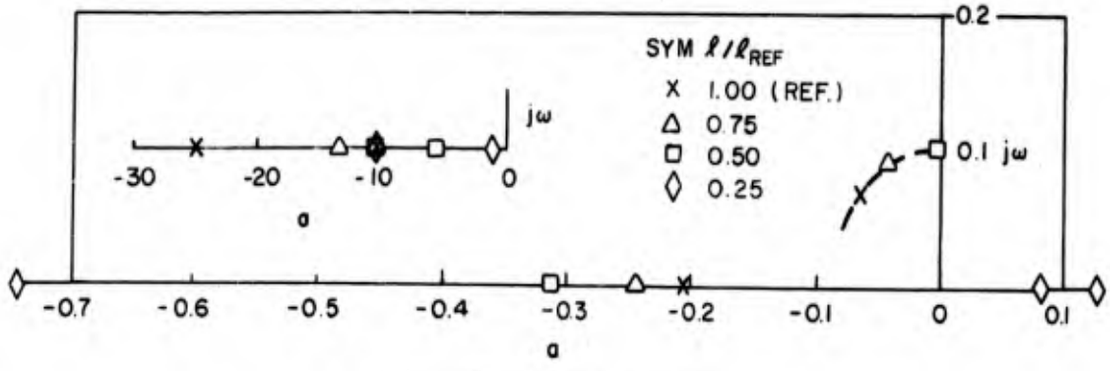

(a) SUBMERGED FOILS CANARD

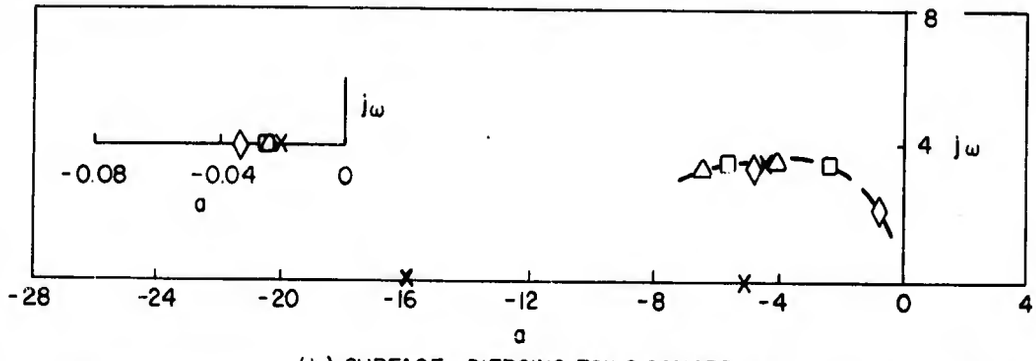

(b) SURFACE-PIERCING FOILS CANARD

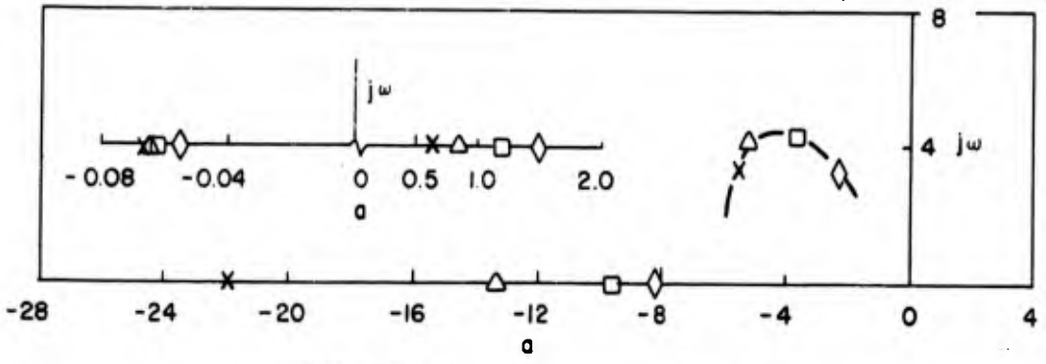

(c) HYBRID SURFACE-PIERCING-AFT-FOIL CANARD

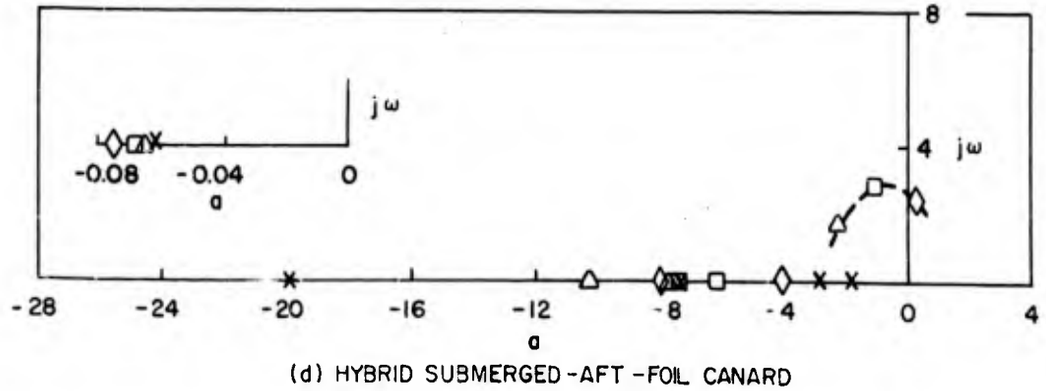

(d) HYBRID SUBMERGED-AFT-FOIL CANARD

FIGURE 8 LONGITUDINAL CHARACTERISTIC ROOTS FOIL SPACING VARIATION

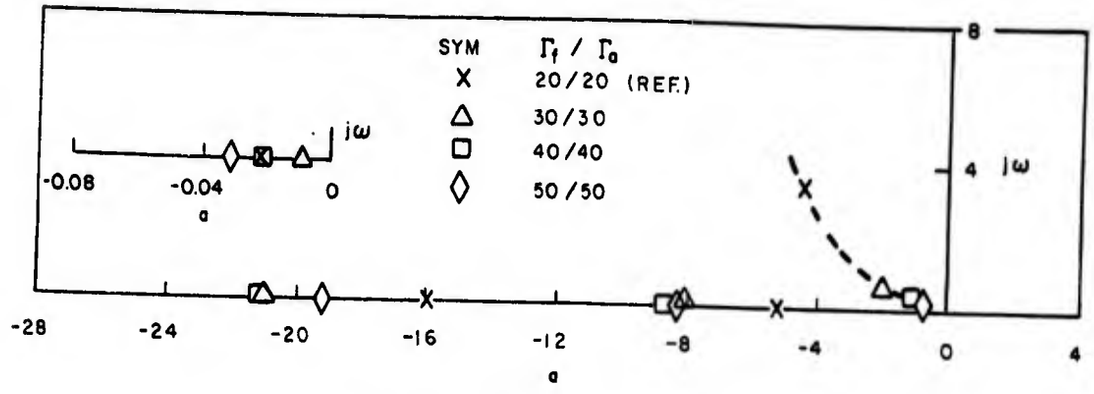

(a) SURFACE-PIERCING FOILS CANARD

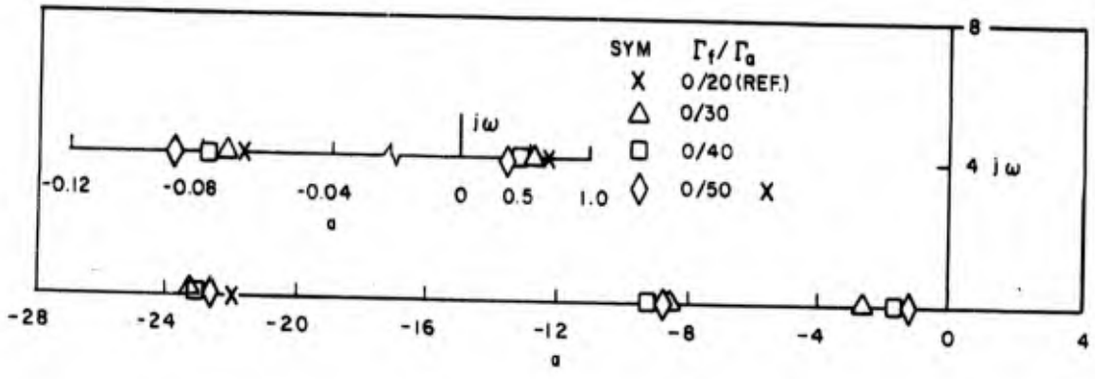

(b) HYBRID SURFACE-PIERCING-AFT-FOIL CANARD

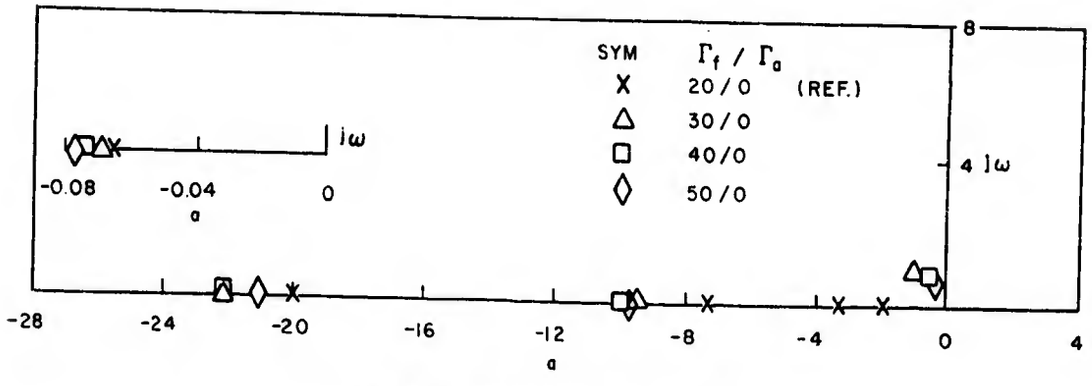

(c) HYBRID SUBMERGED-AFT-FOIL CANARD

FIGURE 9. LONGITUDINAL CHARACTERISTIC ROOTS SURFACE-PIERCING-FOIL DIHEDRAL VARIATION

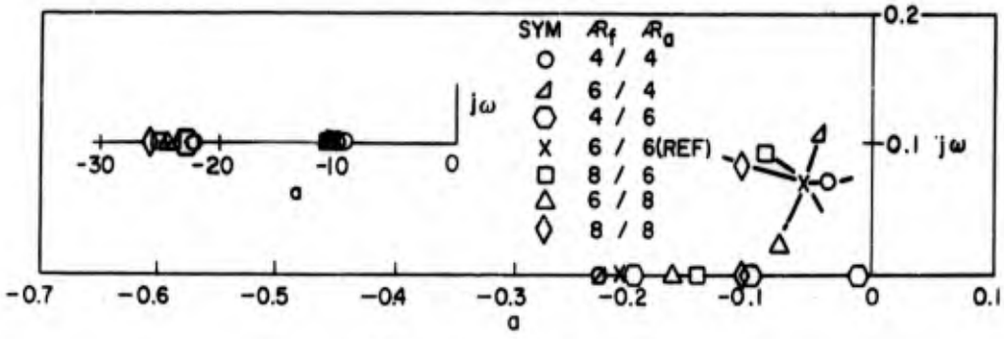

(a) SUBMERGED FOILS CANARD

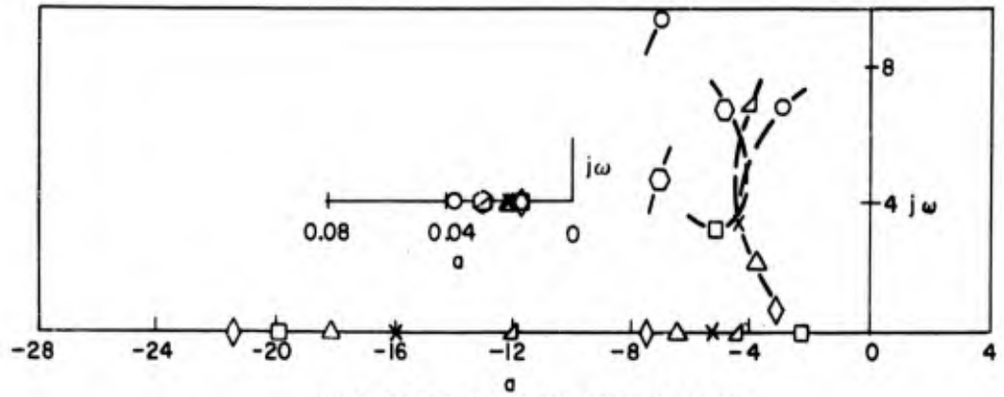

(b) SURFACE-PIERCING FOILS CANARD

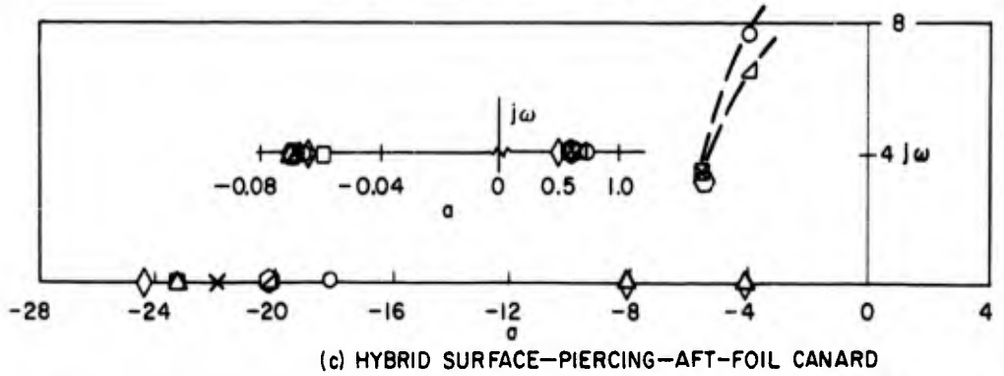

(c) HYBRID SURFACE-PIERCING-AFT-FOIL CANARD

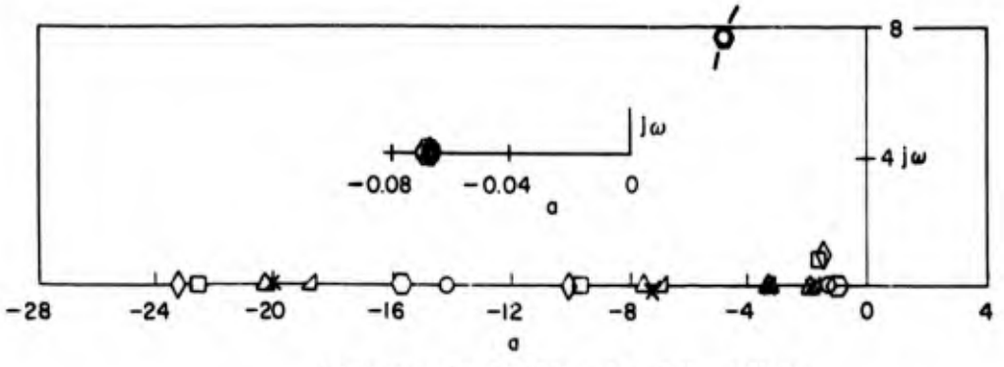

(d) HYBRID SUBMERGED-AFT-FOIL CANARD

FIGURE 10 LONGITUDINAL CHARACTERISTIC ROOTS ASPECT RATIO VARIATION

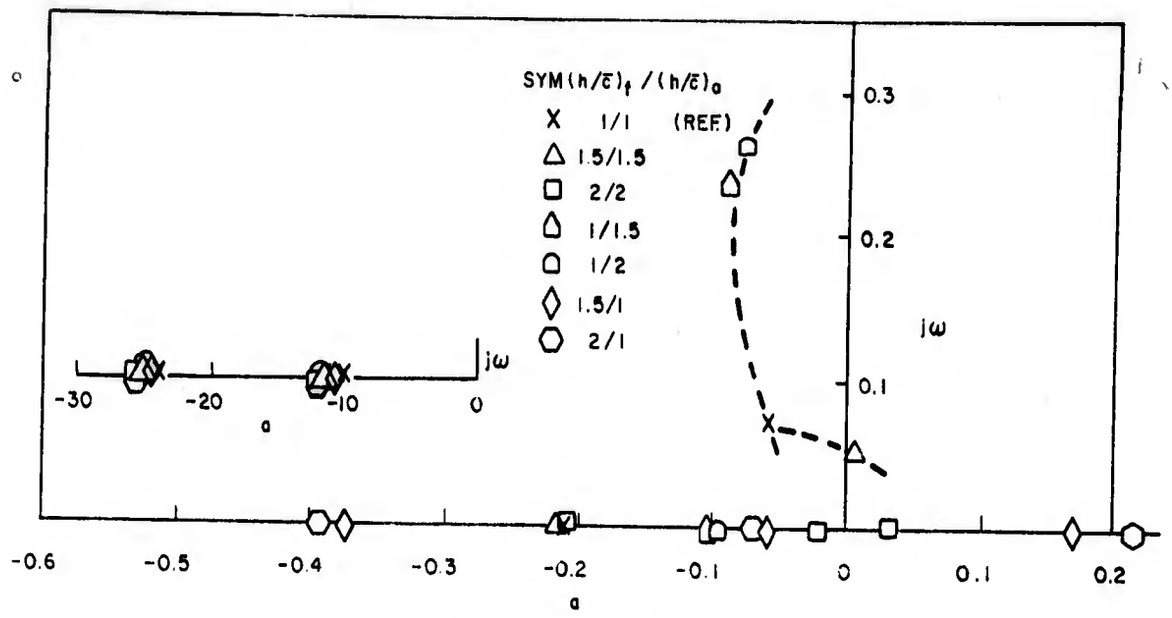

(a) SUBMERGED FOILS CANARD

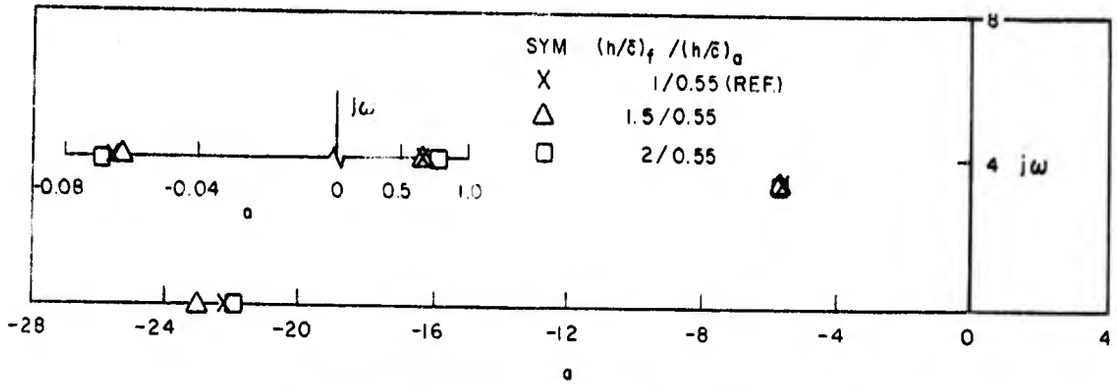

(b) HYBRID SURFACE-PIERCING-AFT-FOIL CANARD

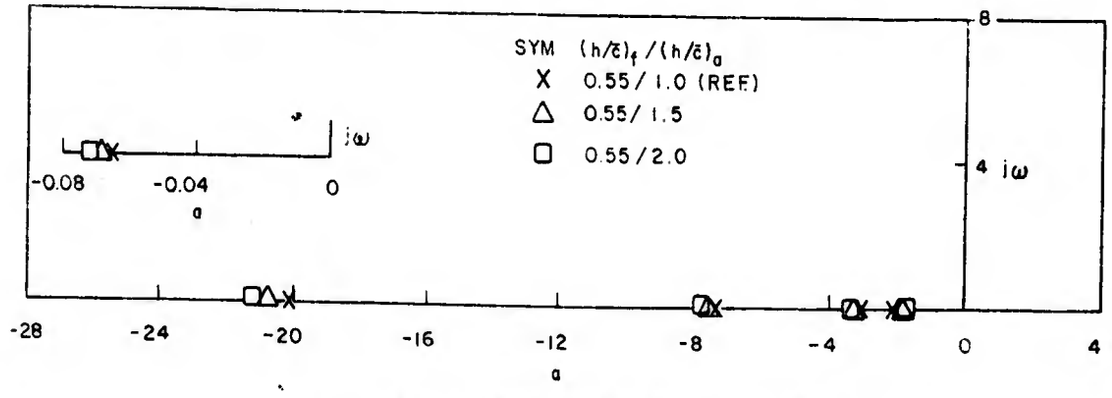

(c) HYBRID SUBMERGED-AFT-FOIL CANARD

FIGURE 11 LONGITUDINAL CHARACTERISTIC ROOTS FOIL DEPTH VARIATION

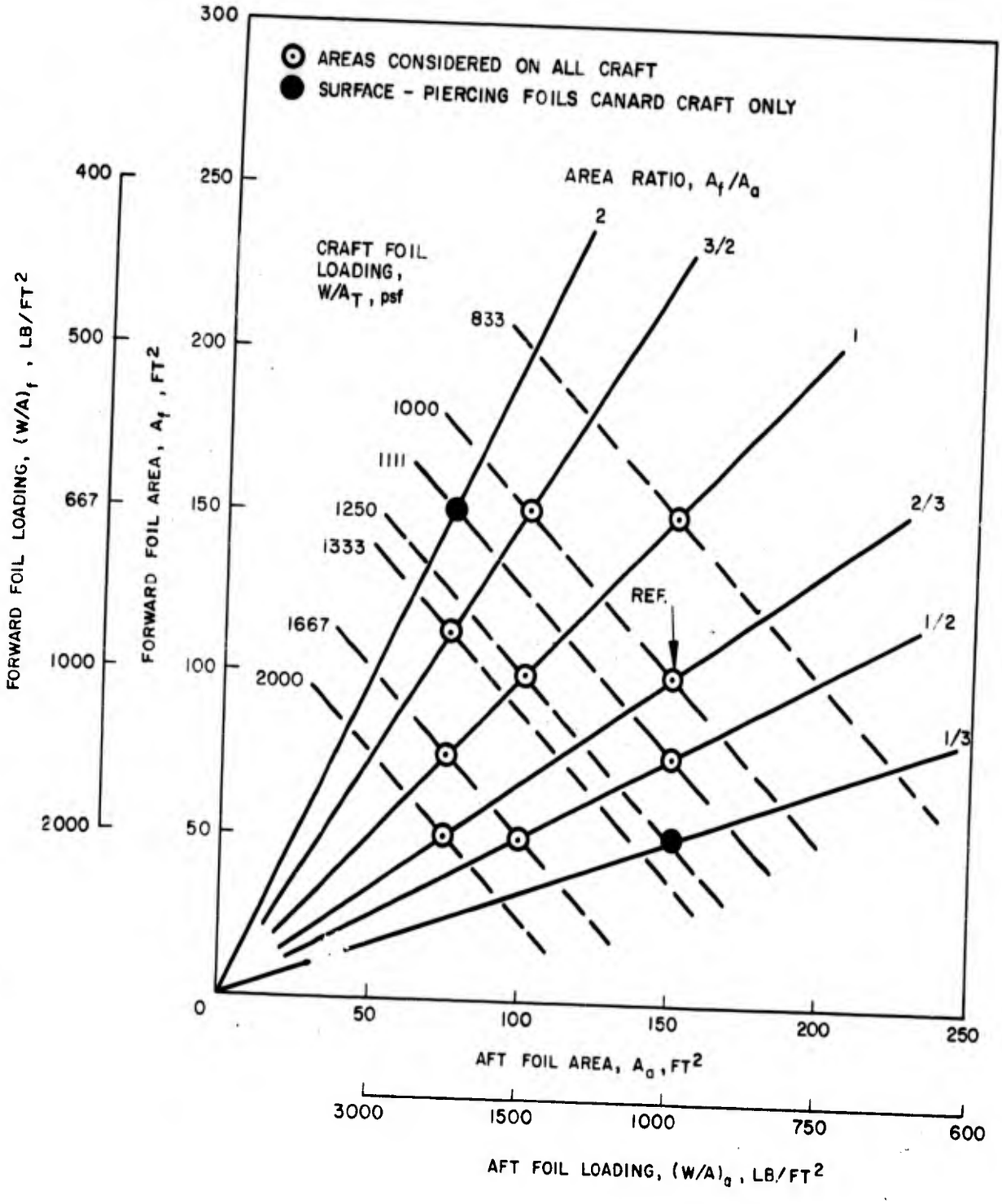

FIGURE 12 FOIL AREA VARIATION

(a) SUBMERGED FOILS CANARD

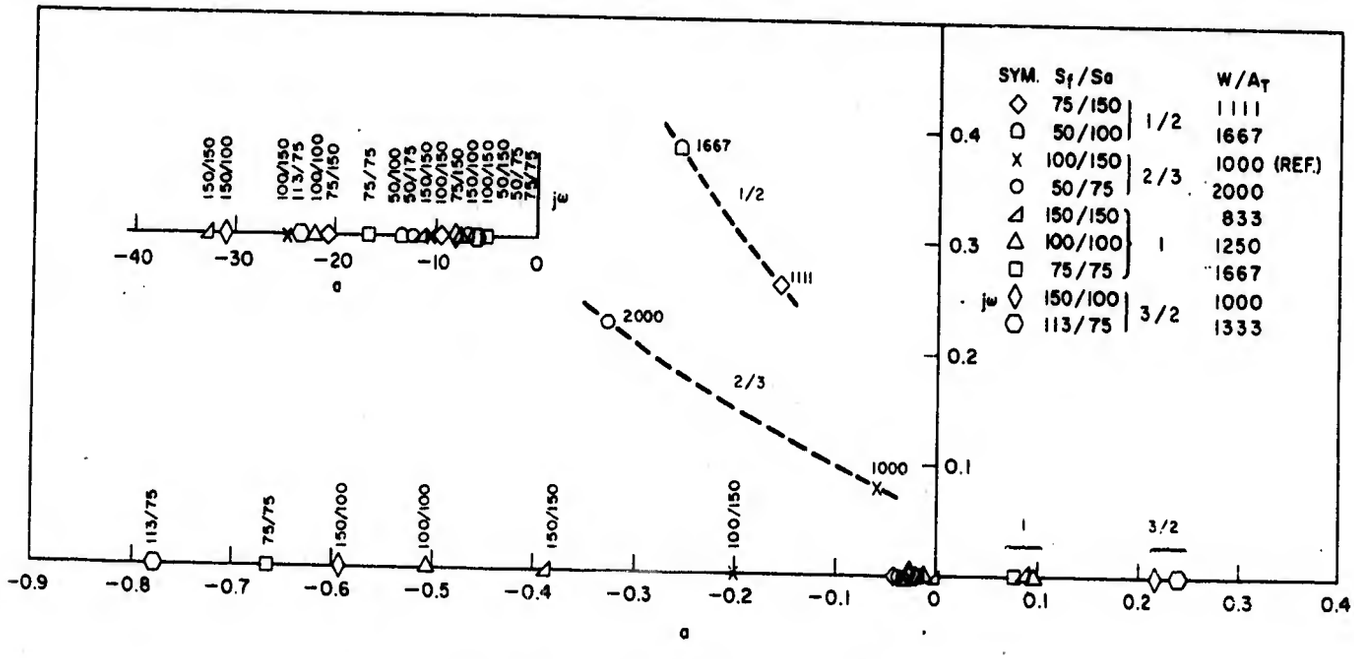

FIGURE 13 LONGITUDINAL CHARACTERISTIC ROOTS FOIL AREA VARIATION

(b) SURFACE-PIERCING FOILS CANARD

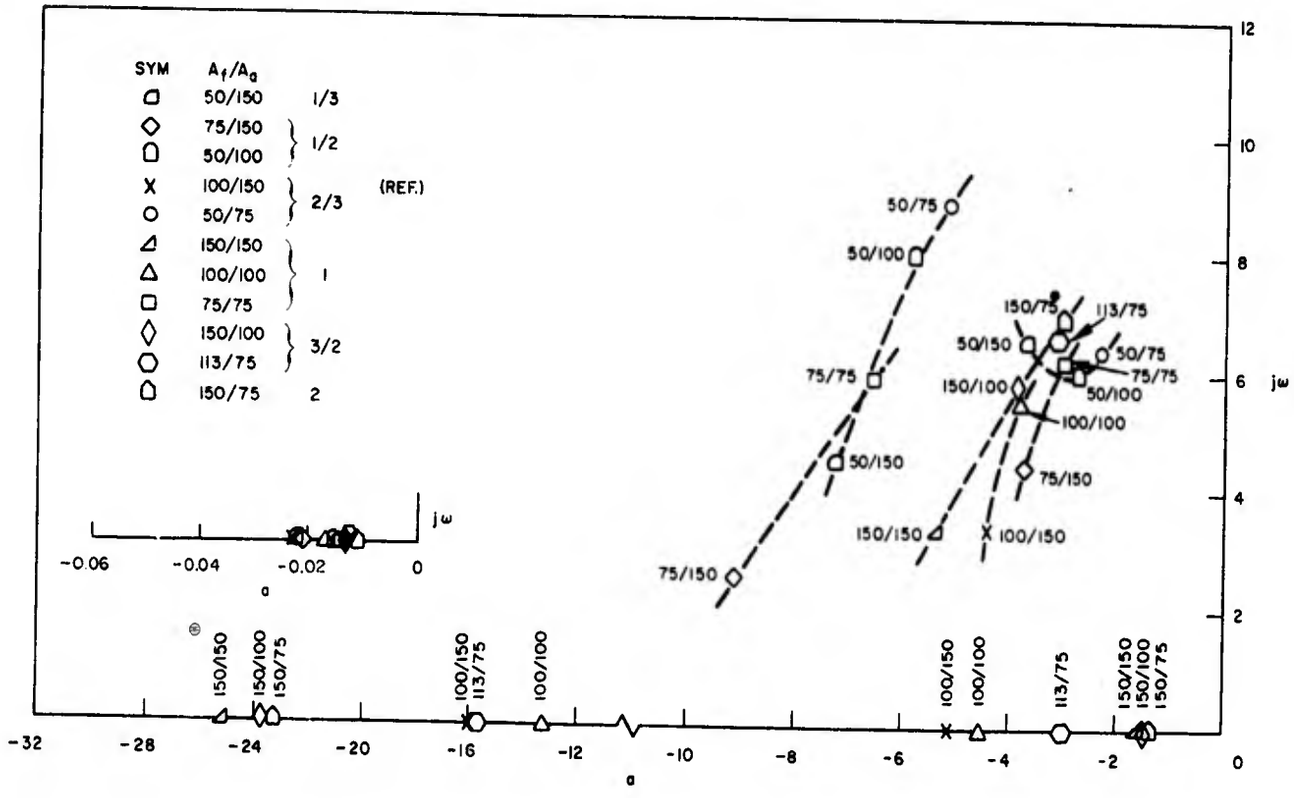

FIGURE 13 (CONT'D) LONGITUDINAL CHARACTERISTIC ROOTS FOIL AREA VARIATION

(c) HYBRID SURFACE-PIERCING-AFT-FOIL CANARD

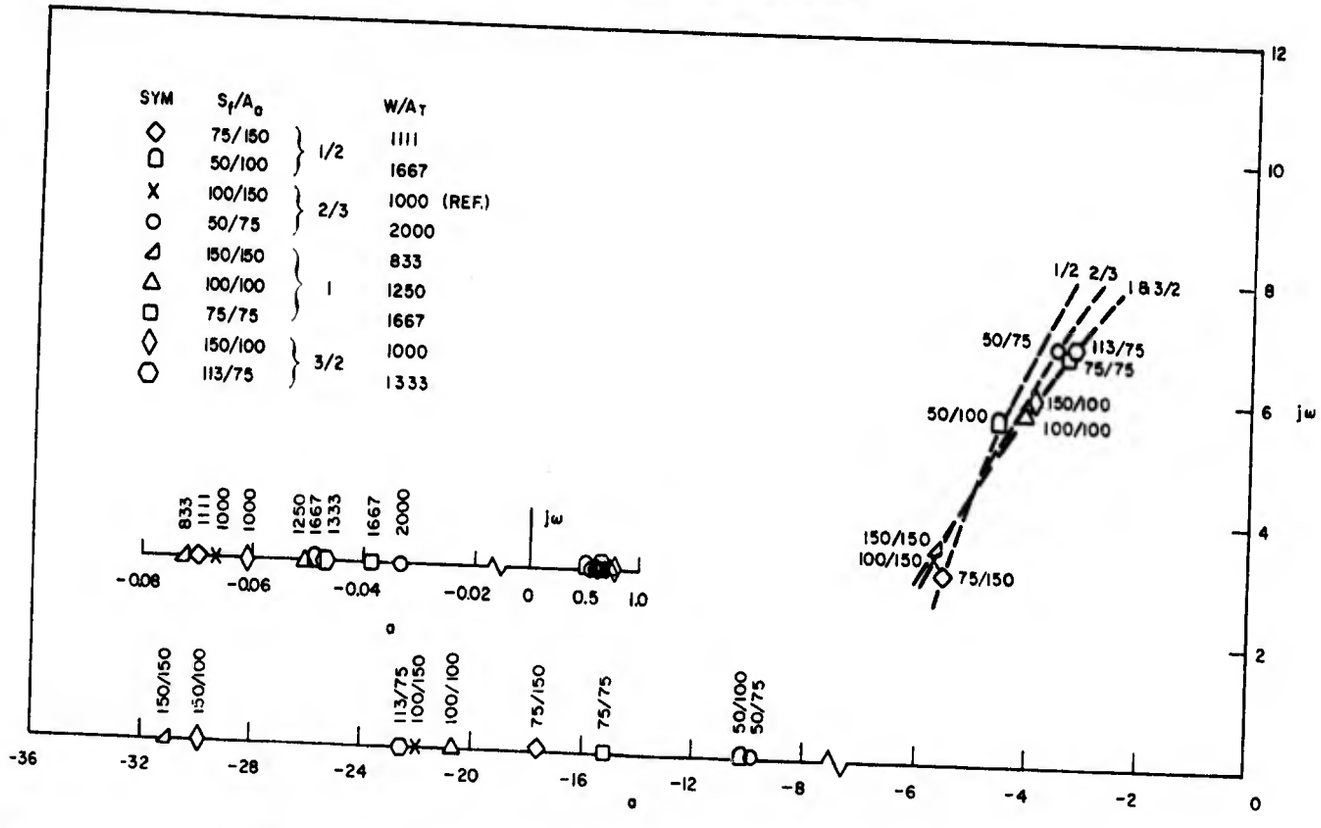

FIGURE 13 (CONT'D) LONGITUDINAL CHARACTERISTIC ROOTS FOIL AREA VARIATION

(d) HYBRID SUBMERGED-AFT-FOIL CANARD

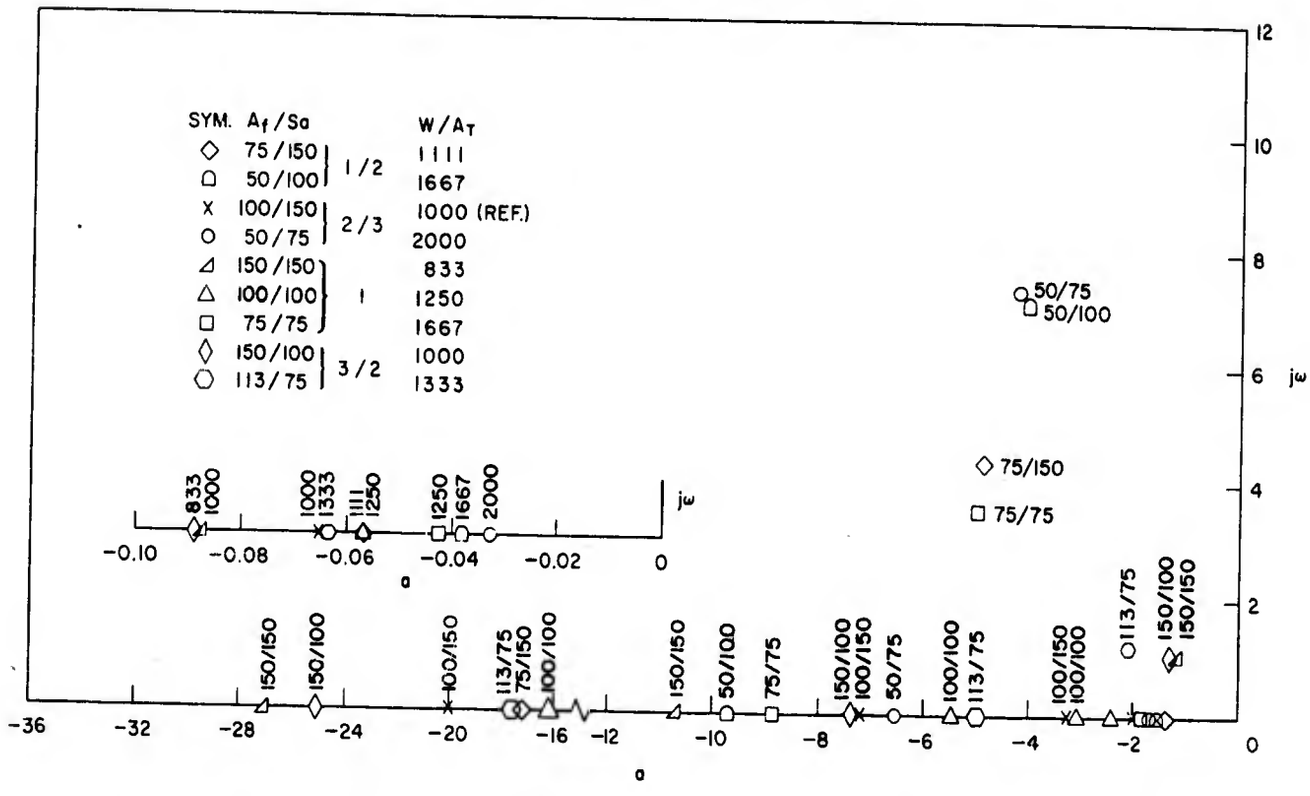

FIGURE 13 (CONCLUDED) LONGITUDINAL CHARACTERISTIC ROOTS FOIL AREA VARIATION

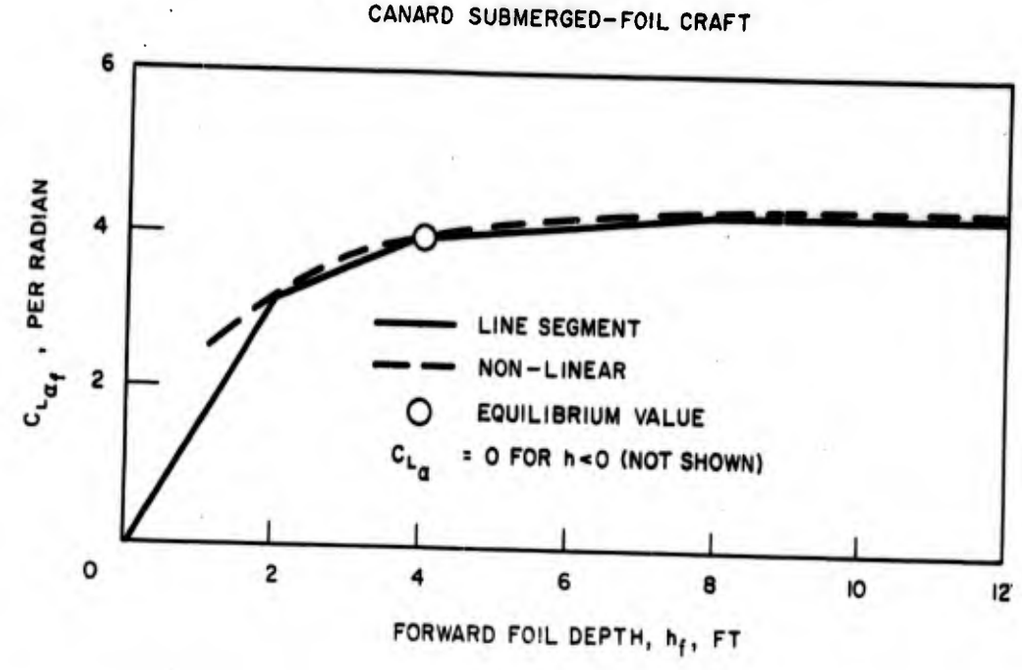

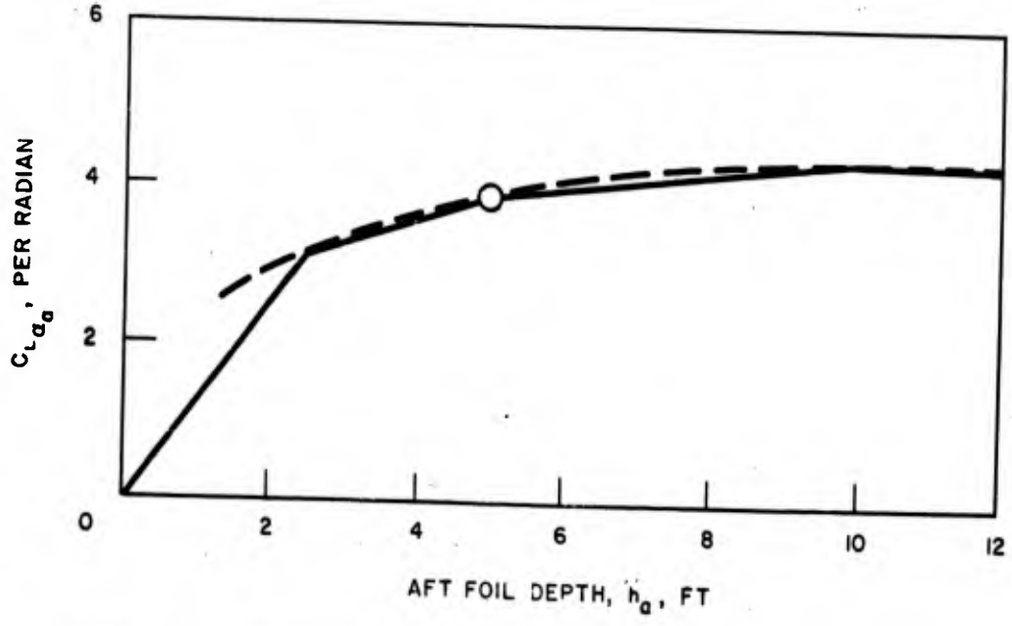

FIGURE 14 COMPARISON BETWEEN NON-LINEAR AND STRAIGHT LINE SEGMENT C_{L_α} VS. h CURVES

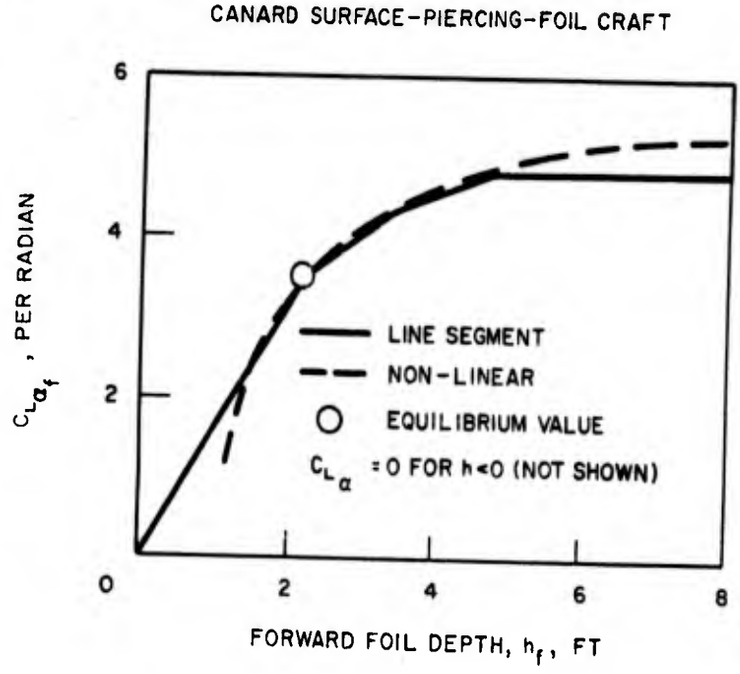

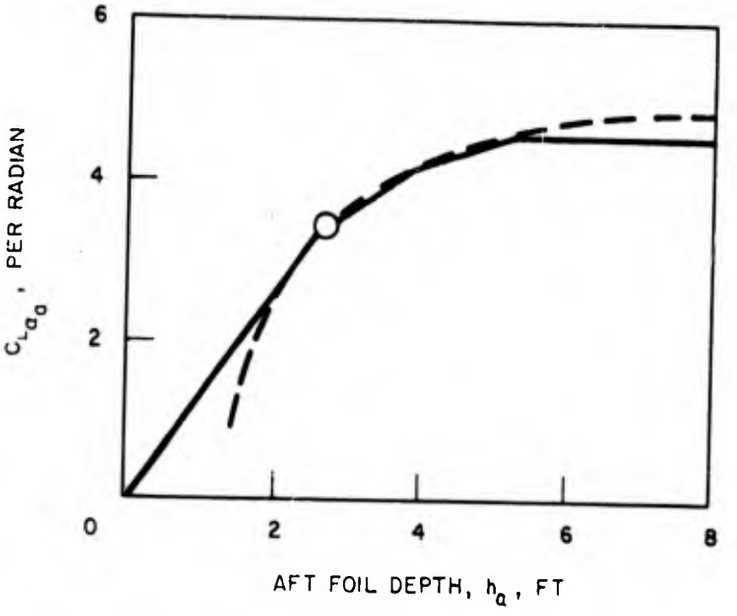

FIGURE 15 COMPARISON BETWEEN NON-LINEAR AND STRAIGHT LINE SEGMENT C_{L_α} VS. h CURVES

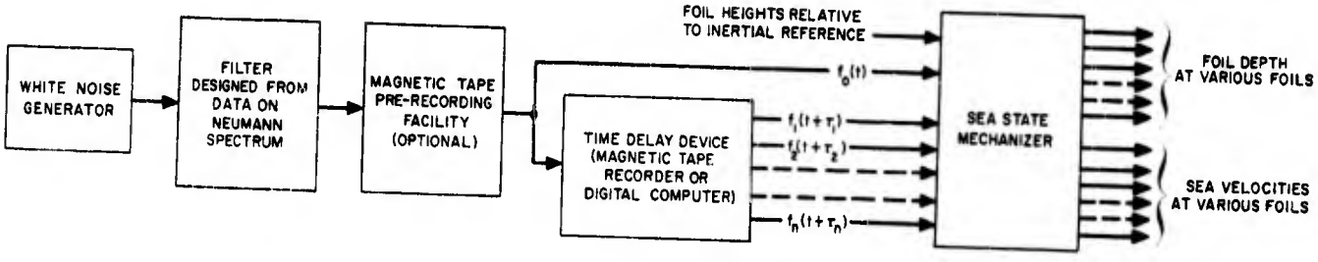

FIGURE 16 FUNCTIONAL BLOCK DIAGRAM OF RANDOM SEA SIMULATION PROCEDURE

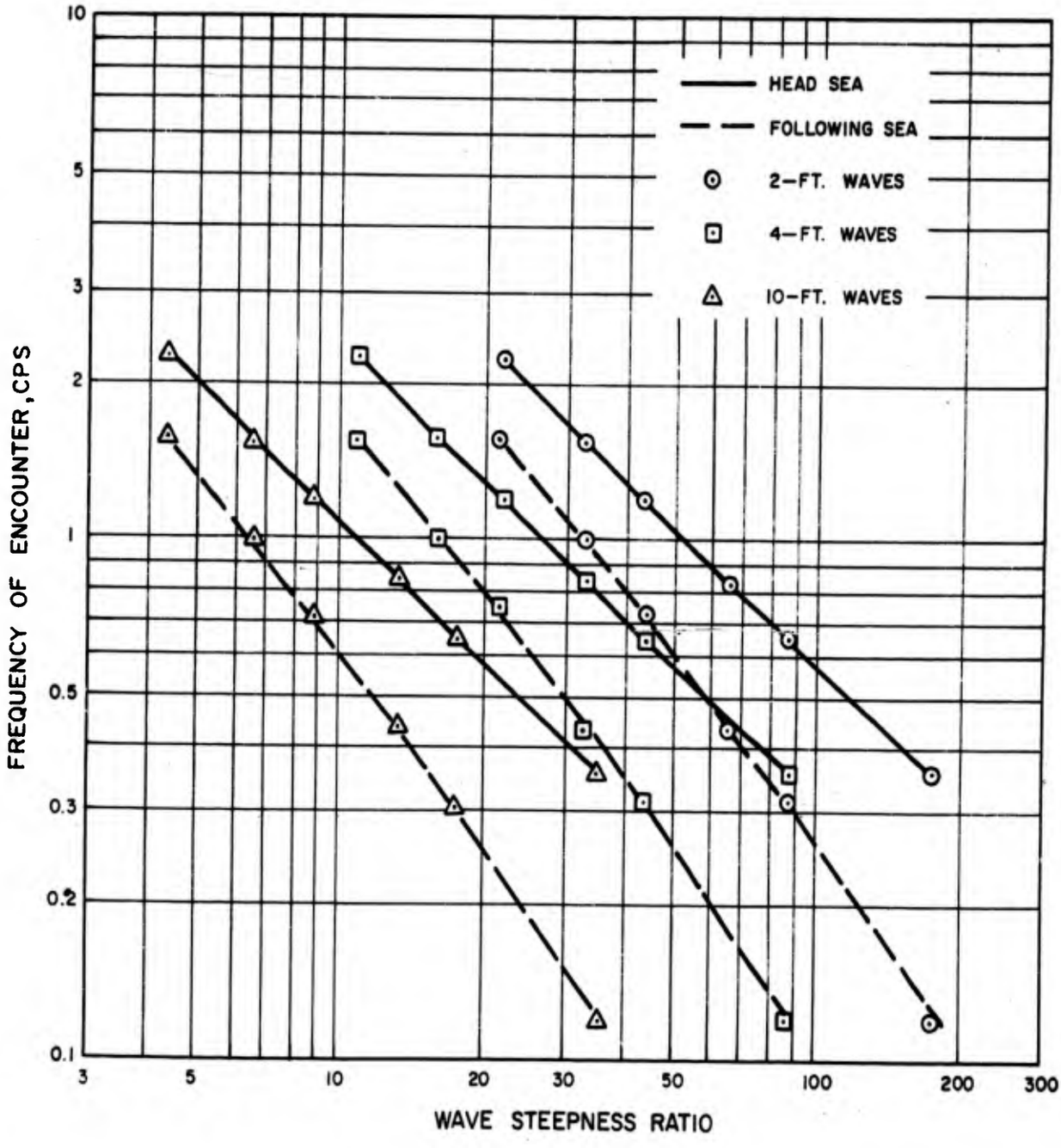

FIGURE 17 RANGE OF SEA STATES STUDIED ON ANALOG SIMULATOR

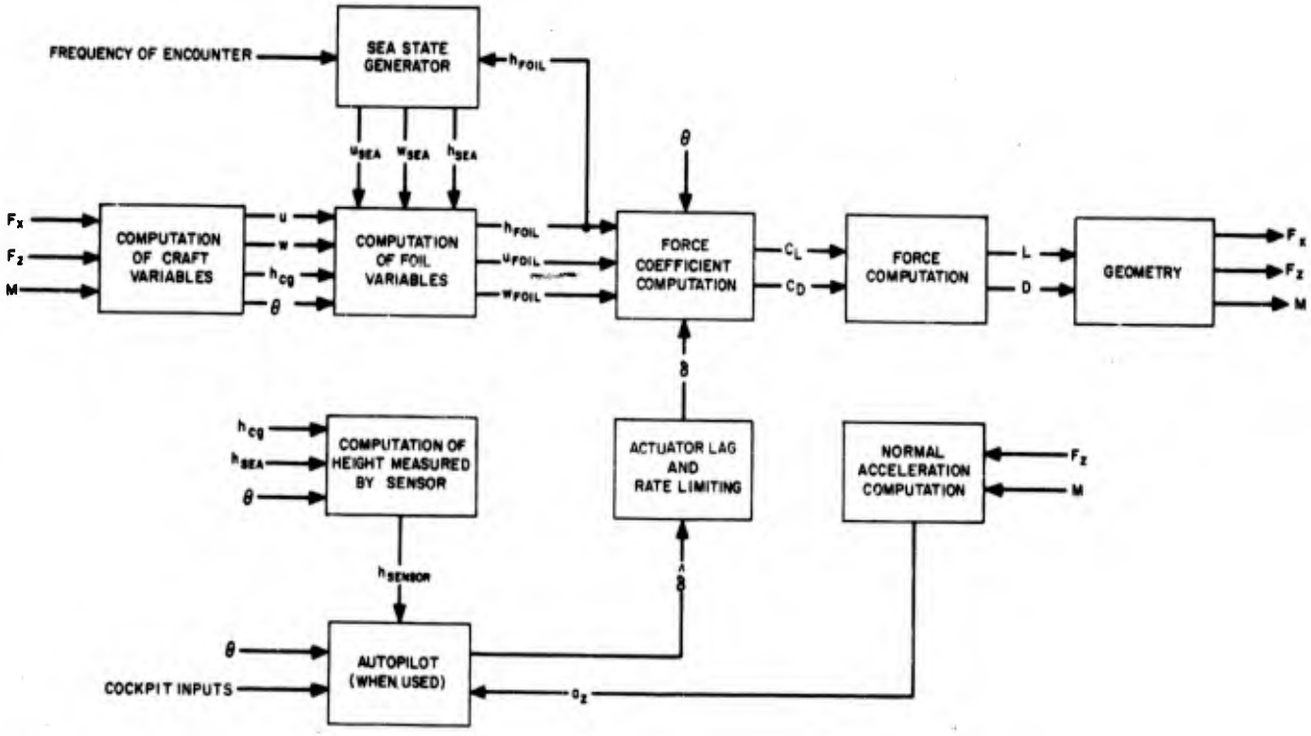

FIGURE 18 FUNCTIONAL BLOCK DIAGRAM OF SIMULATION PROCEDURE

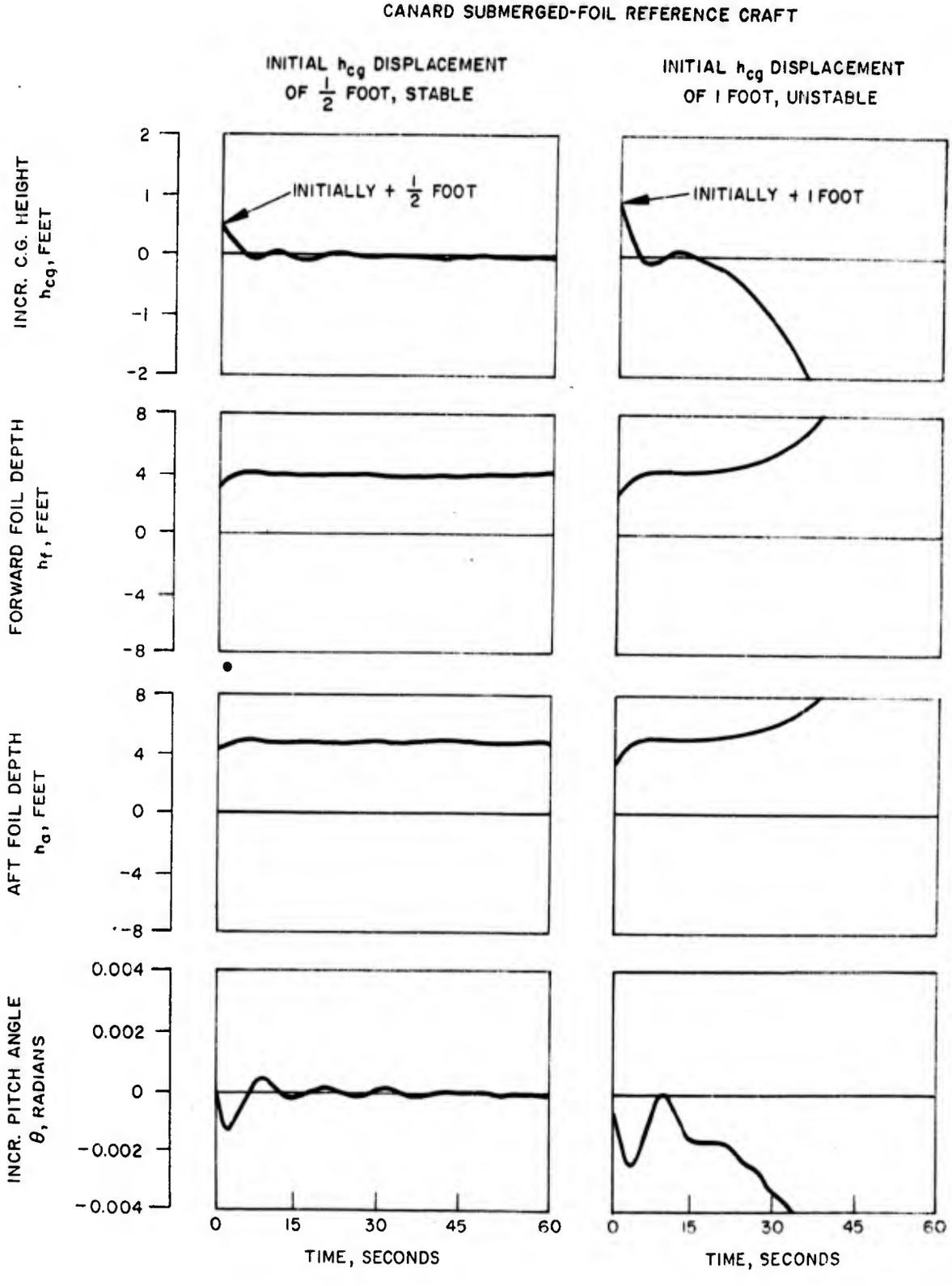

FIGURE 19. CRAFT ALONE RESPONSE AT 50 KNOTS

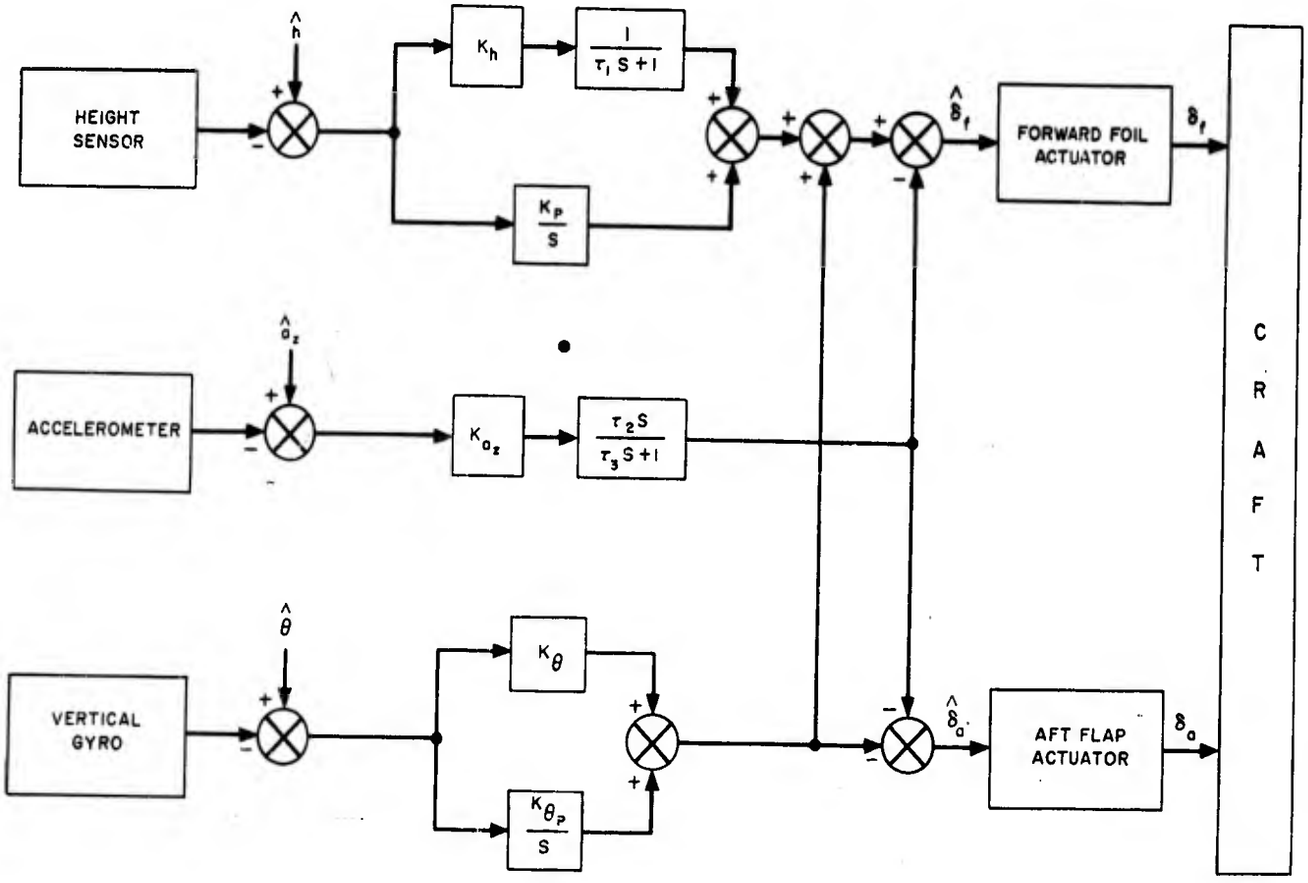

FIGURE 20. FUNCTIONAL BLOCK DIAGRAM OF AUTOPILOT

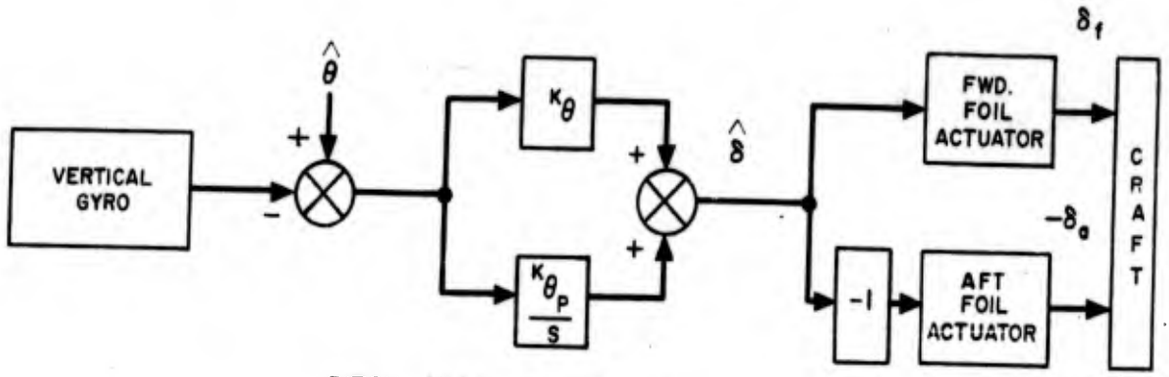

a. PITCH STABILIZATION LOOP

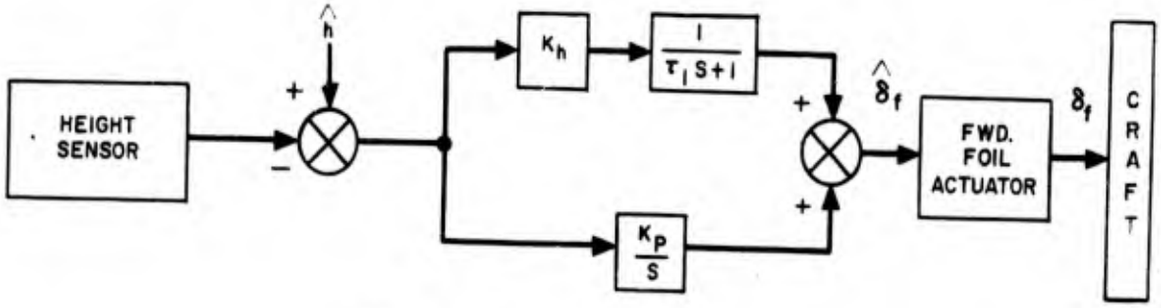

b. VERTICAL STABILIZATION LOOP

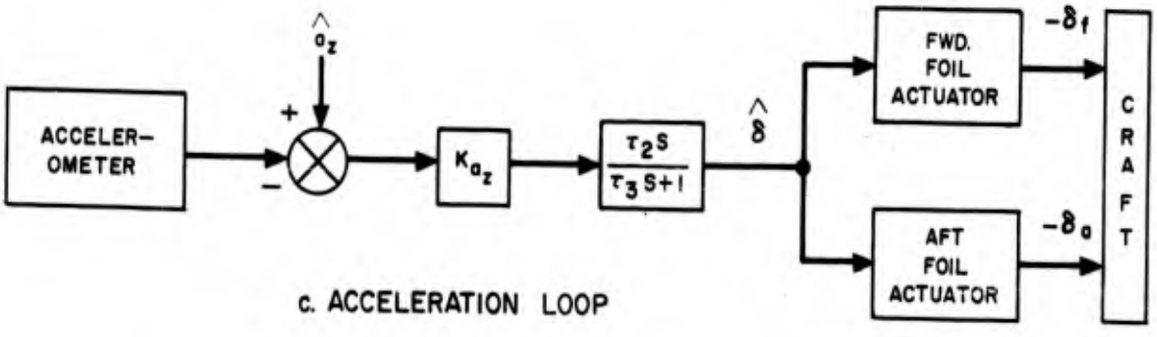

c. ACCELERATION LOOP

FIGURE 21 FUNCTIONAL BLOCK DIAGRAMS SHOWING INDIVIDUAL AUTOPILOT LOOPS

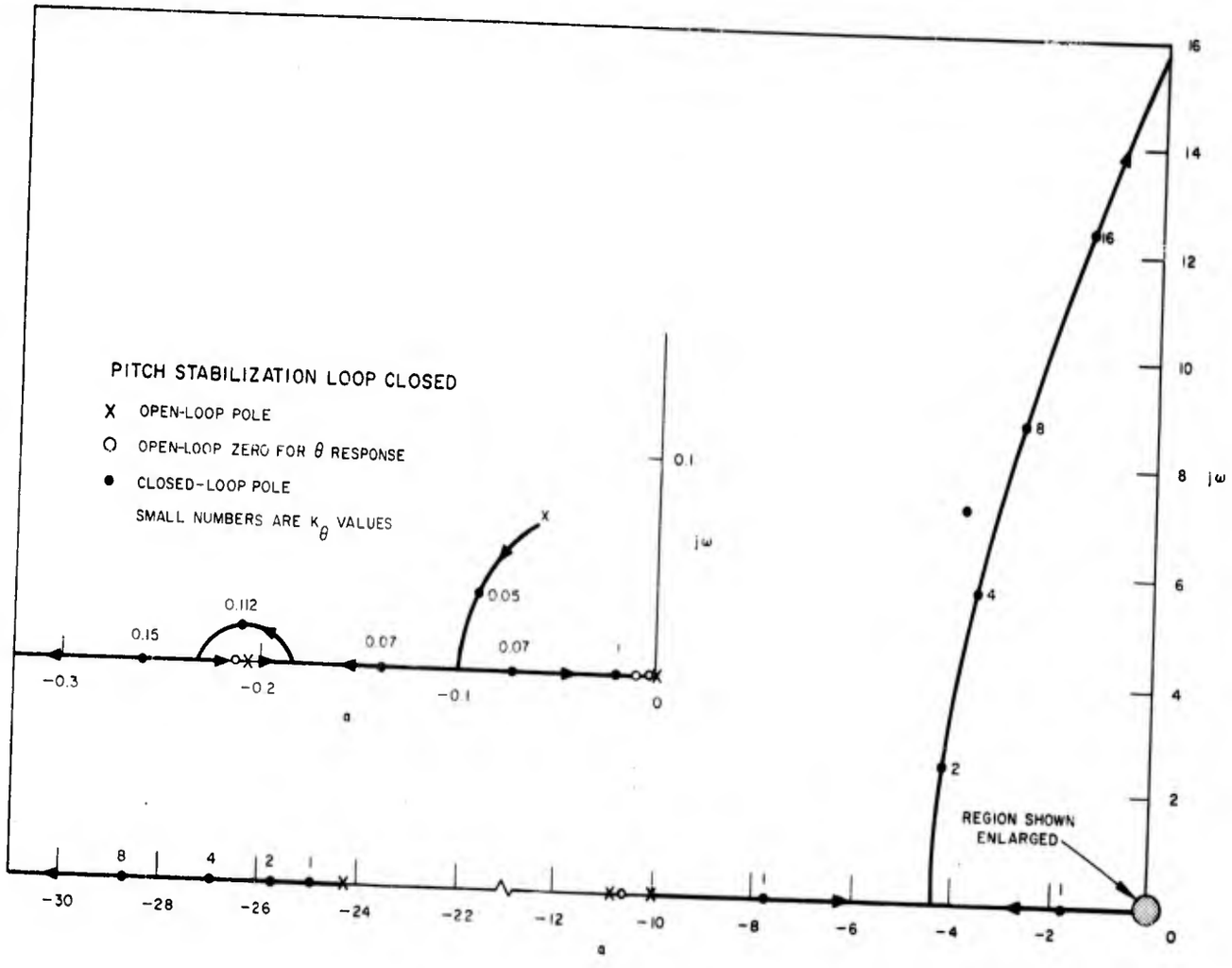

FIGURE 22 ROOT LOCUS FOR CANARD SUBMERGED-FOIL REFERENCE CRAFT AT 50 KNOTS

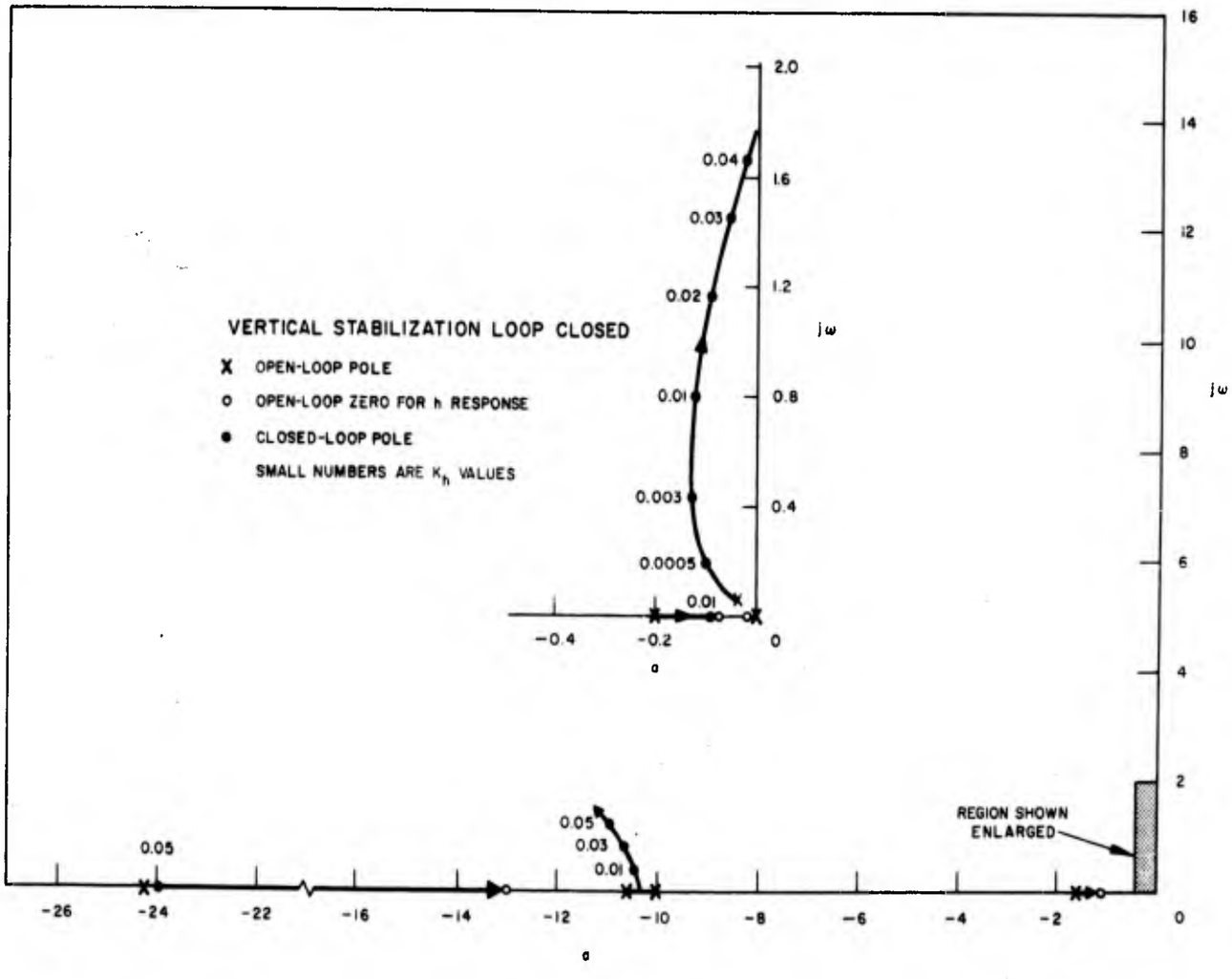

FIGURE 23 ROOT LOCUS FOR CANARD SUBMERGED-FOIL REFERENCE CRAFT AT 50 KNOTS

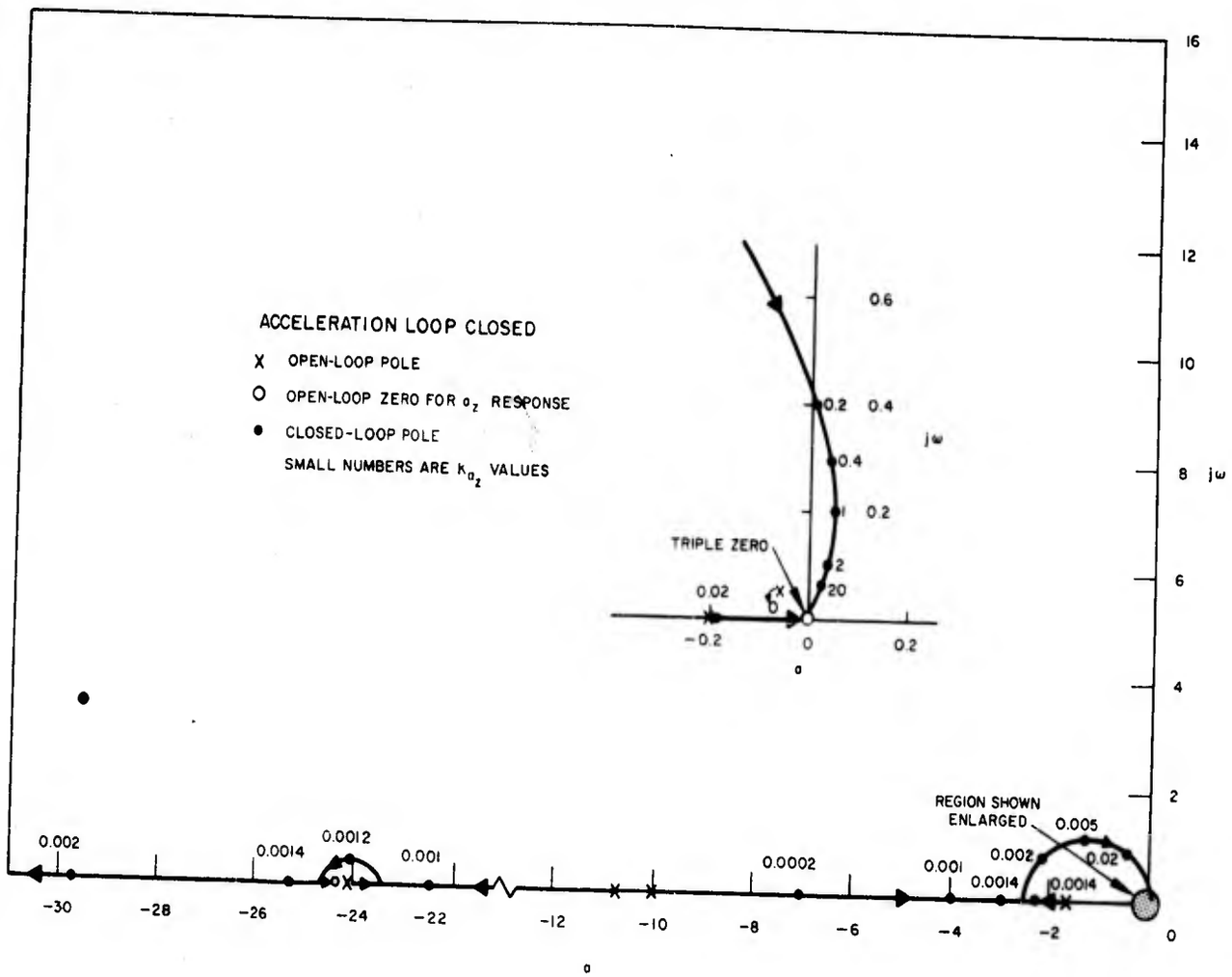

FIGURE 24 ROOT LOCUS FOR CANARD SUBMERGED-FOIL REFERENCE CRAFT AT 50 KNOTS

BOTH VERTICAL AND PITCH STABILIZATION LOOPS CLOSED

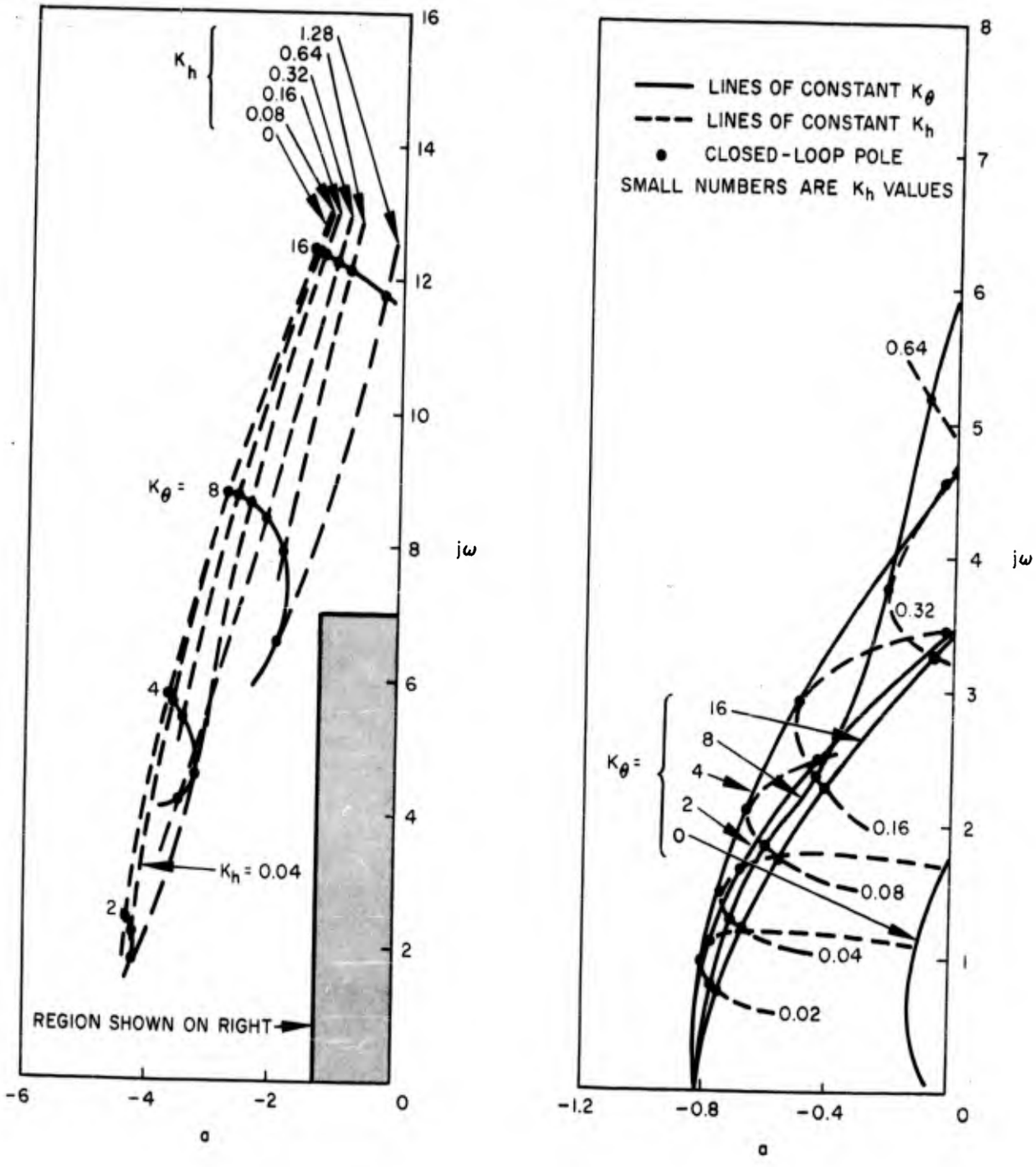

FIGURE 25 FAMILY OF LOCI SHOWING ONLY COMPLEX CONJUGATE ROOTS FOR CANARD SUBMERGED-FOIL REFERENCE CRAFT AT 50 KNOTS

CANARD SUBMERGED-FOIL REFERENCE CRAFT

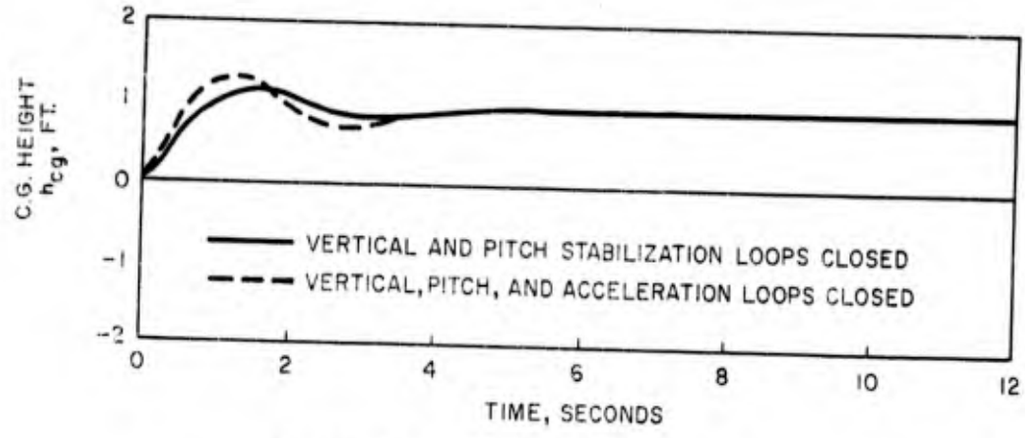

RESPONSE TO +1 FOOT STEP HEIGHT TRIM COMMAND

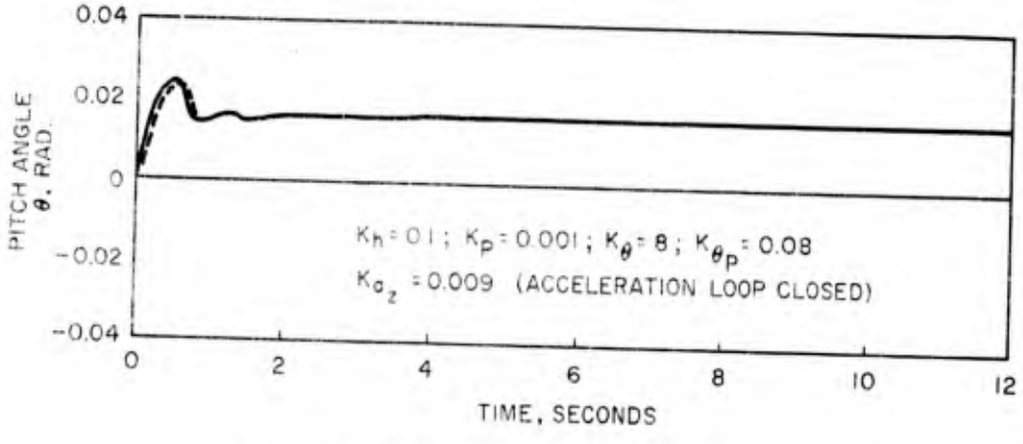

RESPONSE TO +1 DEGREE STEP PITCH TRIM COMMAND

FIGURE 26 AUGMENTED CRAFT RESPONSE AT 50 KNOTS TO STEP HEIGHT AND PITCH TRIM COMMANDS

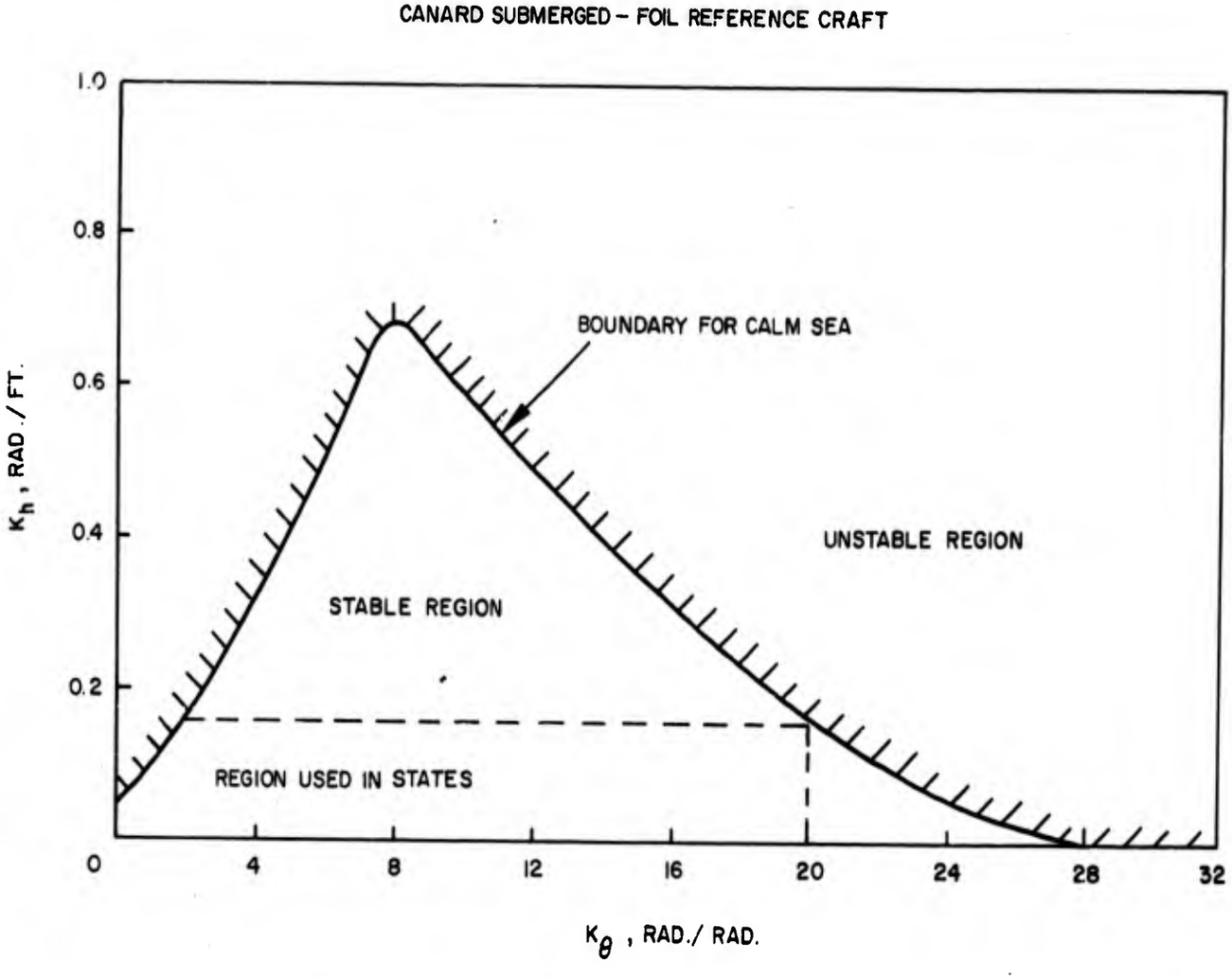

FIGURE 27 HEIGHT ERROR GAIN VS. PITCH ERROR GAIN

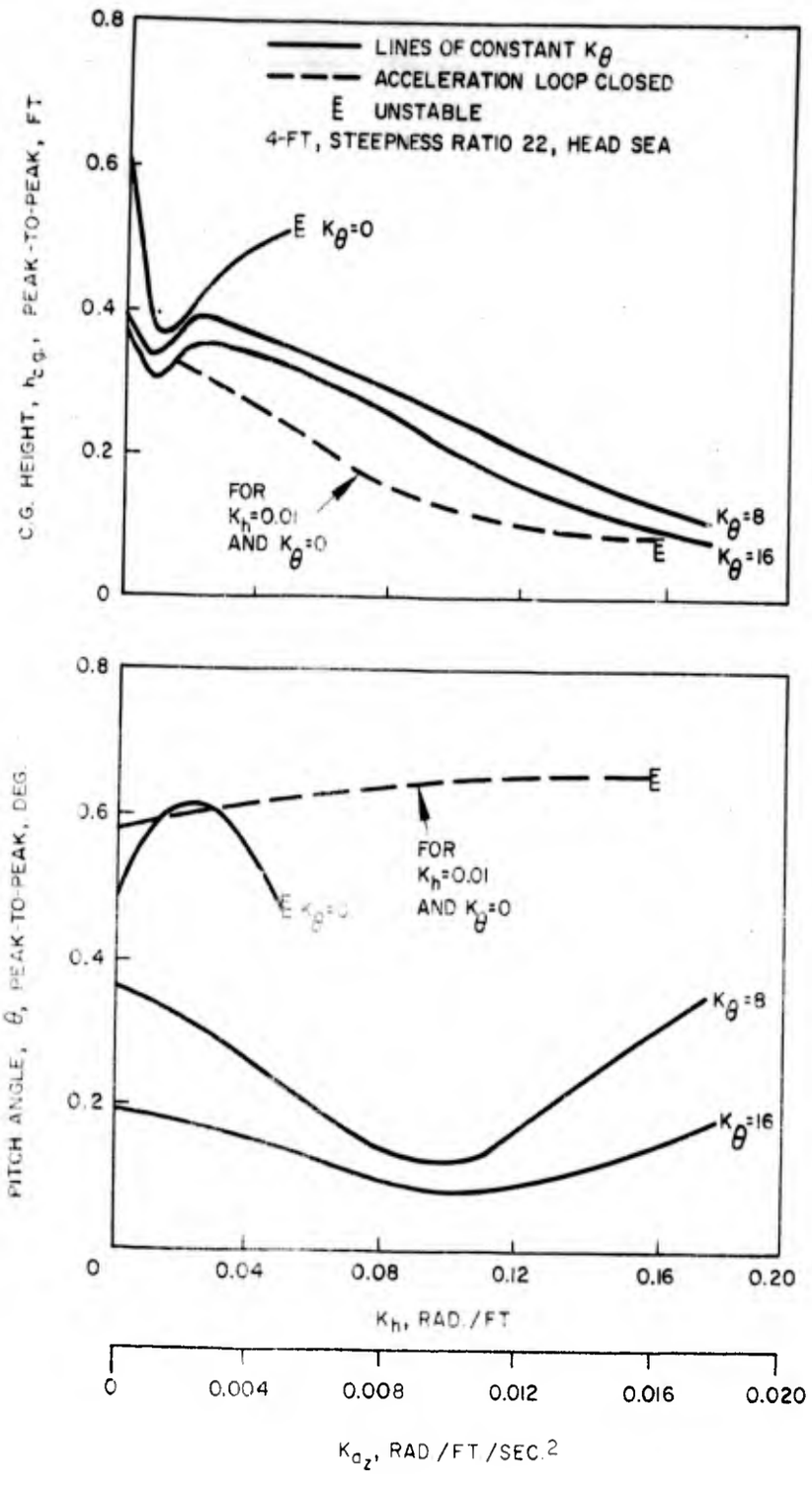

FIGURE 28 EFFECTS OF AUTOPILOT PARAMETER SETTINGS ON C.G. HEIGHT AND PITCH RESPONSES IN SEA STATE

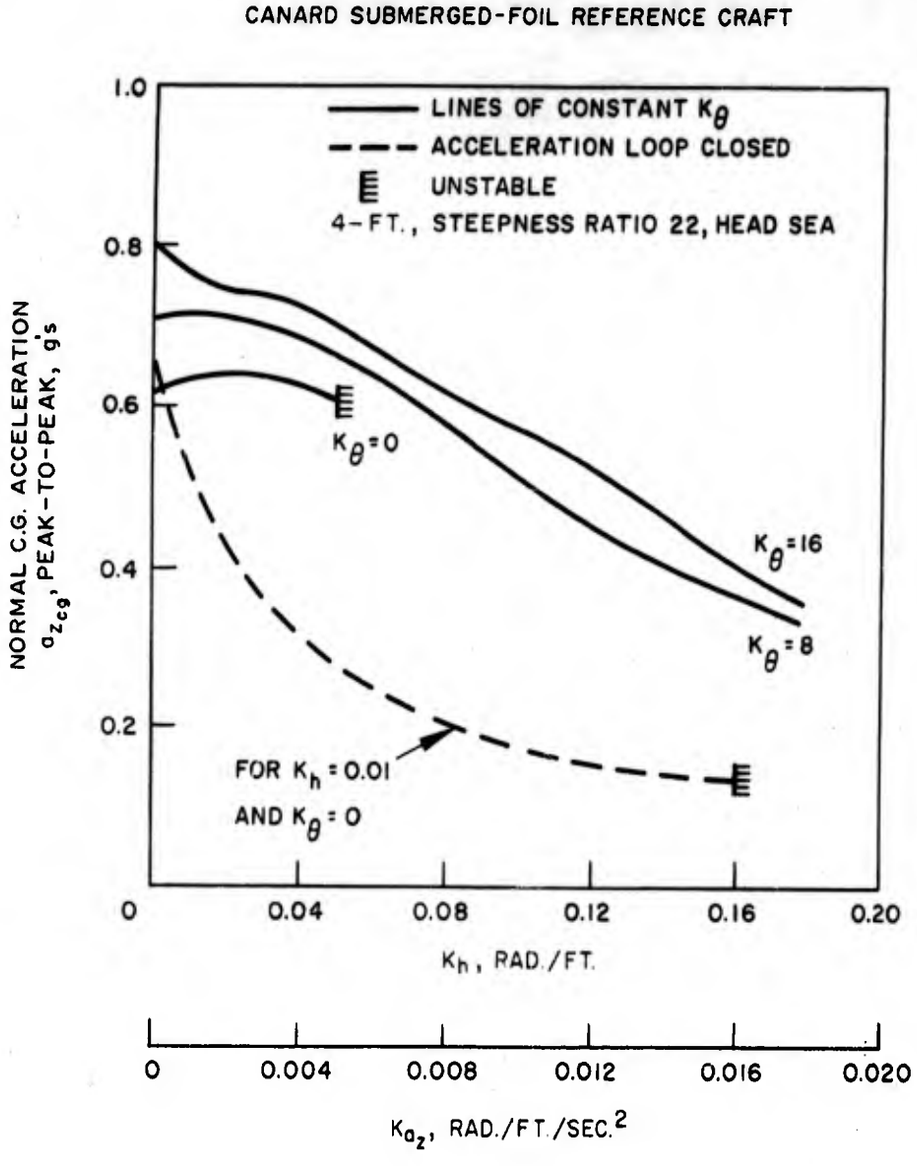

FIGURE 29. EFFECTS OF AUTOPILOT PARAMETER SETTINGS ON NORMAL C.G. ACCELERATION IN SEA STATE

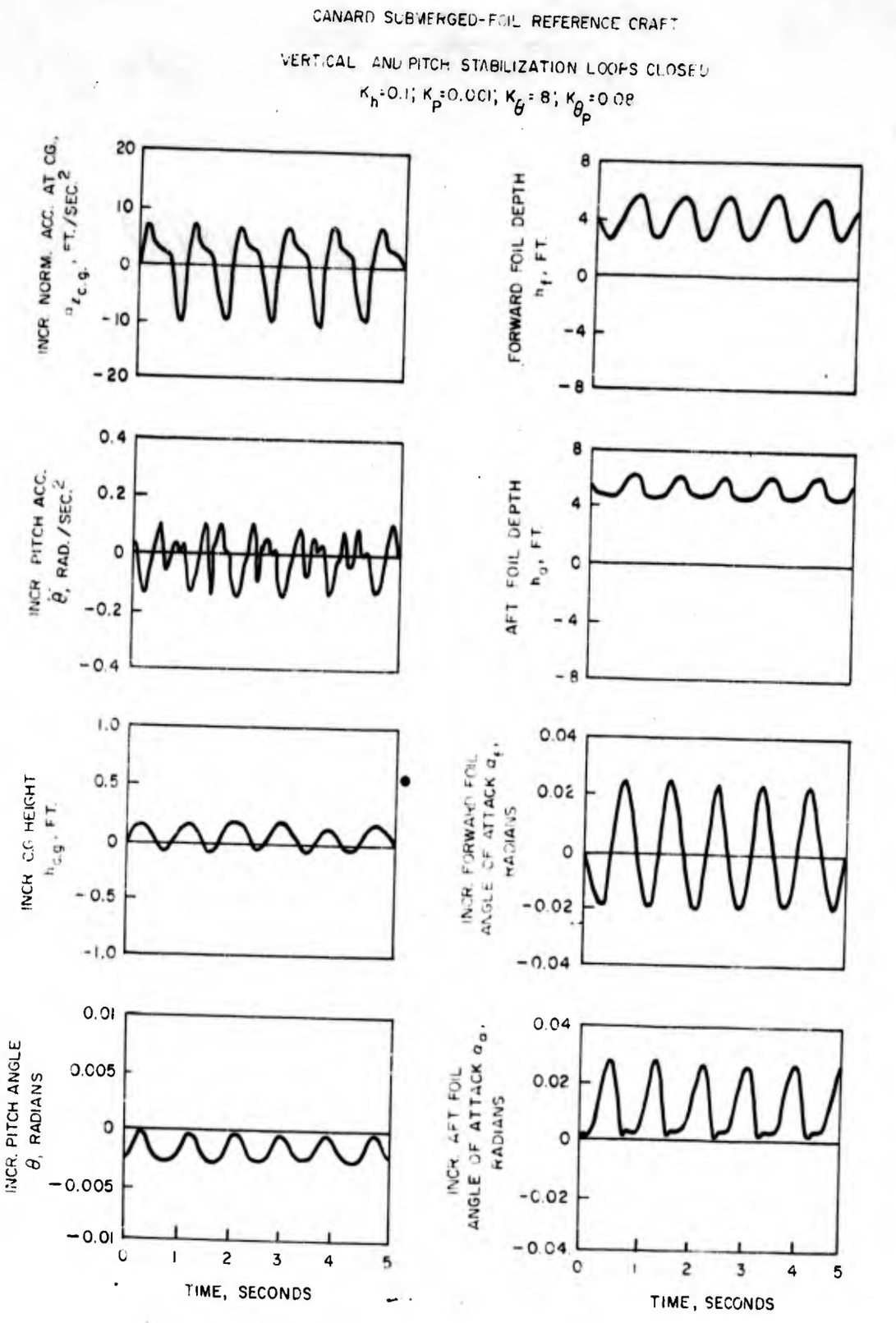

FIGURE 30 AUGMENTED CRAFT RESPONSE TO 4-FT., STEEPNESS RATIO 22, HEAD SEA

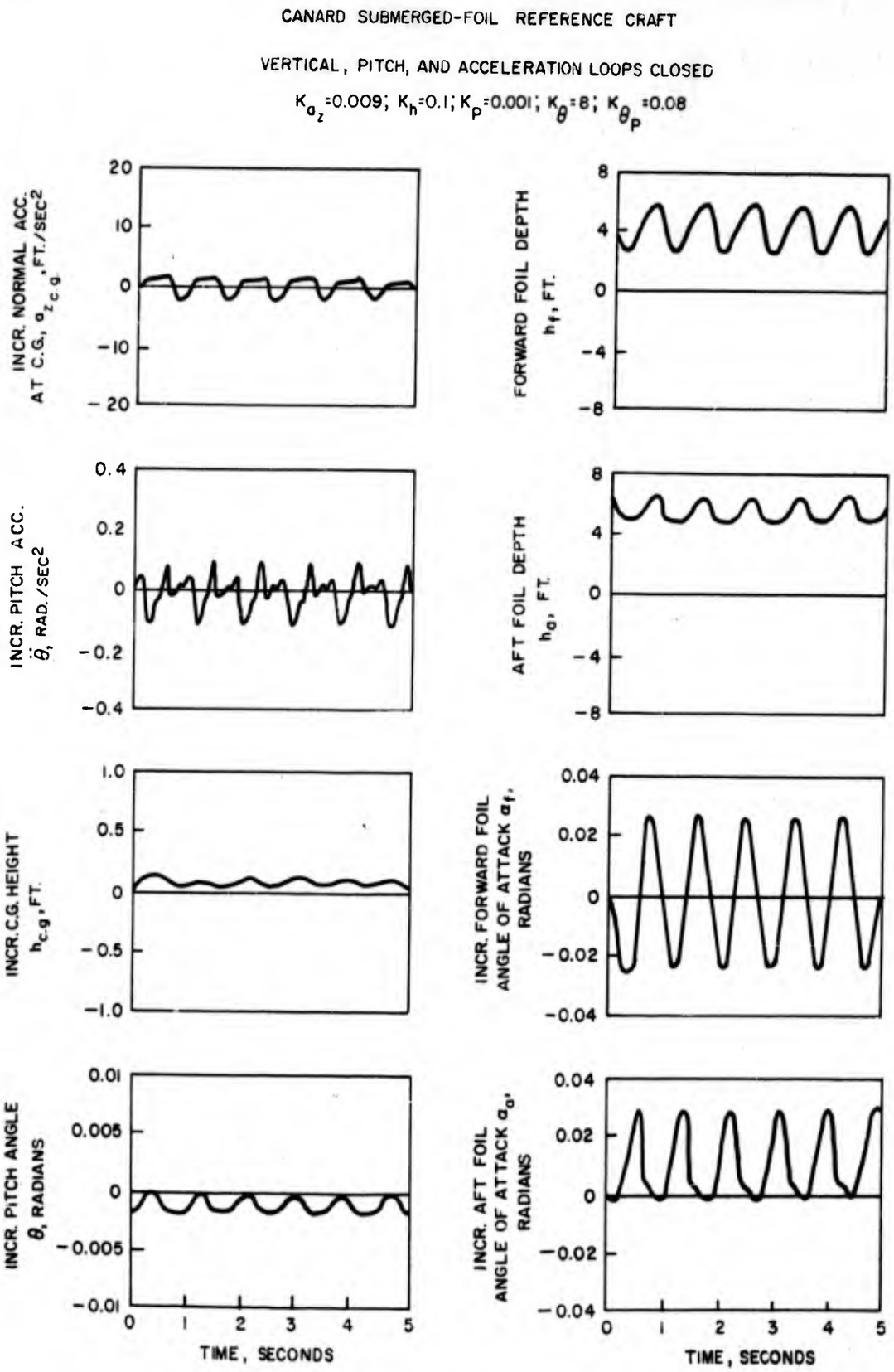

FIGURE 31 AUGMENTED CRAFT RESPONSE TO 4-FT., STEEPNESS RATIO 22, HEAD SEA

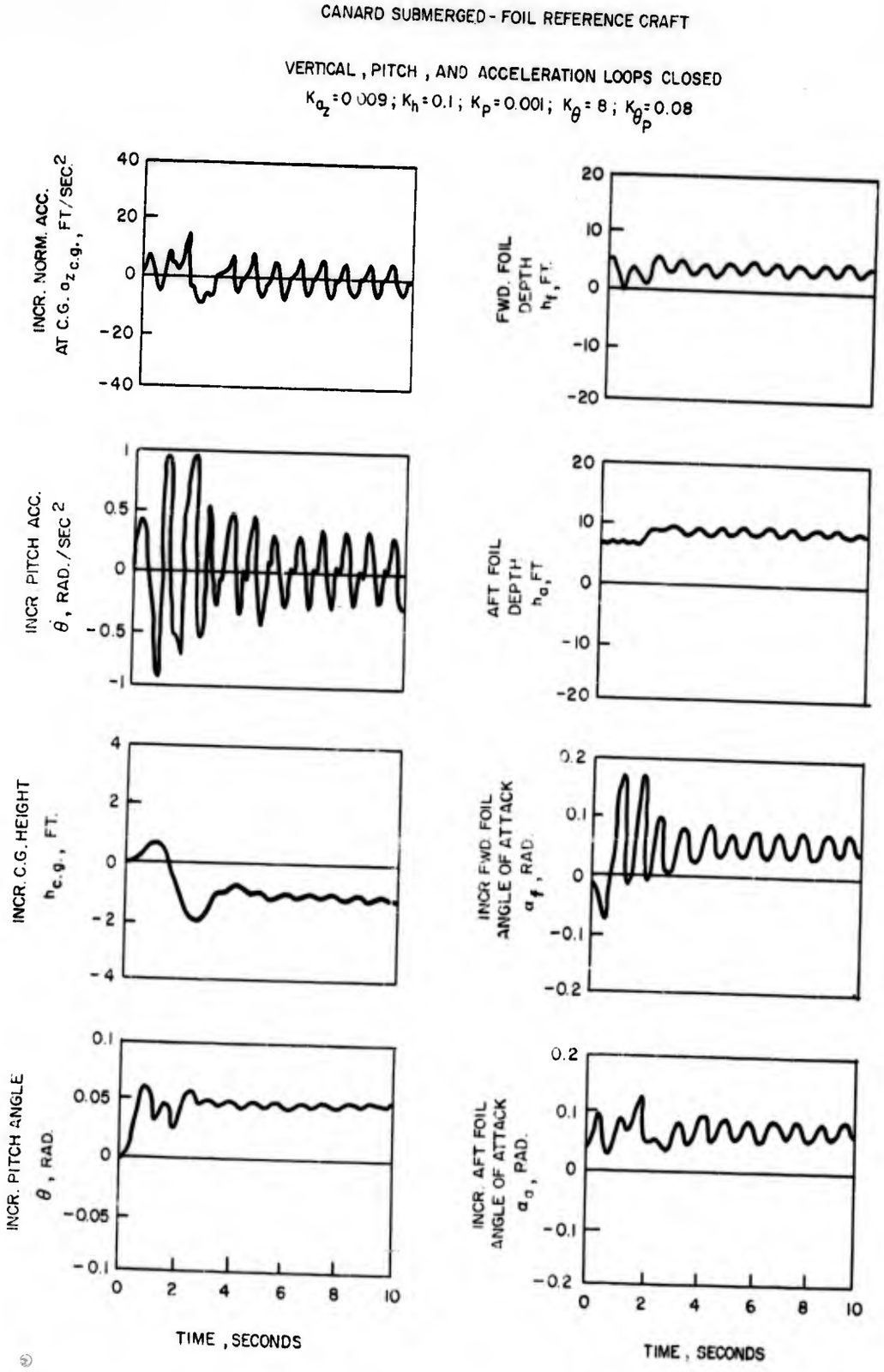

FIGURE 32 AUGMENTED CRAFT RESPONSE TO 3 DEG. STEP PITCH TRIM COMMAND IN 4 - FT., STEEPNESS RATIO 22 , HEAD SEA

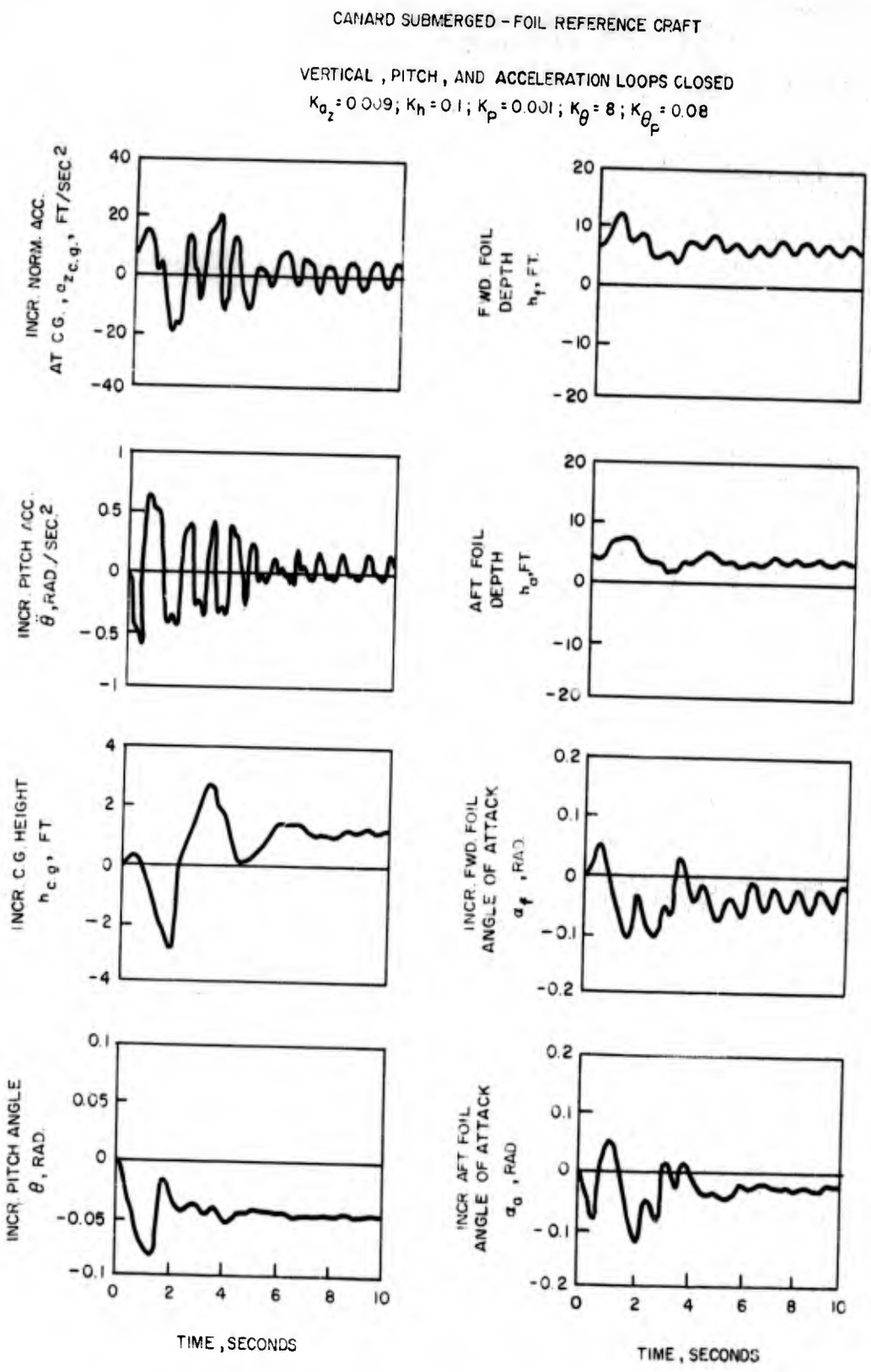

FIGURE 33 AUGMENTED CRAFT RESPONSE TO -3 DEG. STEP PITCH TRIM COMMAND IN 4-FT., STEEPNESS RATIO 22, HEAD SEA

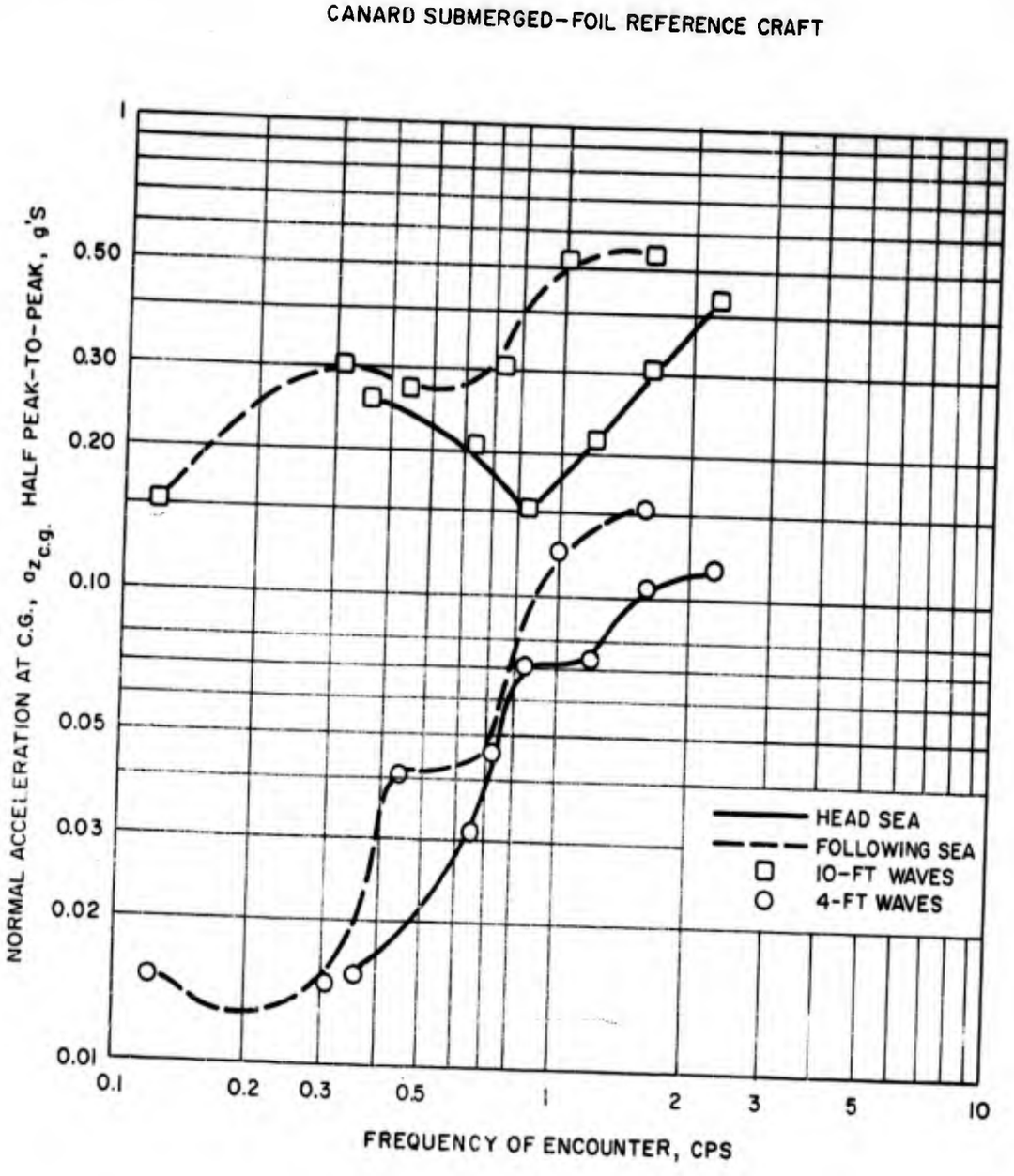

FIGURE 34 AUGMENTED CRAFT NORMAL ACCELERATION (AT C.G.) RESPONSE IN SEA STATES

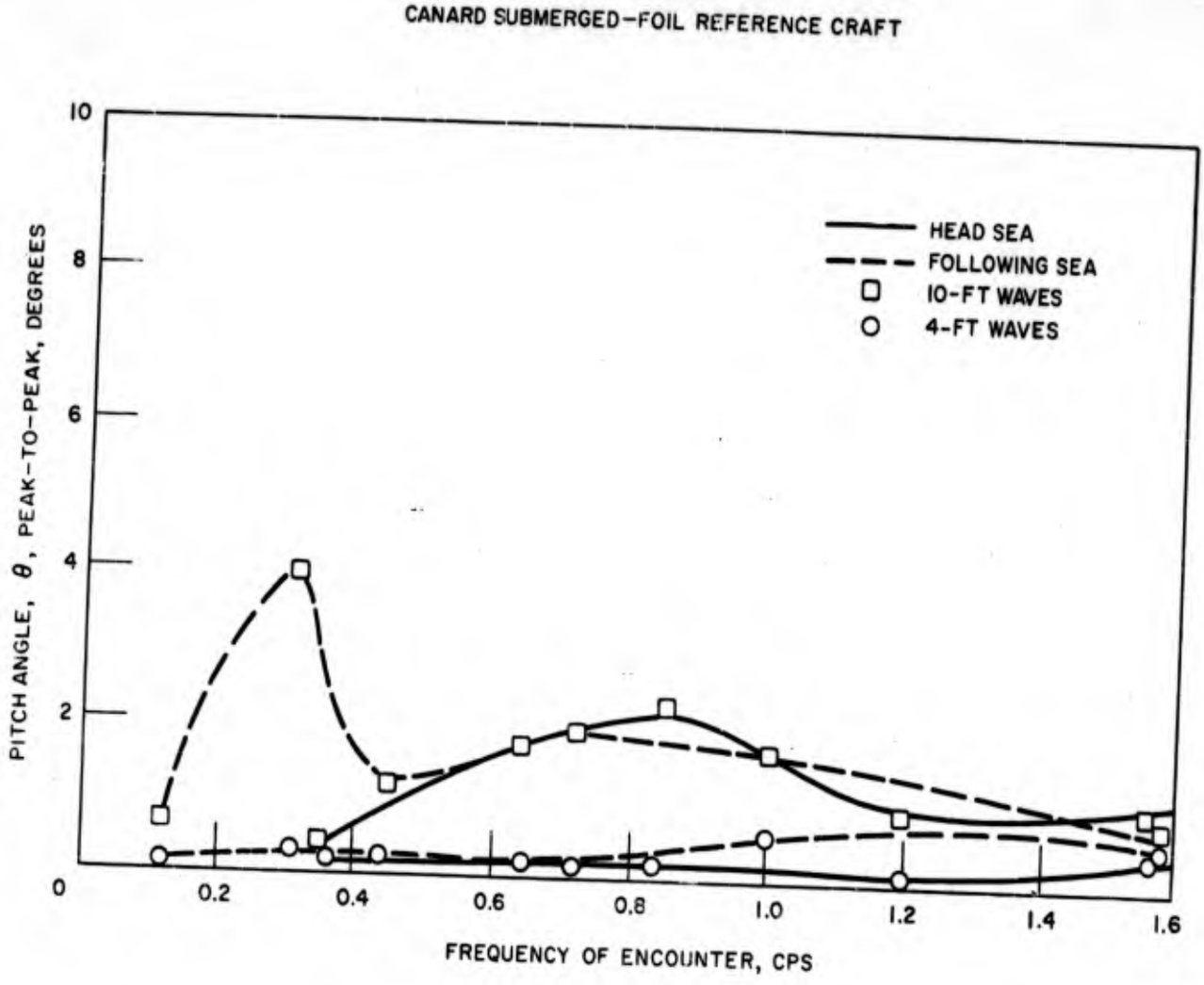

FIGURE 35 AUGMENTED CRAFT PITCH ANGLE RESPONSE IN SEA STATES

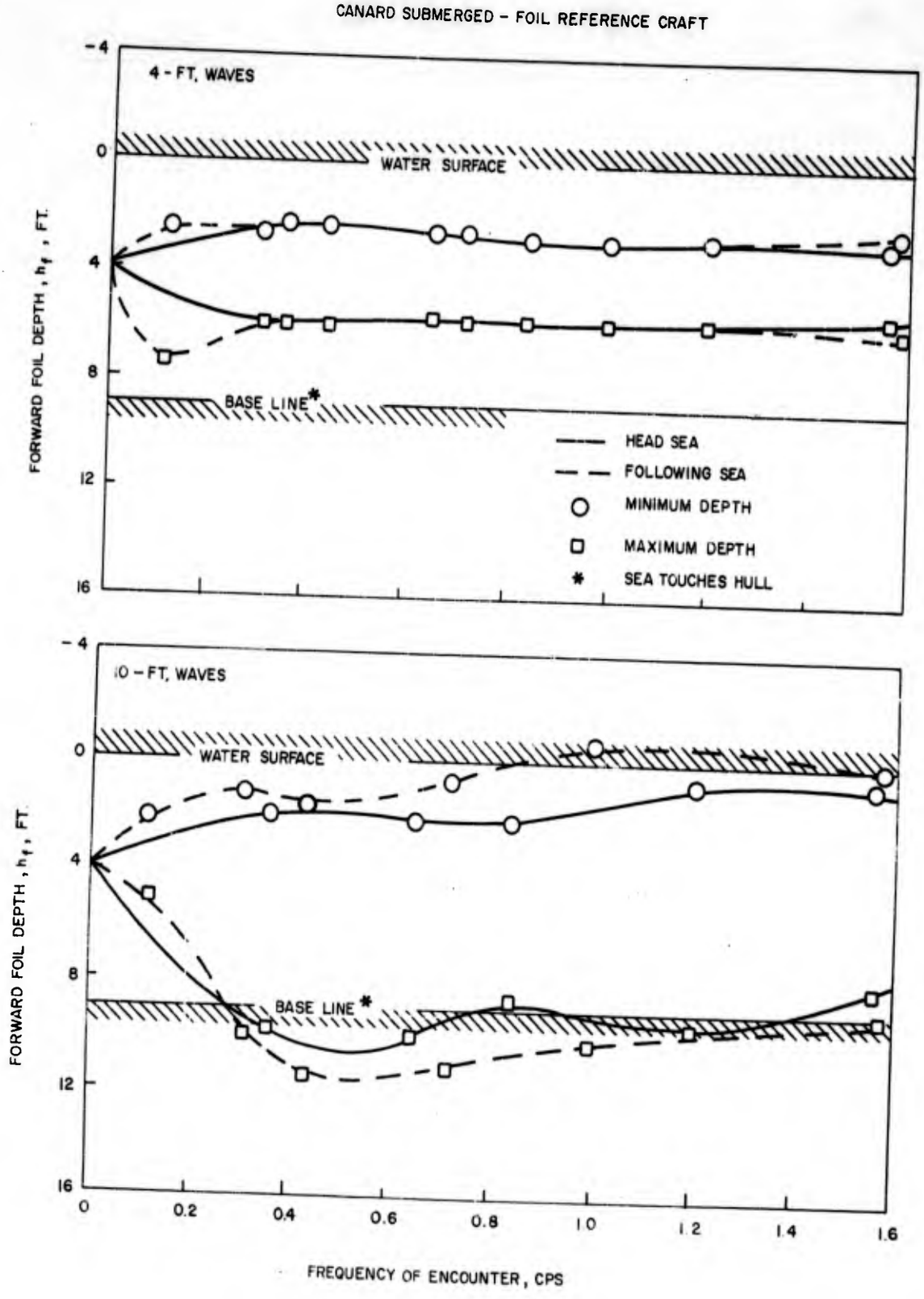

FIGURE 36 AUGMENTED CRAFT FORWARD FOIL DEPTH RESPONSE IN SEA STATES

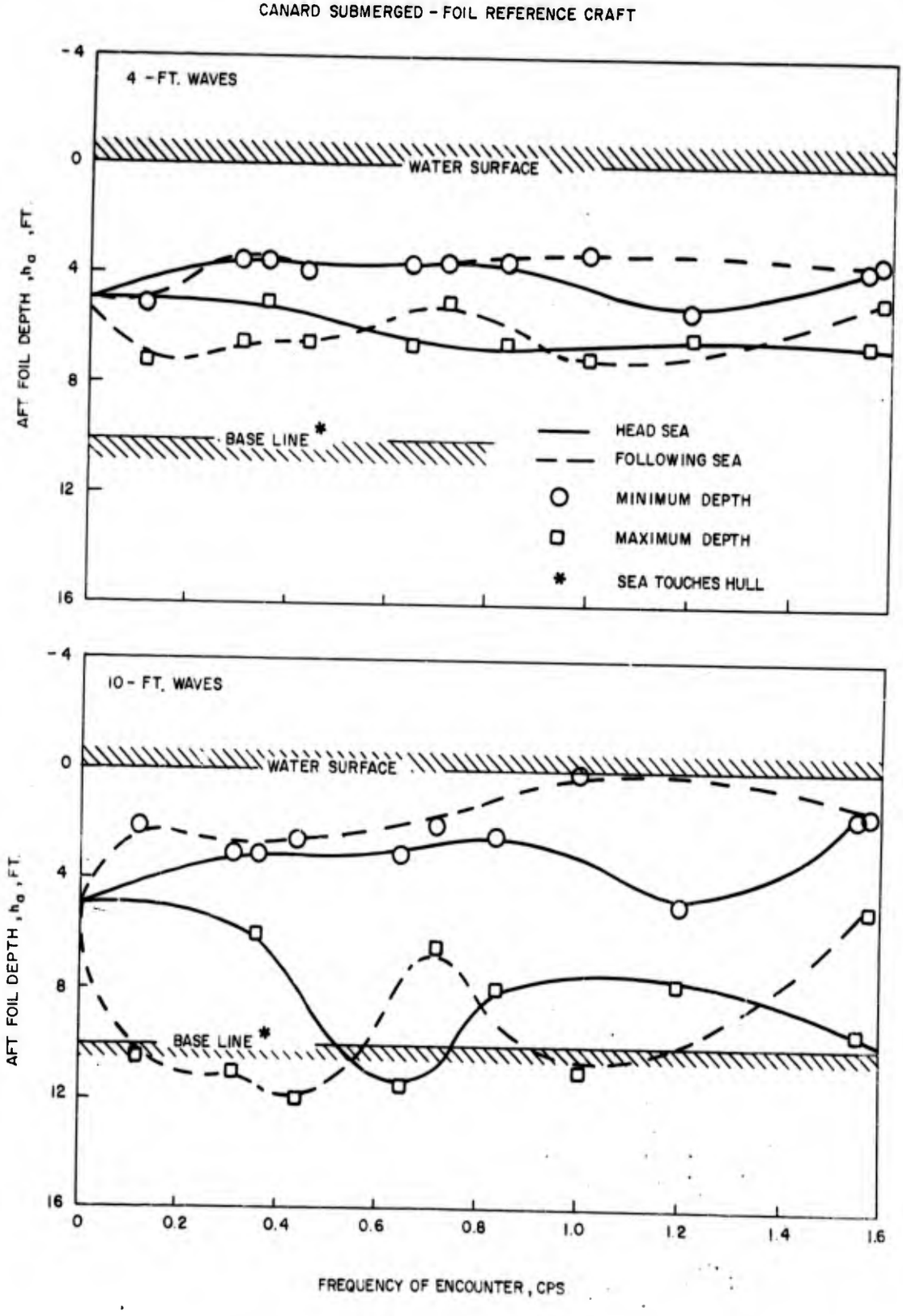

FIGURE 37 AUGMENTED CRAFT AFT FOIL DEPTH RESPONSE IN SEA STATES

CANARD SURFACE-PIERCING-FOIL REFERENCE CRAFT

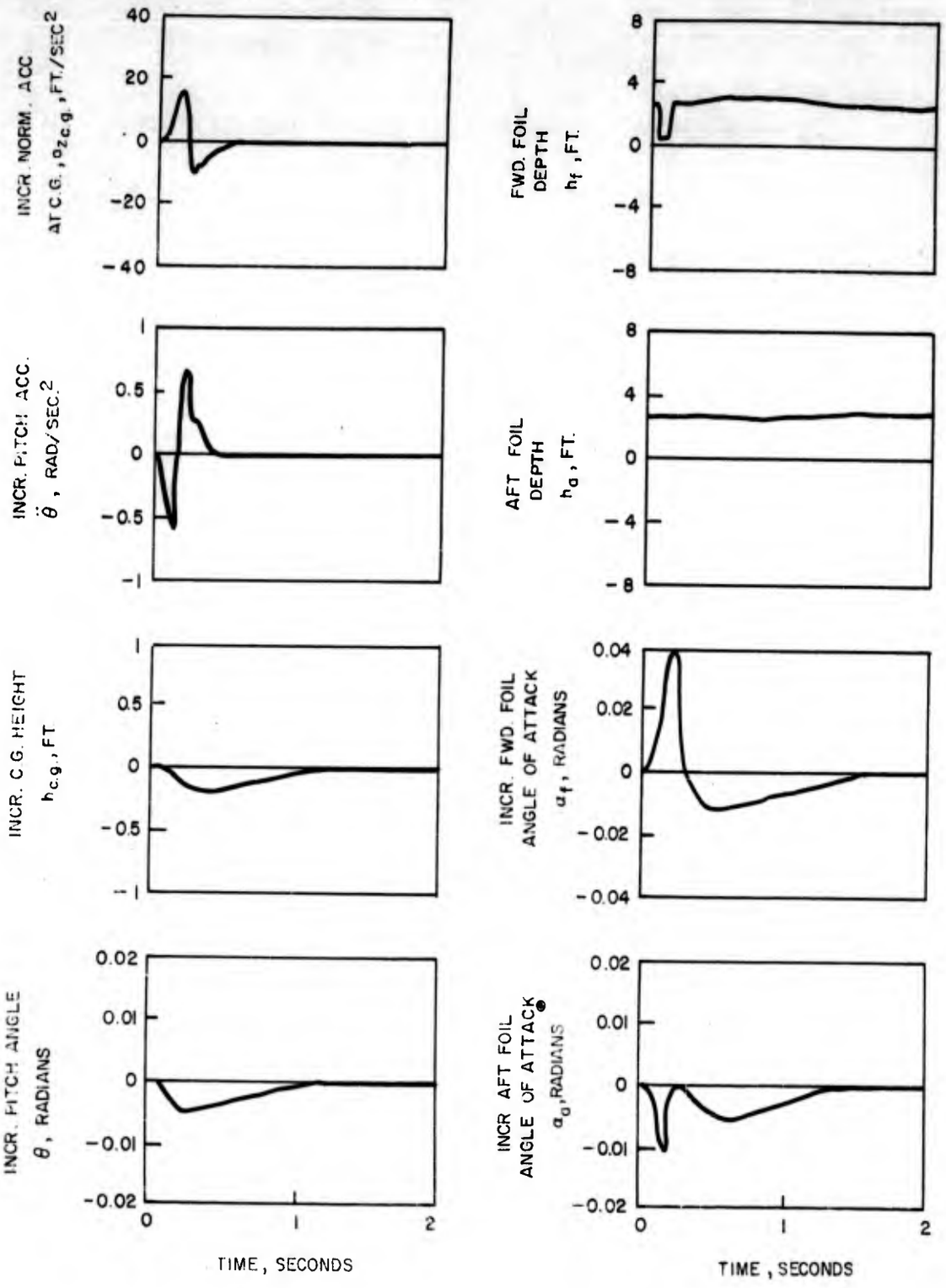

FIGURE 38 UNAUGMENTED CRAFT RESPONSE TO MOMENTARY REDUCTION IN FORWARD FOIL DEPTH

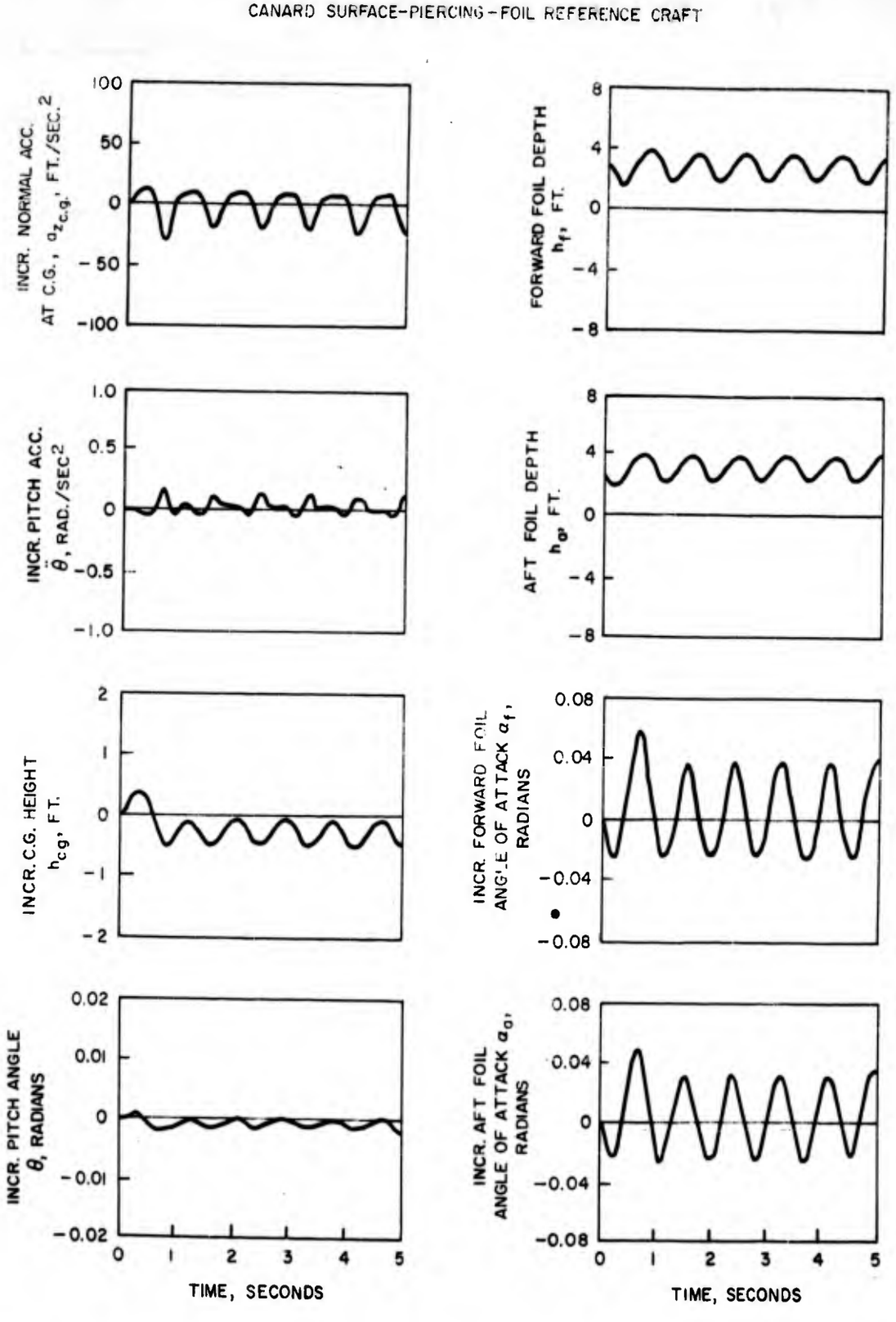

FIGURE 39 UNAUGMENTED CRAFT RESPONSE TO 2-FT., STEEPNESS RATIO 44, HEAD SEA

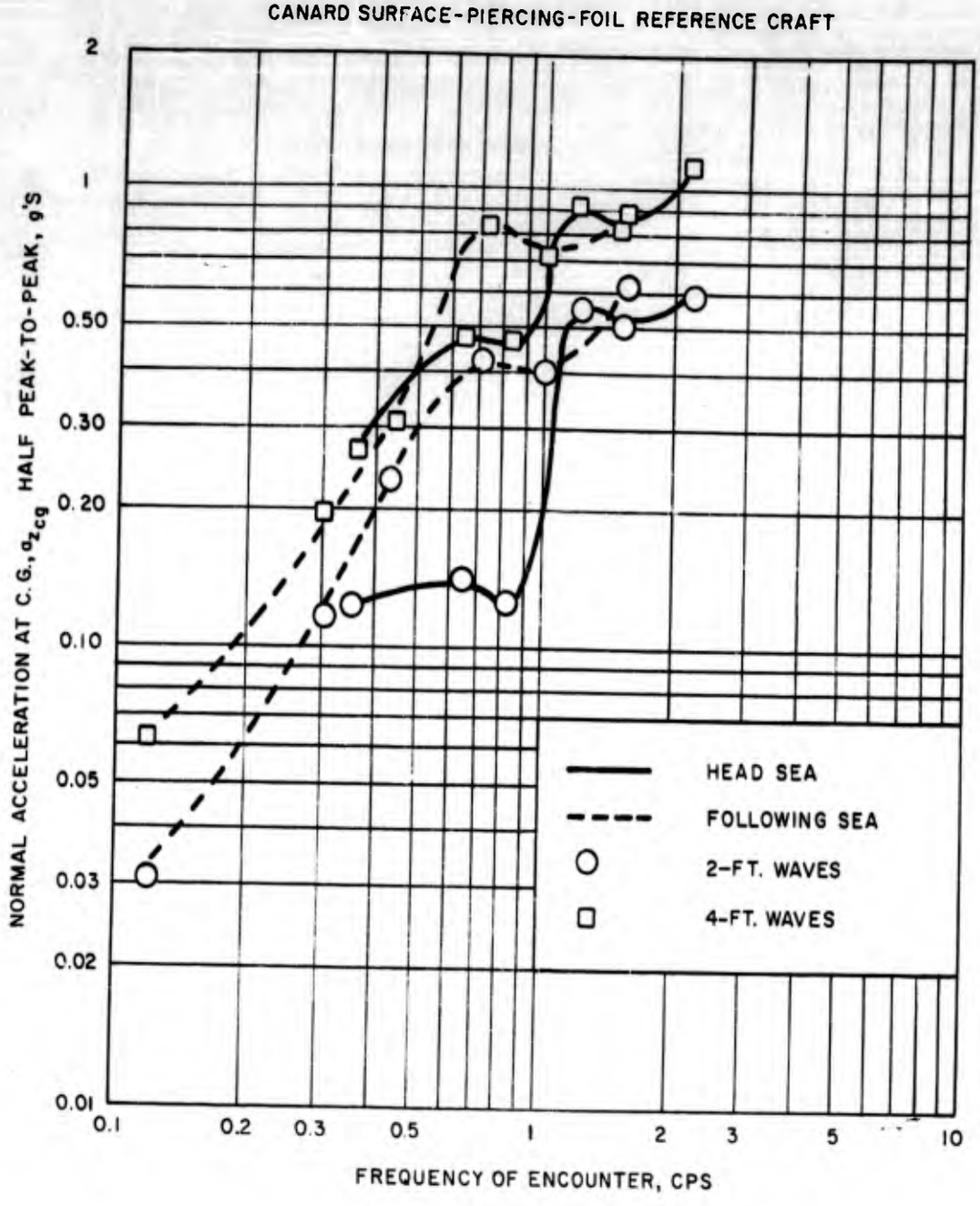

FIGURE 40. UNAUGMENTED CRAFT NORMAL ACCELERATION (AT C.G.) RESPONSE IN SEA STATES

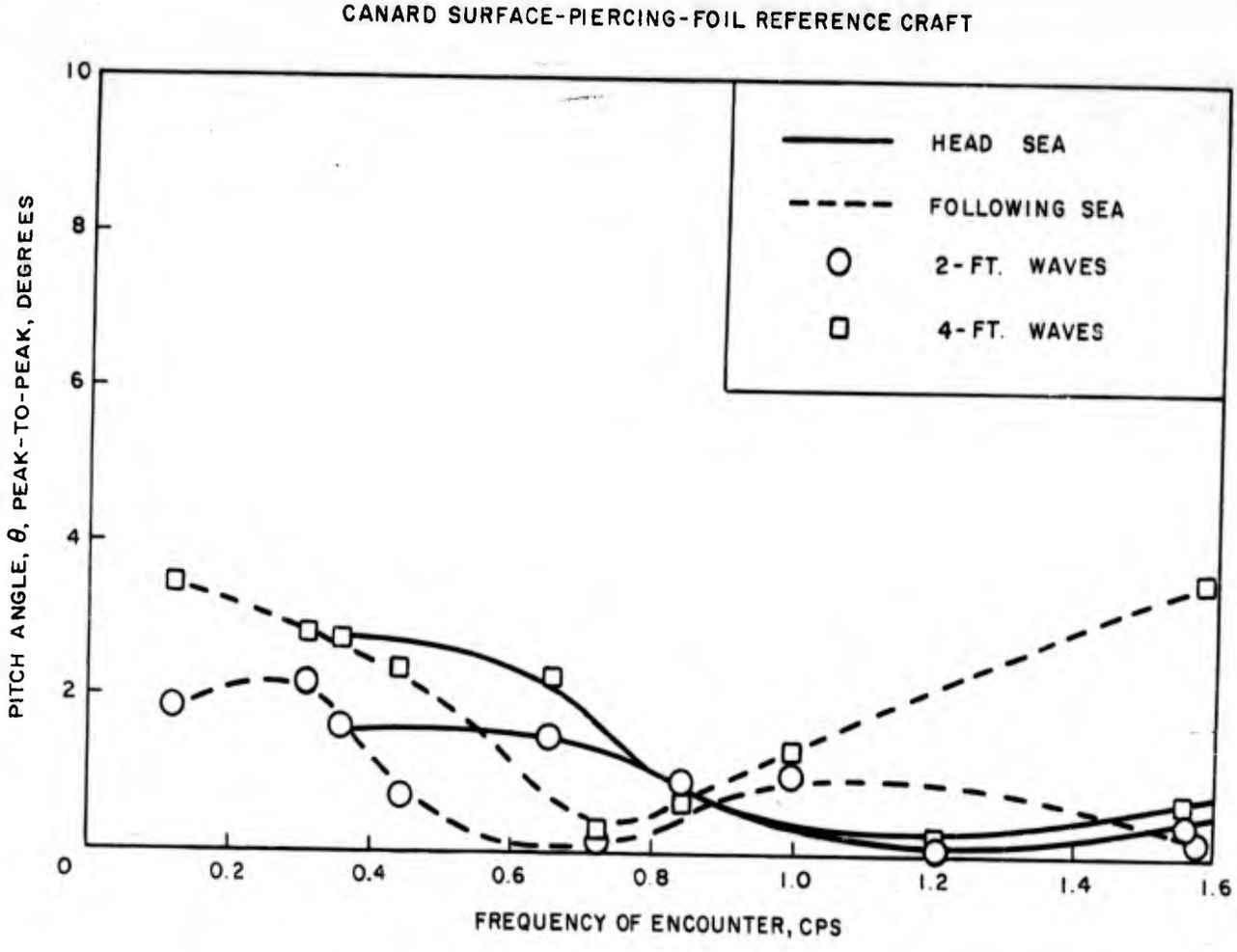

FIGURE 41. UNAUGMENTED CRAFT PITCH ANGLE RESPONSE IN SEA STATES

CANARD SURFACE - PIERCING - FOIL REFERENCE CRAFT

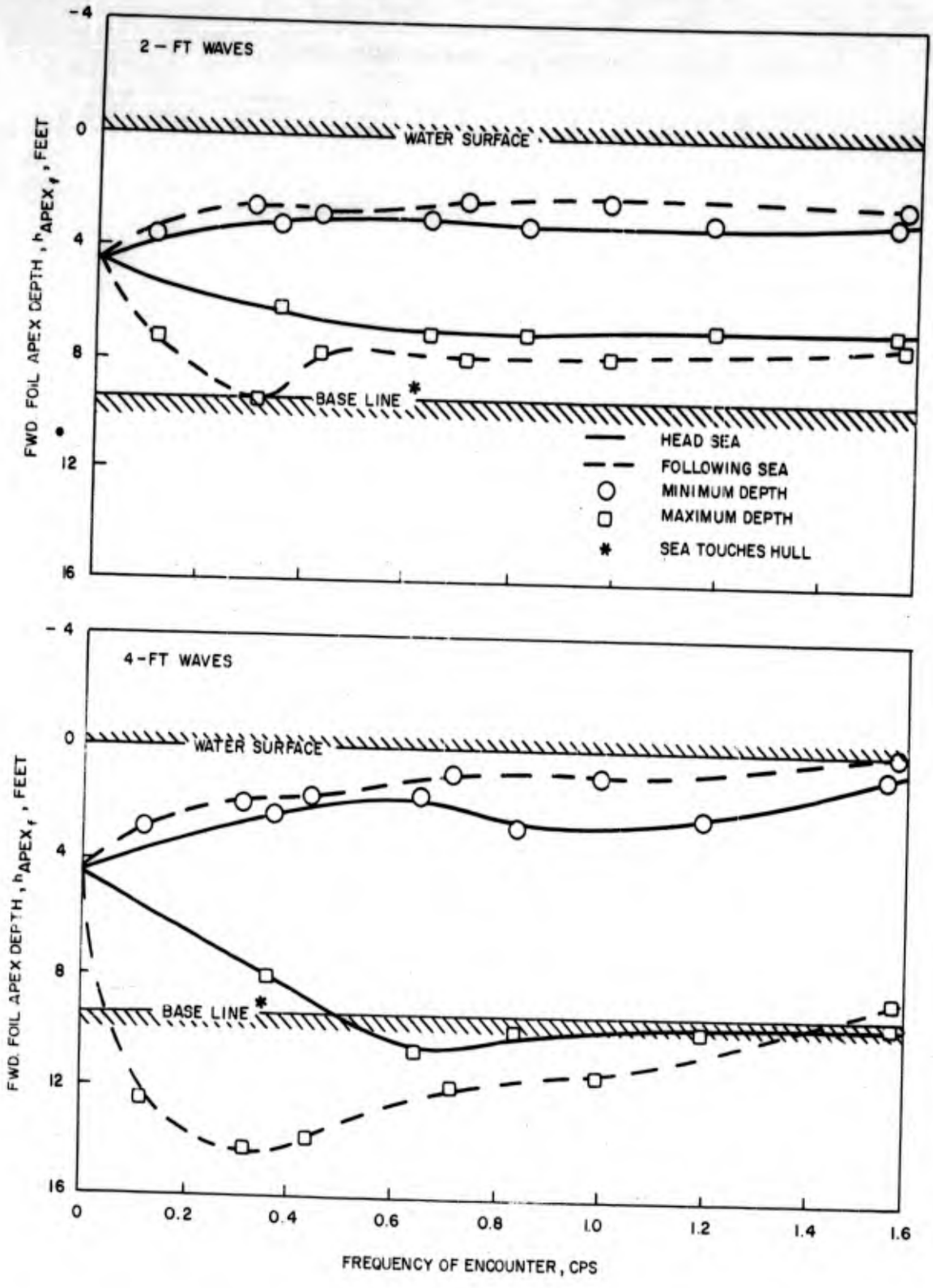

FIGURE 42 UNAUGMENTED CRAFT FORWARD FOIL APEX DEPTH RESPONSE IN SEA STATES

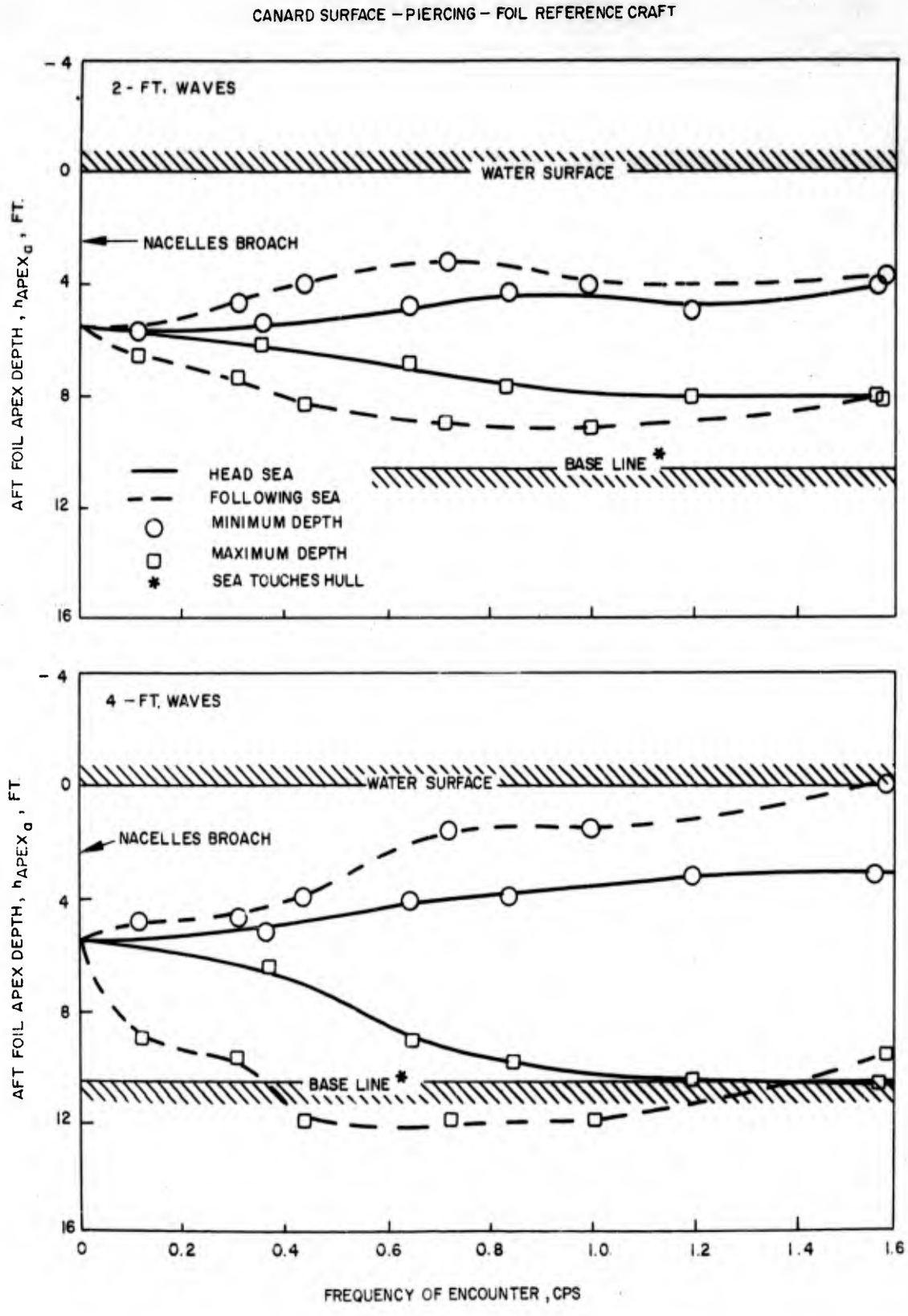

FIGURE 43 UNAUGMENTED CRAFT AFT FOIL APEX DEPTH RESPONSE IN SEA STATES

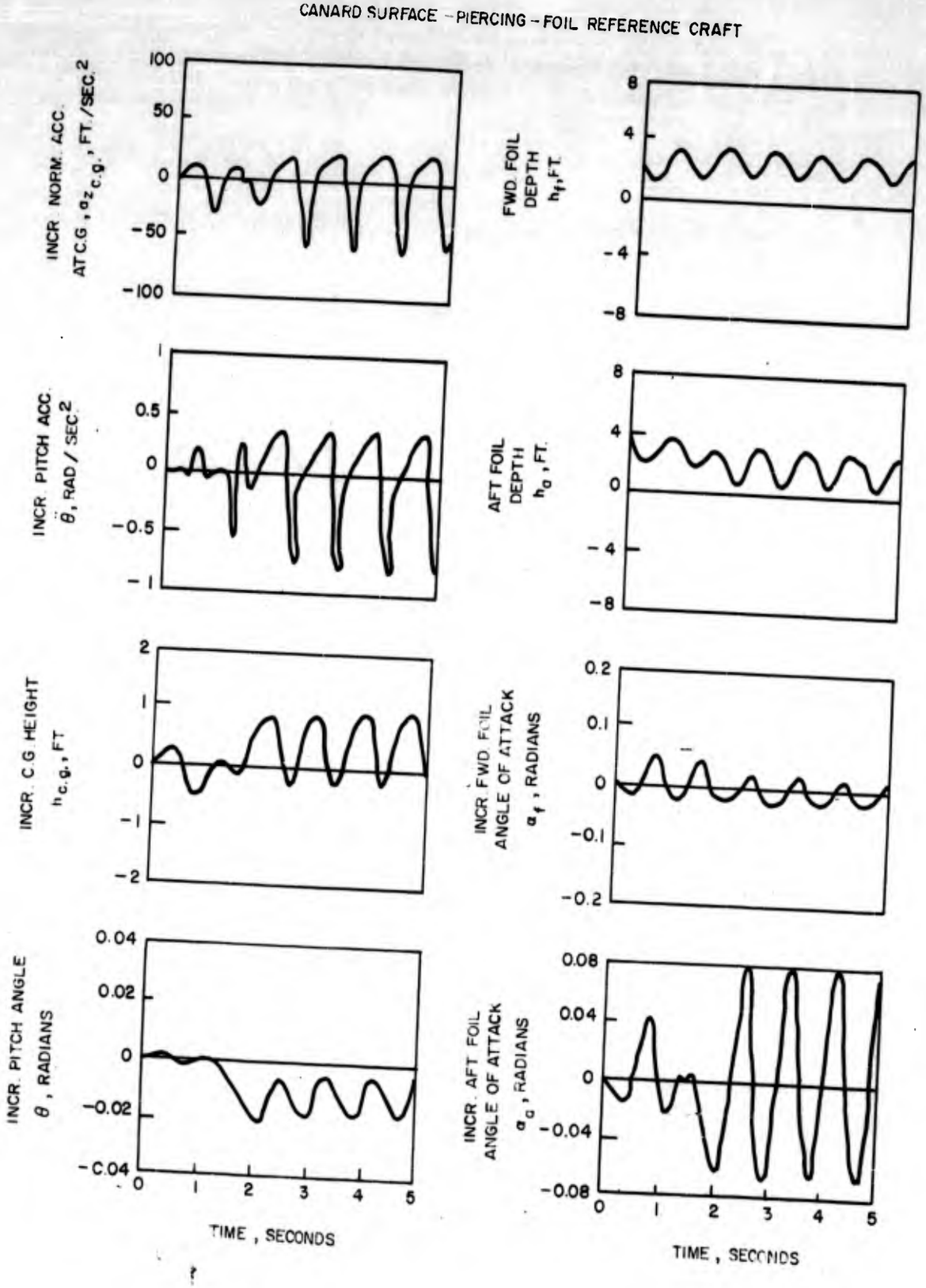

FIGURE 44 UNAUGMENTED CRAFT RESPONSE TO -0.8 DEG. STEP AFT FLAP TRIM COMMAND IN 2-FT., STEEPNESS RATIO 44, HEAD SEA

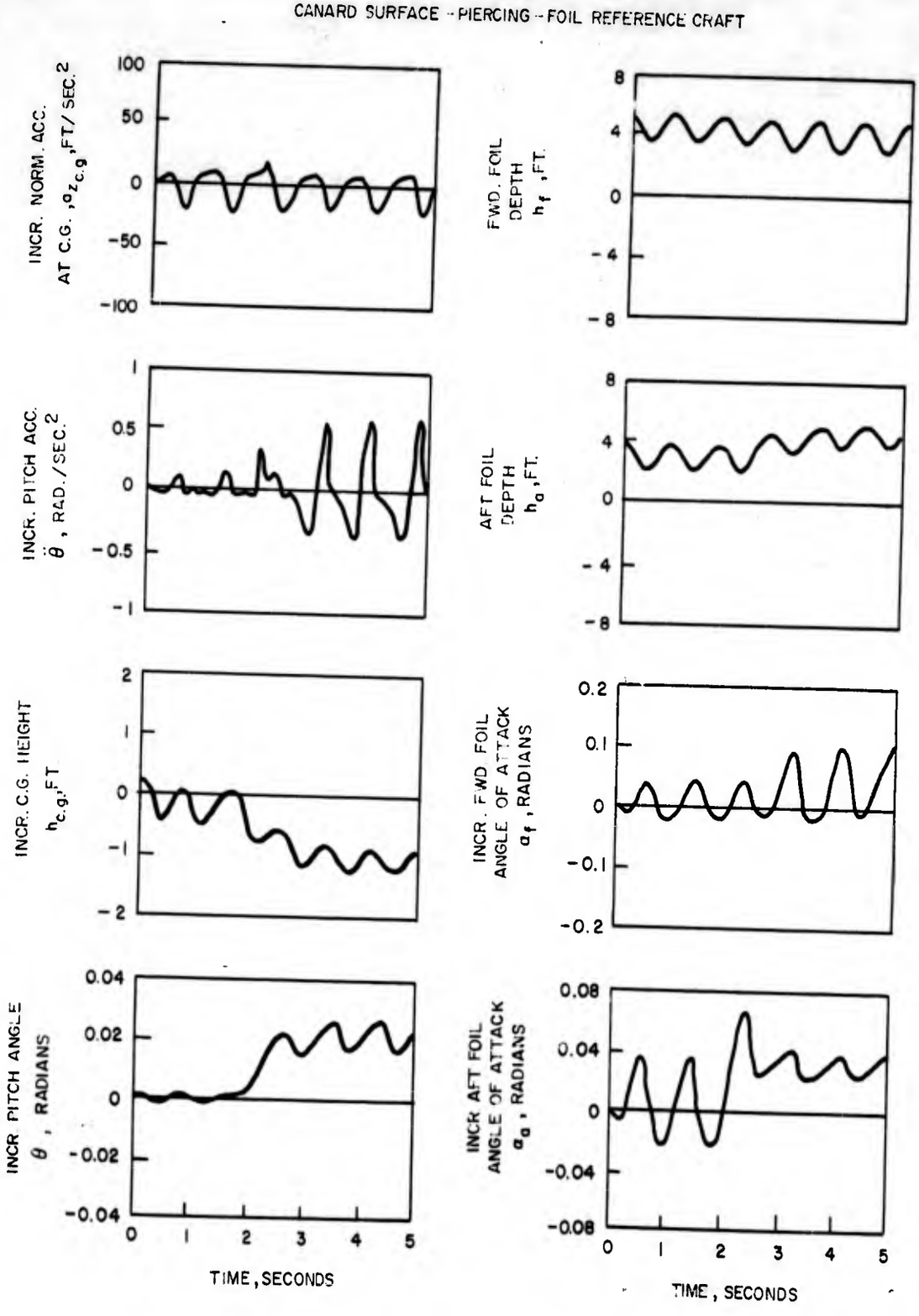

FIGURE 45 UNAUGMENTED CRAFT RESPONSE TO 1.2 DEG. STEP AFT FLAP TRIM COMMAND IN 2-FT., STEEPNESS RATIO 44, HEAD SEA

CANARD AND CONVENTIONAL CONFIGURATIONS

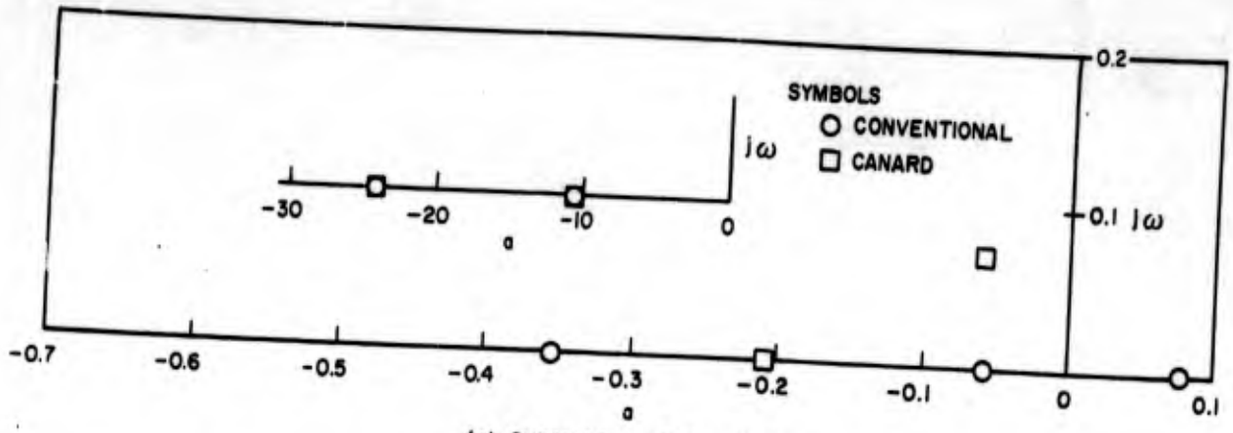

(a) SUBMERGED-FOIL CRAFT

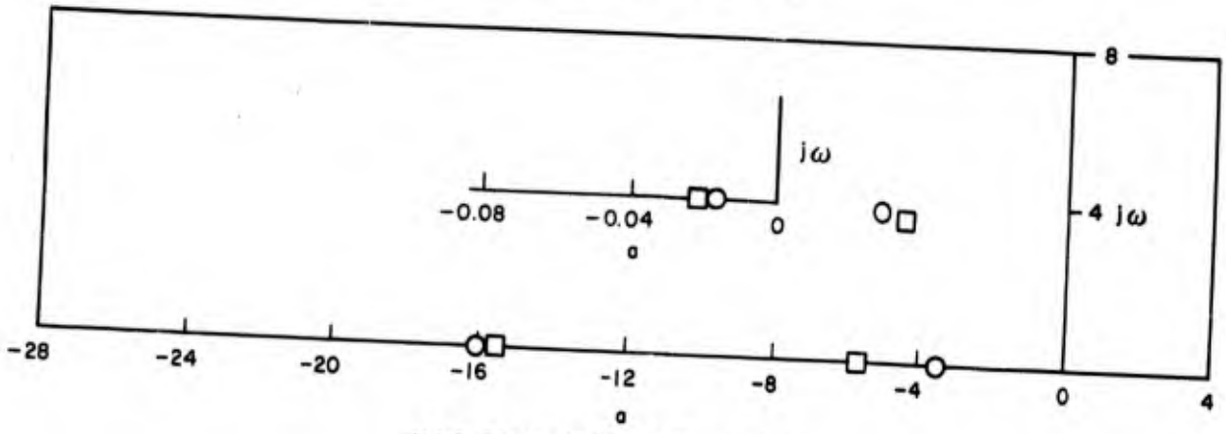

(b) SURFACE-PIERCING-FOIL CRAFT

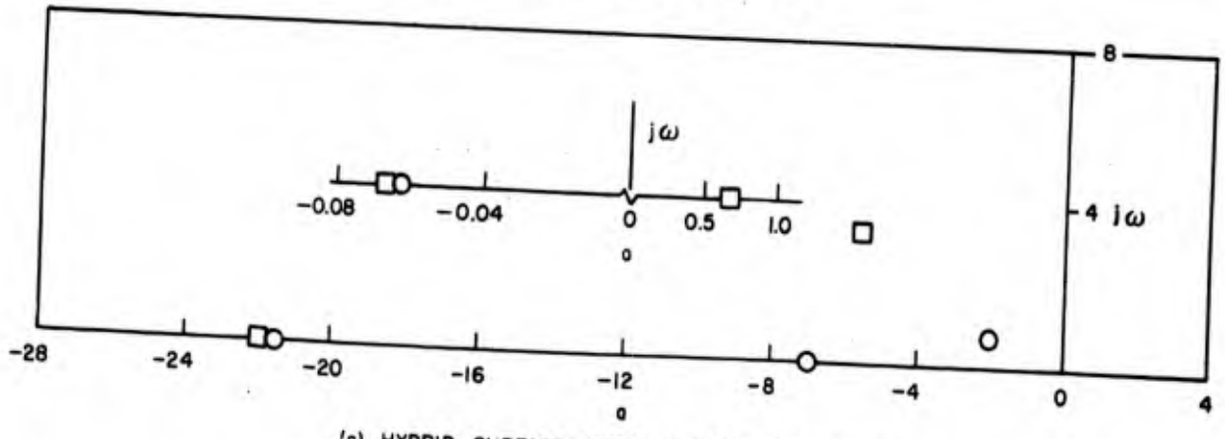

(c) HYBRID SURFACE-PIERCING-MAIN-FOIL CRAFT

FIGURE 46 REFERENCE CRAFT LONGITUDINAL CHARACTERISTIC ROOTS

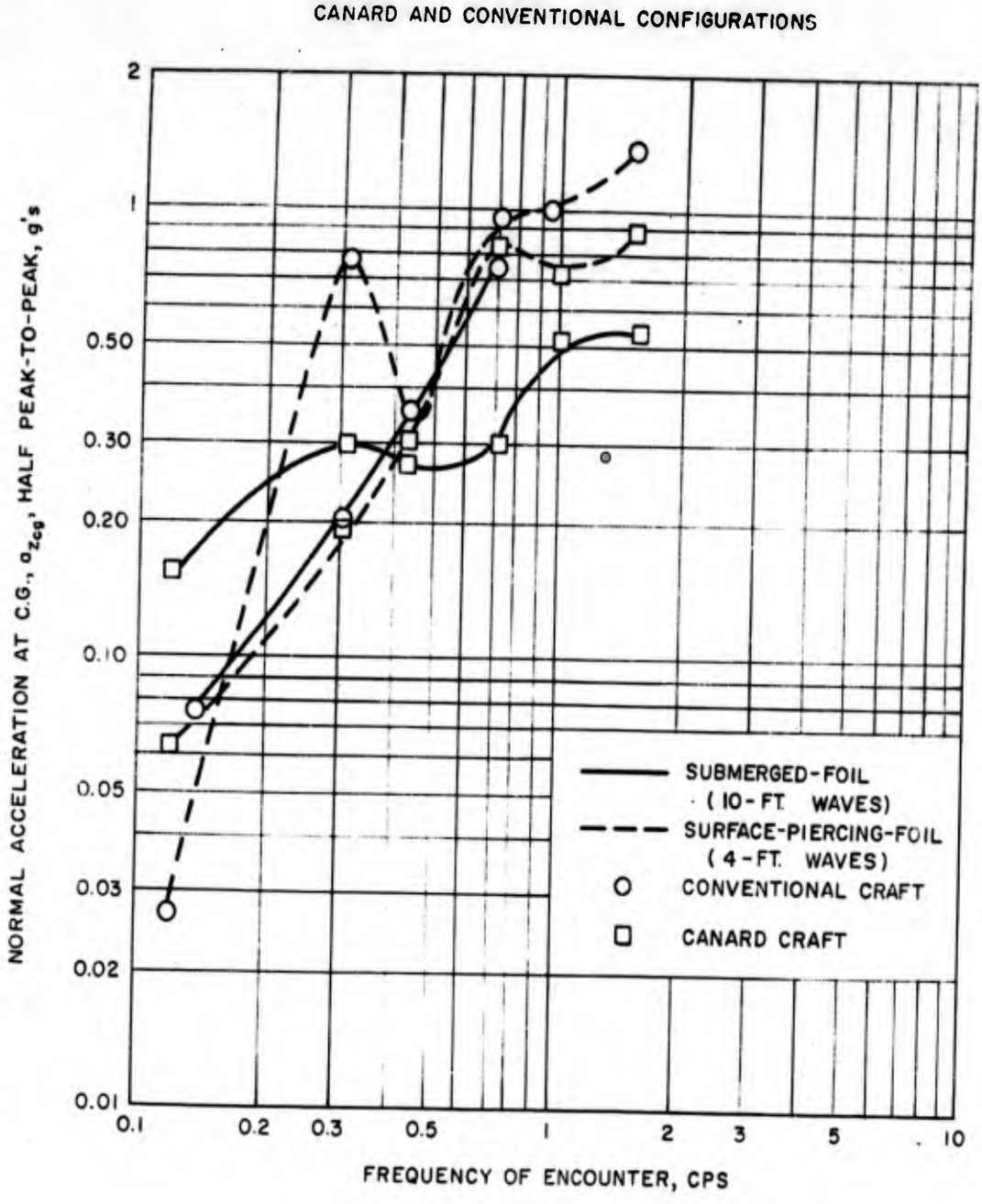

FIGURE 47. NORMAL ACCELERATION RESPONSES IN SEA STATES FOR SUBMERGED-FOIL AND SURFACE-PIERCING-FOIL REFERENCE CRAFT

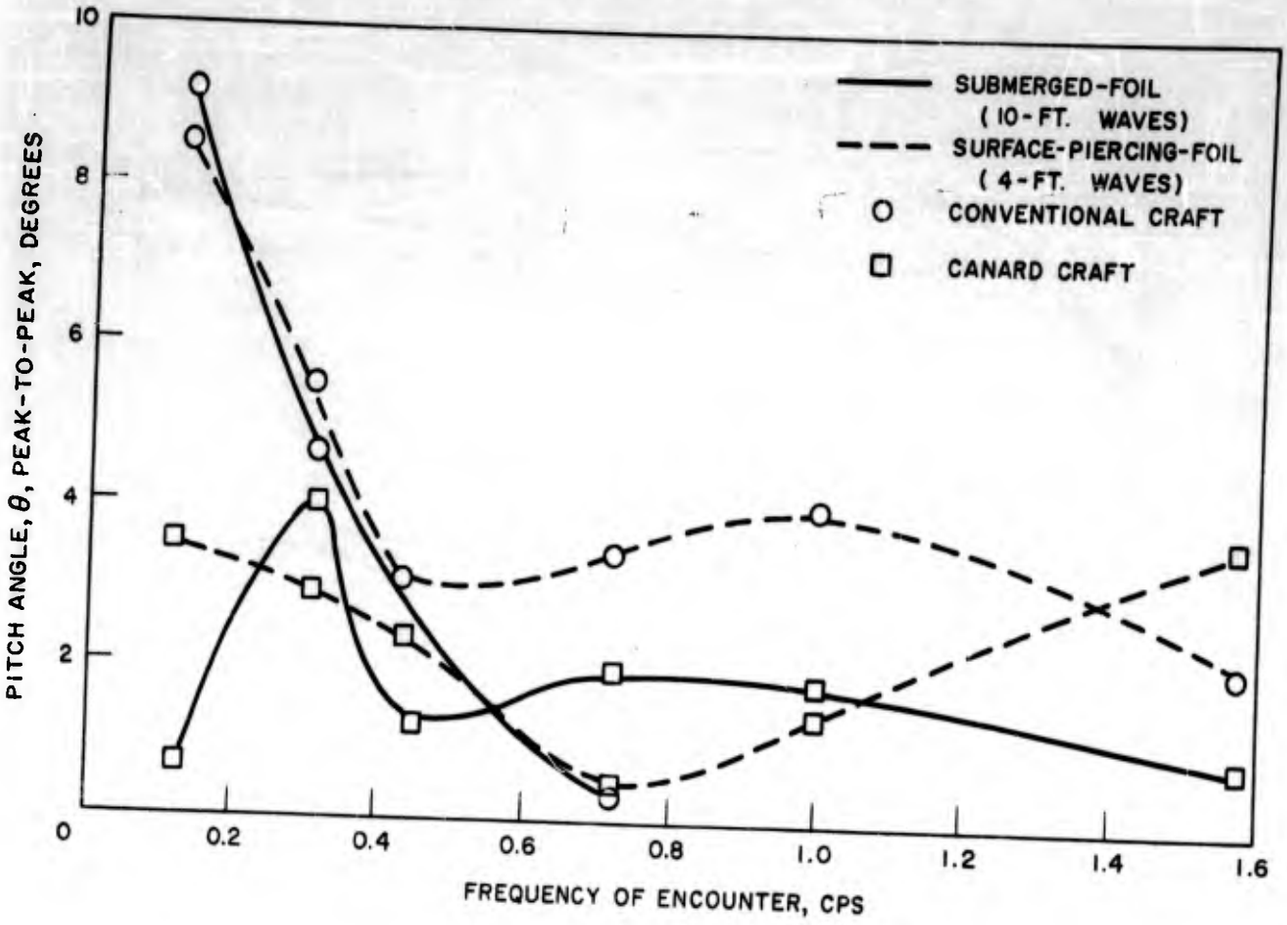

FIGURE 48. CRAFT PITCH ANGLE RESPONSES IN SEA STATES FOR SUBMERGED-FOIL AND SURFACE-PIERCING-FOIL REFERENCE CRAFT

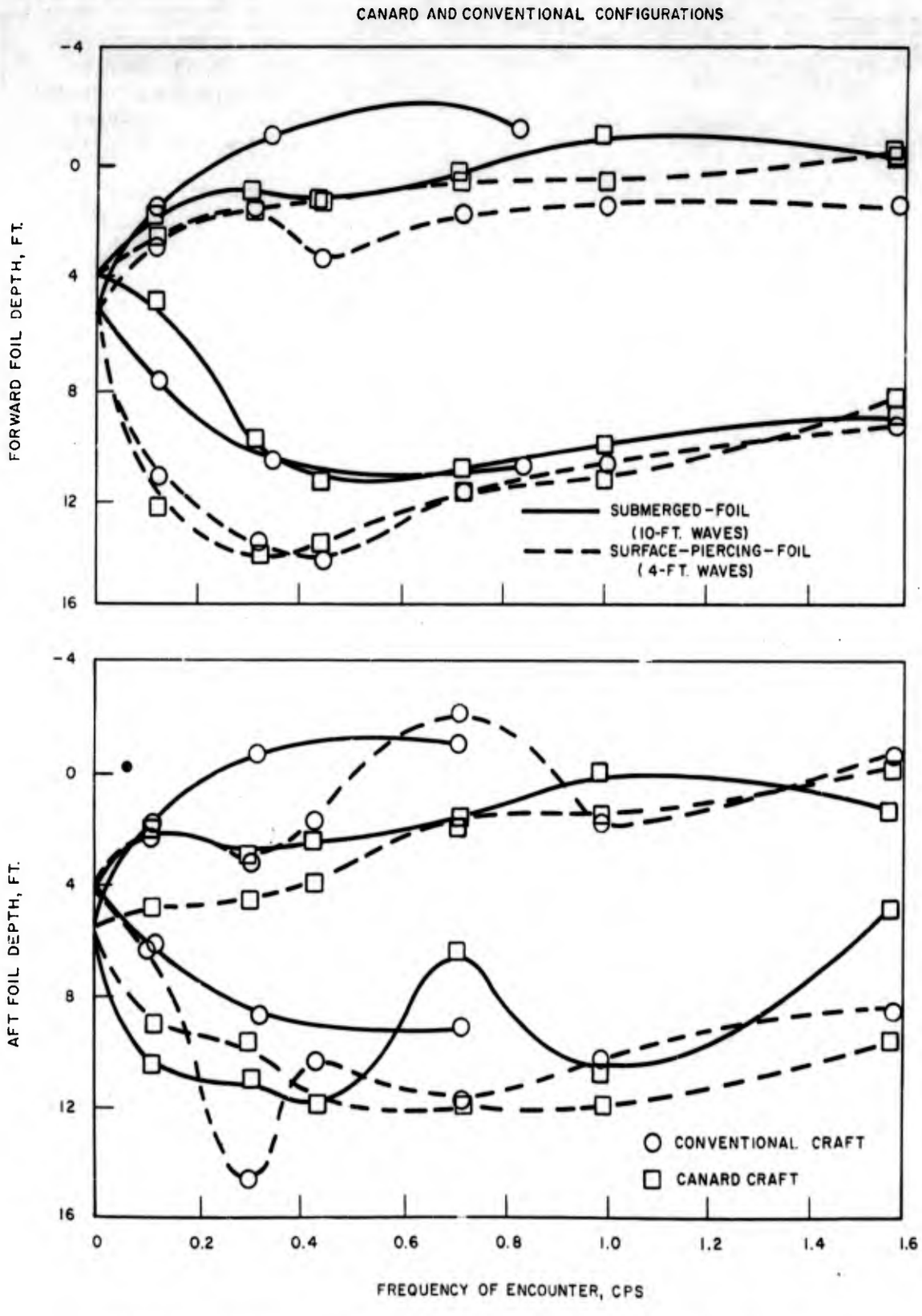

FIGURE 49 CRAFT FOIL DEPTH RESPONSES IN SEA STATES FOR SUBMERGED-FOIL AND SURFACE-PIERCING-FOIL REFERENCE CRAFT

Table 1

CONFIGURATION VARIATIONS MADE FOR INHERENT CRAFT STABILITY STUDY

Foil Types, fwd/aft foils	submerged/ submerged	surface-pierc./ surface-pierc.	submerged/ surface-pierc.	surface-pierc./ submerged
Cruise speed, knots	30, 40, 50*	30, 40, 50*	30, 40, 50*	30, 40, 50*
Horizontal c.g.+ $\Delta x/\ell$	.1, 0*, -.1, -.2, -.3	.1, 0*, -.1, -.2, -.3	.1, 0*, -.1, -.2, -.3	.1, 0*, -.1, -.2, -.3
Vertical c.g.,++ $\Delta z/h_{c.g.ref}$	+.43, 0*, -.43	+.43, 0*, -.43	+.43, 0*, -.43	+.43, 0*, -.43
Foil Spacing, % ref. value	100*, 75, 50, 25	100*, 75, 50, 25	100*, 75, 50, 25	100*, 75, 50, 25
Dihedral Angle, in deg. fwd/aft foils	0/0*	20/20*, 30/30, 40/40, 50/50	0/20*, 0/30 0/40, 0/50	20/0*, 30/0 40/0, 50/0
Aspect Ratio, fwd/aft foils	4/4, 4/6, 6/4, 6/6*, 6/8, 8/6, 8/8	4/4, 4/6, 6/4, 6/6*, 6/8, 8/6, 8/8	4/4, 4/6, 6/4, 6/6*, 6/8, 8/8, 8/8	4/4, 4/6, 6/4, 6/6*, 6/8, 8/6, 8/8
Foil Depth, $h/\bar{c}$, fwd/aft foils	1/1* 1/1.5, 1.5/1, 1.5/1.5, 1/2, 2/1, 2/2	.55/.55*	1/.55*, 1.5/.55, 2/.55	.55/1*, .55/1.5, .55/2
Foil Area, horiz. project area in ft^2, fwd/aft foils	50/75, 50/100, 75/75, 75/150, * 100/100, 100/150 113/75, 150/100, 150/150	50/50, 50/100, 50/150, 75/75, 75/150, 100/100, 100/150*, 113/75, 150/75, 150/100, 150/150	50/50, 50/100 75/75, 75/150, * 100/100, 100/150* 113/75, 150/100, 150/150	50/75, 50/100 75/75, 75/150, * 100/100, 100/150*, 113/75, 150/100, 150/150
Total No. of Variations	32	31	31	31

* Reference Values

\+ Δx is the c.g. location relative to the horizontal projected foil area centroid using quarter-chord points as individual foil area centers. Δx is negative for c.g. aft of craft area centroid.

++ Δz is measured relative to the reference value, positive up; $h_{c.g.ref.}$ is the c.g. height above flying water line (14ft.).

Table 2

PHYSICAL PARAMETERS FOR HORIZONTAL C.G. VARIATION

W_f/W_a	50/50	40/60	30/70	20/80	10/90
$x_{c.g.}$ ft	44.0	52.8	61.6	70.4	79.2
$\Delta x/\ell$	+.1	0	-.1	-.2	-.3
$(W/A)_f$ psf	1250	1000	750	500	250
$(W/A)_a$ psf	833	1000	1167	1333	1500

Notes: 1. W_f/W_a : load distribution in percent gross weight on forward/aft foils.
2. $x_{c.g.}$: c.g. location aft of forward foil $\bar{c}/4$ line.
3. $\Delta x/\ell$: c.g. location relative to craft area centroid; negative for c.g. aft of area centroid.

Table 3

FOIL SPACING PARAMETERS

ℓ/ℓ_{ref}	1.00	.75	.50	.25
ℓ ft.	88	66	44	22
x_f, ft.	52.8	39.6	26.4	13.2
x_a, ft.	35.2	26.4	17.6	8.8

Notes: 1. ℓ : distance between foil $\bar{c}/4$ lines; $\ell_{ref.}$ = 88 ft.
2. x_f: c.g. to forward foil $\bar{c}/4$ line.
3. x_a: c.g. to aft foil $\bar{c}/4$ line.

Table 4

SURFACE-PIERCING-FOIL DIHEDRAL ANGLE VARIATION DATA

	Forward Foil				Aft Foil			
Γ, deg	20	30	40	50	20	30	40	50
S, ft^2	106.4	115.5	130.5	155.6	159.6	173.2	195.8	233.4
$h/\bar{c}$	.55	.87	1.26	1.79	.55	.87	1.26	1.79
h, ft	2.23	3.54	5.14	7.30	2.73	4.33	6.29	8.94

Notes:
1. S: wetted plan area; $h/\bar{c}$: mean-depth-to-mean-chord ratio; h: mean depth (half apex depth).
2. For all foils: AR = 6, TR = 1, Λ = 0.
3. Forward foil: b = 24.5 ft, $\bar{c}$ = 4.08 ft, A = 100 ft^2
4. Aft foil: b = 30.0 ft., $\bar{c}$ = 5.00 ft, A = 150 ft^2
5. Foil span b measured at flying water line.

Table 5

PHYSICAL DATA FOR ASPECT RATIO VARIATIONS

Submerged Foils

	Forward			Aft		
AR	4	6	8	4	6	8
b, ft.	20.0	24.5	28.3	24.5	30.0	34.6
$\bar{c}$, ft	5.00	4.08	3.54	6.12	5.00	4.33
S, ft^2	100	100	100	150	150	150
h, ft	5.00	4.08	3.54	6.12	5.00	4.33
$h/\bar{c}$	1.0	1.0	1.0	1.0	1.0	1.0

Surface-Piercing Foils

	Forward			Aft		
AR	4	6	8	4	6	8
b, ft	20.0	24.5	28.3	24.5	30.0	34.6
$\bar{c}$, ft	5.00	4.08	3.54	6.12	5.00	4.33
S, ft^2	106.4	106.4	106.4	159.6	159.6	159.6
h, ft	1.82	2.23	2.57	2.23	2.73	3.15
$h/\bar{c}$	.36	.55	.73	.36	.55	.73

Notes:
1. For all foils: TR = 1, Λ = 0.
2. Forward foil: A = 100 ft^2; aft foil: A = 150 ft^2.
3. Surface-piercing foil: b and AR measured at flying water line; 20 degs. dihedral.
4. AR = 6 are reference foils.

NOMENCLATURE

A - horizontal projected area of wetted foil, $ft.^2$

AR - foil aspect ratio, dimensionless

a - real part of complex root, per sec.

a_z - normal acceleration, $ft./sec.^2$

b - foil span (at flying water line for surface-piercing foil), ft.

C_D - drag coefficient, dimensionless

C'_{D_o} - sum of constant drag coefficients, dimensionless

C_{D_α} - partial derivative of C_D with respect to α, per rad.

C_{D_h} - partial derivative of C_D with respect to h, per ft.

C_{D_v} - partial derivative of C_D with respect to v, per ft./sec.

C_{D_δ} - partial derivative of C_D with respect to δ, per rad.

C_L - lift coefficient, dimensionless

C_{L_h} - partial derivative of C_L with respect to h, per ft.

C_{L_v} - partial derivative of C_L with respect to v, per ft./sec.

C_{L_α} - lift curve slope, per rad.

C_{L_δ} - partial derivative of C_L with respect to δ, per rad.

$\bar{c}$ - mean chord of wetted foil, ft.

D - drag, lbs.

F_x - force along craft x-axis, positive forward, lbs.

F_z - force along craft z-axis, positive downward, lbs.

f - frequency of wave encounter, cps

g - gravity constant, ft./sec^2.

H_{sea} - wave amplitude (1/2 crest-to-trough height), ft.

h - foil mean depth below free water surface, positive down; or height above free water surface, positive up; ft.

h_{apex} - surface-piercing-foil depth below water surface to foil apex, ft.

h_{sea} - height of free water surface above mean free surface, positive up, ft.

h_{sensor} - height as measured by height sensor, ft.

$h/\bar{c}$ - mean-depth-to-chord ratio

I_x, I_y, I_z - roll, pitch, and yaw moments of inertia respectively, slug-ft.^{2}

i - foil incidence, rad.

$j = \sqrt{-1}$

K_D - sum of induced and wave drag coefficients

K_E - correction factor for box foil configuration

K_{a_z} - normal acceleration error gain, rad/ft./sec.^{2}

K_h - height error gain, rad/ft.

K_p - height error integral gain, rad/ft-sec.

K_θ - pitch error gain, rad/rad.

K_{θ_p} - pitch error integral gain rad/rad-sec.

L - lift, lbs.

ℓ - distance between foil quarter-chord lines, ft.

M - pitching moment, ft-lbs.

m - craft mass, slugs

S - foil wetted planform area, ft^2.

S_h - partial of S with respect to h, ft^2/ft.

s - Laplace transform variable

TR - foil taper ratio (wetted, tip/root)

t - real time, sec.

u - pertubation velocity along x-axis, positive forward, ft/sec.

u_{sea} - local sea velocity along x-axis, positive forward, ft/sec.

V - velocity, ft/sec.

$V_{orb.}$ - wave orbital velocity, ft/sec.

V_{sea} - wave velocity, positive when crest is traveling in negative x direction, ft/sec.

W - total gross weight of craft, lbs.

w - pertubation velocity along z-axis, positive down, ft/sec.

w_{sea} - local sea velocity along z-axis, positive up, ft/sec.

x, y, z - distances along craft x-, y-, and z-axis, positive forward, starboard, and down respectively, ft.

Δx - horizontal c.g. location relative to horizontal projected foil area centroid, positive forward of a.c., ft.

Δz - vertical c.g. location relative to reference value, positive up, ft.

α - angle of attack, rad.

α_δ - flap effectiveness parameter, dimensionless

Γ - foil dihedral angle, deg.

Δ - unaugmented craft longitudinal characteristic equation

δ - control surface deflection, rad.

ζ - foil planform correction factor, dimensionless

ζ_o - constant in linear approximation of ζ

$\zeta_1 = 0.0348/\bar{c} \tan\Gamma$

θ - craft pitch angle, rad.

Λ - quarter-chord sweep angle, deg.

$\lambda_1 = 2gh/V^2$

λ_{sea} - sea wave length, ft.

$\rho = 1.994$ slugs/ft^3, density of sea water

σ - Munk's interference factor

$\tau = \ell/V_o$, sec.

τ_1 - height error filter time constant, sec.

$\tau_2; \tau_3$ - normal acceleration error filter time constants, sec.

ω - imaginary part of complex root, rad/sec.

Subscripts

$( )_a$ - aft foil or aft foil arrangement

$( )_f$ - forward foil or forward foil arrangment

$( )_{c.g.}$ - center of gravity

$( )_n$ - nacelle

$( )_{ref.}$ - reference quantity

$( )_s$ - strut

$( )_{trim}$ - trim quantity

$( )_o$ - equilibrium quantity

Superscripts

$\hat{( )}$ - command quantity

$\dot{( )}$ - first derivative with respect to time

$\ddot{( )}$ - second derivative with respect to time

Other notation

$( )(s)$ - function of Laplace transform variable

$( )(t)$ - function of time

REFERENCES

1. Chuck, G., Luke, R.K.C., and Scroggs, S. J., Study of Hydrofoil Stability and Control, Hughes Aircraft Company, SRS-399, December, 1960.

2. H.O. Publ. No. 603, Practical Methods for Observing and Forecasting Ocean Waves, U.S. Navy Hydrographic Office, 1955.

3. St. Denis, M. and Pierson, W. J., On the Motion of Ships in Confused Seas, Transactions of the Society of Naval Architects and Marine Engineers, 1953.

4. Bigelow, H. B. and Edmondson, W. T., Wind Waves at Sea Breakers and Surf, H. O. Publ. No. 602, 1947.

5. Hughes Aircraft Company Correspondence No. 60H-12894/5467-002, Proposal For a Hydrofoil Stability and Control Study, Hughes Aircraft Company, December 1960.

APPENDIX A

HYDRODYNAMIC DATA

Hydrodynamic data for the reference craft and parametric variations, as computed by the digital computer programs, are tabulated in this appendix. These coefficients may be used with the forms given in Appendix B of Reference 1 to compute dimensional stability derivatives, which are then used to compute the characteristic roots. The coefficients are listed according to components (foil, strut, and nacelle) since the same component is used in more than one craft. For example, the forward surface-piercing-foil arrangement is used on both the surface-piercing-foil craft and the hybrid submerged-aft-foil craft.

Table A-1

REFERENCE CRAFT HYDRODYNAMIC DATA

Coef.	Forward Components			Aft Components			
	Surface-Piercing Foil	Submerged Foil	Strut*	Surface-Piercing Foil	Submerged Foil	Strut*	Nacelle+
C_L	.1405	.1405	0	.1405	.1405	0	0
C_{L_α} per rad	3.56	3.92	0	3.51	3.88	0	.094
C_{L_h} per ft	.1683	.0056	0	.1379	.0046	0	0
C_{L_v} per fps	.00021	.00014	0	.00025	.00017	0	0
C_D	.01361	.01338	.00309	.01371	.01346	.00349	.00180
C_{D_α} per rad	.0925	.0915	0	.0931	.0928	0	0
C_{D_h} per ft	.01253	.00005	.00052	.01034	.00004	.00047	0
C_{D_v} per fps	$.13\times10^{-5}$	$-.7\times10^{-5}$	0	$.17\times10^{-5}$	$-.7\times10^{-6}$	0	0
C_{L_δ} per rad	2.37	1.26	-	2.34	2.59	-	-
C_{D_δ} per rad	.1459	.1428	-	.1468	.1439	-	-
δ trim rad	.0593	.0538	-	.0601	.0543	-	-

* Used with submerged foils only. Coefficients based on associated foil area.

\+ Coefficients based on foil area.

Table A-2

FOIL HYDRODYNAMIC DATA FOR SPEED VARIATION

V_o, kts	40				30			
Coef.	Fwd Foils		Aft Foils		Fwd Foils		Aft Foils	
	S-P	Sub.	S-P	Sub.	S-P	Sub.	S-P	Sub.
C_L	.2195	.2195	.2195	.2195	.3902	.3902	.3902	.3902
C_{L_α} per rad	3.44	3.83	3.36	3.78	3.20	3.66	3.08	3.58
C_{L_h} per ft	.2495	.0089	.2055	.0073	.4536	.0165	.3748	.0138
C_{L_v} per fps	.00059	.00041	.00071	.00048	.00232	.00151	.00273	.00171
C_D	.01826	.01885	.01858	.01910	.03629	.03786	.03781	.03900
C_{D_α} per rad	.1381	.1476	.1393	.1503	.2523	.2777	.2549	.2846
C_{D_h} per ft	.01727	.00014	.01446	.00012	.03680	.00056	.03181	.00050
C_{D_v} per fps	$.70\times10^{-5}$	$-.2\times10^{-5}$	$.90\times10^{-5}$	$-.2\times10^{-5}$	$.62\times10^{-4}$	$-.1\times10^{-4}$	$.82\times10^{-4}$	$-.9\times10^{-4}$
C_{L_δ} per rad	2.29	2.55	2.24	2.51	2.13	2.44	2.05	2.38
C_{D_δ} per rad	.1904	.1949	.1922	.1973	.3041	.3155	.3087	.3217
δ trim rad	.0901	.0861	.0921	.0873	.1723	.1602	.1784	.1637

Note: Strut and nacelle coefficients same as those at 50 knots (Table A-1).

Table A-3

FOIL HYDRODYNAMIC DATA FOR HORIZONTAL C.G. VARIATION

(a) Submerged Foils

	Forward Foil				Aft Foil			
$\Delta x/\ell$	+.1	-.1	-.2	-.3	+.1	-.1	-.2	-.3
C_L	.1756	.1053	.0702	.0351	.1171	.1639	.1873	.2107
C_{L_α} per rad	3.92	3.92	3.92	3.92	3.88	3.88	3.88	3.88
C_{L_h} per ft	.0070	.0042	.0028	.0014	.0038	.0053	.0061	.0069
C_{L_v} per fps	.00018	.00011	.00007	.00004	.000142	.00020	.00023	.00026
C_D	.01544	.01160	.01011	.00891	.01222	.01482	.01633	.01796
C_{D_α} per rad	.1144	.0687	.0458	.0229	.0773	.1082	.1237	.1872
C_{D_h} per ft	.00008	.00003	.00001	.000003	.00003	.00006	.00008	.00010
C_{D_v} per fps	$-.10\times10^{-5}$	$-.38\times10^{-6}$	$-.17\times10^{-6}$	$-.42\times10^{-7}$	$-.51\times10^{-6}$	$-.99\times10^{-6}$	$-.13\times10^{-5}$	$-.16\times10^{-5}$
C_{L_δ} per rad	2.61	2.61	2.61	2.61	2.59	2.59	2.59	2.59
C_{D_δ} per rad	.1642	.1214	.1000	.0786	.1294	.1583	.1727	.1872
δ_{trim} rad	.0673	.0403	.0269	.0135	.0453	.0634	.0724	.0815

Note: Strut and nacelle coefficients same as reference values (Table A-1).

Table A-3 (concluded)

(b) Surface-Piercing Foils

	Forward Foil				Aft Foil			
$\Delta x/\ell$	+.1	-.1	-.2	-.3	+.1	-.1	-.2	-.3
C_L	.1756	.1053	.0702	.0351	.1171	.1639	.1873	.2107
C_{L_α} per rad	3.56	3.56	3.56	3.56	3.51	3.51	3.51	3.51
C_{L_h} per ft	.2104	.1186	.0791	.0395	.1149	.1511	.1727	.1943
C_{L_v} per fps	.00026	.00015	.00010	.00005	.00021	.00028	.00032	.00036
C_D	.01570	.01149	.01008	.00892	.01244	.01450	.01588	.01736
C_{D_α} per rad	.1156	.0652	.0434	.0217	.0776	.1021	.1167	.1313
C_{D_h} per ft	.01459	.01047	.00912	.00802	.00932	.01097	.01209	.01330
C_{D_v} per fps	$.20\times10^{-5}$	$.64\times10^{-6}$	$.29\times10^{-6}$	$.70\times10^{-7}$	$.12\times10^{-5}$	$.21\times10^{-5}$	$.27\times10^{-5}$	$.34\times10^{-5}$
C_{L_δ} per rad	2.37	2.37	2.37	2.37	2.34	2.34	2.34	2.34
δ trim rad	.0741	.0418	.0279	.0139	.0501	.0659	.0753	.0847
C_{D_δ} per rad	.1681	.1197	.0989	.0780	.1318	.1554	.1694	.1834

Note: Nacelle coefficients same as reference values (Table A-1).

Table A-4

SURFACE-PIERCING FOILS HYDRODYNAMIC DATA FOR DIHEDRAL ANGLE VARIATION

	Forward Foil			Aft Foil		
Γ, deg	30	40	50	30	40	50
C_L	.1405	.1405	.1405	.1405	.1405	.1405
C_{L_α} per rad	4.25	4.65	4.95	4.21	4.60	4.90
C_{L_h} per ft	.0938	.0615	.0420	.0767	.0502	.0343
C_{L_v} per fps	.00017	.00015	.00015	.00020	.00018	.00017
C_D	.01256	.01201	.01162	.01264	.01208	.01169
C_{D_α} per rad	.1021	.1039	.1033	.1032	.1052	.1047
C_{D_h} per ft	.00707	.00462	.00314	.00582	.00380	.00258
C_{D_v} per fps	$-.44\times10^{-7}$	$-.47\times10^{-6}$	$-.68\times10^{-6}$	$.33\times10^{-7}$	$-.50\times10^{-6}$	$-.76\times10^{-6}$
C_{L_δ} per rad	2.83	3.10	3.30	2.80	3.07	3.26
C_{D_δ} per rad	.1479	.1471	.1455	.1489	.1483	.1467
δ trim rad	.0496	.0453	.0426	.0501	.0458	.0430

Note: Nacelle coefficients same as reference values (Table A-1).

Table A-5
HYDRODYNAMIC DATA FOR ASPECT RATIO VARIATION

	Surface-Piercing Foils				Submerged Foils			
	Forward		Aft		Forward		Aft	
AR	4	8	4	8	4	8	4	8
C_L	.1405	.1405	.1405	.1405	.1405	.1405	.1405	.1405
C_{L_α} per rad	2.232	4.177	2.165	4.133	3.525	4.177	3.489	4.141
C_{L_h} per ft	.2834	.1242	.2361	.1015	.0046	.0061	.0038	.0050
C_{L_v} per fps	.00042	.00015	.00052	.00018	.00015	-.00013	.00018	.00016
C_D	.01668	.01220	.01699	.01226	.01444	.01281	.01453	.01288
C_{D_α} per rad	.0791	.0788	.0781	.0798	.1101	.0795	.1112	.0807
C_{D_h} per ft	.02125	.0095	.01783	.0078	.000060	-.00055	.000052	.000041
C_{D_v} per fps	$.10\times10^{-4}$	$.33\times10^{-6}$	$.13\times10^{-4}$	$-.33\times10^{-6}$	$.31\times10^{-7}$	$-.98\times10^{-6}$	$.12\times10^{-6}$	$-.11\times10^{-5}$
C_{L_δ} per rad	1.49	2.78	1.44	2.75	2.35	2.78	2.32	2.76
C_{D_δ} per rad	.1506	.1314	.1511	.1323	.1579	.1333	.1590	.1343
ϵ_{trim} rad	.0888	.0475	.0915	.0480	.0598	.0505	.0605	.0509
					Struts			
C_D	-	-	-	-	.00358	.00281	.00402	.00318
C_{D_h} per ft	-	-	-	-	.00052	.00052	.00047	.00047

Note: Nacelle coefficient same as reference values (Table A-1).

Table A-6

HYDRODYNAMIC DATA FOR SUBMERGED-FOIL DEPTH VARIATION

	Forward Components				Aft Component			
	Foil		Strut		Foil		Strut	
$h/\bar{c}$	1.5	2.0	1.5	2.0	1.5	2.0	1.5	2.0
C_L	.1405	.1405	0	0	.1405	.1405	0	0
C_{L_α} per rad	4.135	4.255	0	0	4.104	4.220	0	0
C_{L_h} per ft	.00235	.00141	0	0	.00193	.00118	0	0
C_{L_v} per fps	.00013	.00011	0	0	.00015	.00014	0	0
C_D	.01302	.01313	.00416	.00523	.01310	.01290	.00467	.00584
C_{D_α} per rad	.0893	.0737	0	0	.0906	.0882	0	0
C_{D_h} per ft	$.32\times10^{-5}$	$.47\times10^{-6}$	.00052	.00052	$.32\times10^{-5}$	$-.40\times10^{-5}$	.00047	.00047
C_{D_v} per fps	$-.11\times10^{-5}$	$-.16\times10^{-5}$	0	0	$-.12\times10^{-5}$	$-.14\times10^{-5}$	0	0
C_{L_δ} per rad	2.76	2.58	-	-	2.73	2.81	-	-
C_{D_δ} per rad	.1400	.1312	-	-	.1411	.1389	-	-
δ trim rad	.0510	.0545	-	-	.0514	.0500	-	-

Note: Nacelle coefficients same as reference values (Table A-1).

Table A-7

HYDRODYNAMIC DATA FOR FOIL AREA VARIATION

(a) Submerged Foils

	Forward Foil				Aft Foil	
Area, ft^2	50	75	113	150	75	100
C_L	.2809	.1873	.1243	.0936	.2809	.2107
C_{L_α} per rad	3.970	3.943	3.910	3.883	3.943	3.920
C_{L_h} per ft	.01563	.00854	.00463	.00305	.01286	.00836
C_{L_V} per fps	.00021	.00017	.00013	.00011	.00025	.00021
C_D	.02303	.01612	.01254	.01111	.02321	.01780
C_{D_α} per rad	.1780	.1211	.0813	.0618	.1816	.1373
C_{D_h} per ft	.000262	.000100	.000038	.000019	.00022	.00011
C_{D_V} per fps	$-.22\times10^{-5}$	$-.11\times10^{-5}$	$-.54\times10^{-6}$	$-.32\times10^{-6}$	$-.25\times10^{-5}$	$-.15\times10^{-5}$
C_{L_δ} per rad	2.64	2.63	2.60	2.59	2.63	2.61
C_{D_δ} per rad	.2256	.1705	.1332	.1150	.2272	.1856
δ trim rad	.1063	.0713	.0477	.0362	.1070	.0807
	Forward Strut				Aft Strut	
C_D	.00247	.00281	.00233	.00358	.00280	.00305
C_{D_h} per ft	.000525	.000525	.000525	.000525	.000470	.000470

Note: Nacelle coefficients same as reference values (Table A-1).

Table A-7 (concluded)

(b) Surface-Piercing Foils

	Forward Foil				Aft Foil	
A, ft^2	50	75	113	150	75	100
C_L	.2809	.1873	.1243	.0936	.2809	.2107
C_{L_α} per rad	3.625	3.589	3.544	3.509	3.589	3.558
C_{L_h} per ft	.4452	.2429	.1318	.0864	.3643	.2372
C_{L_v} per fps	.00028	.00023	.00018	.00016	.00034	.00029
C_D	.02180	.01563	.01237	.01105	.0220	.01718
C_{D_α} per rad	.1721	.1154	.07705	.0583	.1731	.1303
C_{D_h} per ft	.02903	.01674	.01066	.00821	.0240	.01605
C_{D_v} per fps	$.28 \times 10^{-5}$	$.17 \times 10^{-5}$	$.97 \times 10^{-6}$	$.68 \times 10^{-6}$	$.37 \times 10^{-5}$	$.26 \times 10^{-5}$
C_{L_δ} per rad	2.41	2.39	2.36	2.34	2.39	2.37
C_{D_δ} per rad	.2219	.1678	.1312	.1133	.2230	.1823
δ_{trim} rad	.1094	.0736	.0495	.03765	.1104	.0836

Note: Nacelle coefficients same as reference values (Table A-1).

APPENDIX B
REFERENCE CRAFT TRANSFER FUNCTIONS

Longitudinal transfer functions for the four canard reference craft are given in this appendix. These transfer functions are computed from the linear model as discussed in Reference 1. The denominator, Δ, is the same for all transfer functions for a given craft and is listed first, followed by the various numerators. These numerators are for: (1) perturbation speed along the craft x-axis, u; (2) perturbation speed along the z-axis, w ; (3) pitch angle, θ; and (4) center of gravity height along the vertical, $h_{c.g.}$; in response to both forward flap deflection, δ_f ; and aft flap deflection, δ_a . For example, the transfer function of $h_{c.g.}$ to δ_f is equal to the numerator of $h_{c.g.}/\delta_f$ divided by the denominator Δ.

Bode and root locus plots may be constructed utilizing these transfer functions.

Submerged-Foil Craft

$$\Delta = (s + 24.17)(s+10.65)(s+.206)(s + .0586 + j.0718)(s + .0586 - j.0718)$$

$$u/\delta_f = -13.08(s + 25.84)(s + 12.45)(s + 1.500)(s - .212)$$

$$w/\delta_f = -239.1(s + 19.99)(s + .699)(s - .528)(s + .00487)$$

$$\theta/\delta_f = 15.05(s + 10.66)(s + .209)(s + .00303)$$

$$h_{c.g.}/\delta_f = 239.1(s + 22.82)(s + 2.585)(s + .0790)$$

$u/\delta_a = -19.75(s + 22.97)(s + 13.79)(s - .425 + j.185)(s - .425 - j.185)$

$w/\delta_a = -355.2(s + 27.1)(s + .0121)(s + .0728 + j.451)(s + .0728 - j.451)$

$\theta/\delta_a = -15.64(s + 10.61)(s + .209)(s + .00830)$

$h_{c.g.}/\delta_a = 355.2(s + 24.96)(s - 1.507)(s + .0770)$

Surface-Piercing-Foil Craft

$\Delta = (s+15.48)(s+5.67)(s+.0225)(s+4.408 +j3.689)(s+4.408 -j3.689)$

$u/\delta_f = -14.22(s + 18.39)(s + 8.096 + j3.322)(s + 8.096 - j3.322)$
$(s - 1.315)$

$w/\delta_f = -216.9(s + 9.082 + j4.409)(s+ 9.082 - j4.409)(s - 1.694)(s + .01936)$

$\theta/\delta_f = 13.63(s + 4.639 + j3.405)(s + 4.639 - j3.405)(s + .01900)$

$h_{c.g.}/\delta_f = 216.9(s + 10.88 + j1.240)(s + 10.88 - j1.240)(s +.04597)$

$u/\delta_a = -10.73(s + 14.03 + j3.079)(s + 14.03 -j3.079)(s + 1.413 + j.381)$
$(s + 1.413 - j.381)$

$w/\delta_a = -160.5(s+ 19.63)(s + 2.044 + j1.724)(s + 2.044 - j1.724)(s+ .02162)$

$\theta/\delta_a = -7.081(s + 4.609 + j4.070)(s + 4.609 - j4.070)(s + .02153)$

$h_{c.g.}/\delta_a = 160.5(s + 16.84)(s + 3.164)(s + .01026)$

Hybrid Surface-Piercing-Aft-Foil Craft

$\Delta = (s + 22.07)(s + 5.612 + j3.328)(s + 5.612 - j3.328)(s - .6560)$
$(s + .0673)$

$u/\delta_f = -13.08(s + 21.74)(s + 8.039 + j2.806)(s + 8.039 - j2.806)(s - .8632)$

$w/\delta_f = -239.1(s + 9.068 + j3.897)(s + 9.068 -j3.897)(s - 1.673)(s + .03165)$

$\theta/\delta_f = 15.05(s + 4.627 + j3.100)(s + 4.627 - j3.100)(s + .03127)$

$h_{c.g.}/\delta_f = 239.1(s + 12.46)(s + 9.300)(s + .04889)$

$u/\delta_a = -20.66(s + 22.22)(s + 12.62)(s - .7480 + j.4123)(s - .7480 - j.4123)$

$w/\delta_a = -321.0(s + 27.13)(s + .1365 + j.4683)(s + .1365 - j.4683)(s - .1193)$

$\theta/\delta_a = -14.15(s + 10.59)(s + .2688)(s - .07267)$

$h_{c.g.}/\delta_a = 321.0(s + 24.99)(s - 1.485)(s + .05696)$

Hybrid Submerged-Aft-Foil Craft

$\Delta = (s + 19.93)(s + 7.275)(s + 3.233)(s + 1.911)(s + .0653)$

$u/\delta_f = -13.70(s + 23.11)(s + 12.16)(s + 1.394)(s - .8399)$

$w/\delta_f = -216.9(s + 19.94)(s + .739)(s - .410)(s - .172)$

$\theta/\delta_f = 13.64(s + 10.68)(s + .278)(s - .0658)$

$h_{c.g.}/\delta_f = 216.9(s + 22.76)(s + 2.572)(s + .0830)$

$u/\delta_a = -19.76(s + 15.28 + j2.867)(s + 15.28 - j2.867)(s + 1.425 + j1.282)$
$(s + 1.425 - j1.282)$

$w/\delta_a = -355.2(s + 19.92)(s + 1.889 + j1.742)(s + 1.889 - j1.742)(s + .0390)$

$\theta/\delta_a = 15.64(s + 4.618 + j3.777)(s + 4.618 - j3.777)(s + .0387)$

$h_{c.g.}/\delta_a = 355.2(s + 17.21)(s + 2.781)(s + .0178)$

APPENDIX C

REFERENCE CRAFT SIMULATION AND ROOT LOCUS DATA

Herein are presented: (1) some craft and fixed autopilot parameters used in the analog simulation of the fully-submerged-foil and surface-piercing-foil canard reference craft at 50 knots, (2) additional information on the root loci plots appearing in Figures 22 through 24, (3) tabulation of the critical open-loop poles and zeros for these plots, and (4) tabulation of variable autopilot parameter settings.

Simulation Parameter Values

Craft parameters pertinent to both vehicles simulated are:

$V_0 = 84.5$ ft/sec

$\rho = 1.994$ slugs/ft^3

$g = 32.16$ ft/sec^2

$m = 7,774$ slugs

$I_y = 6.4 \times 10^6$ slug-ft^2

$\alpha_\delta = .666$ for all flaps

$\dot{\delta} = 20$ deg/sec maximum for all flaps

Other craft and fixed autopilot parameters are tabulated in Table C-1.

Root Locus For the Pitch Stabilization Loop Closed

The root locus plot of Figure 22 shows the effect of closing the pitch stabilization loop on the submerged-foil reference craft at 50 knots in a calm sea and is calculated from the mathematical model of Figure C-1. Pitch-to-flap transfer functions (θ/δ_f and $-\theta/\delta_a$) are obtained from digital computations, and a value of $K_{\theta_p}/K_\theta = .01$ is assumed. The critical open-loop poles and zeros are tabulated below.

Type of Root	Real Part	Imaginary Part
zero	-.00571	0
zero	-.01	0
zero	-.209	0
zero	- 10.64	0
pole	0	0
pole	-.0586	-.0718
pole	-.0586	+.0718
pole	-.206	0
pole	-10	0
pole	-10.65	0
pole	-24.17	0

Root Locus for the Vertical Stabilization Loop Closed

The root locus plot of Figure 23 illustrates the effect of closing the vertical stabilization loop on the submerged-foil reference craft at 50 knots in a calm sea and is computed from the mathematical model of Figure C-2. The sensor height-to-forward flap transfer function (h_{sensor}/δ_f) is obtained by digital computation, and a value of $K_p/K_h = .01$ is used. Critical open-loop poles and zeros are given below.

Type of Root	Real Part	Imaginary Part
zero	-.01	0
zero	-.073	0
zero	-1.135	0
zero	-13.05	0
pole	0	0
pole	-.0586	-.0718
pole	-.0586	+.0718
pole	-.206	0
pole	-1.54	0
pole	-10	0
pole	-10.65	0
pole	-24.17	0

Root Locus For Acceleration Loop Closed

The root locus of Figure 24 presents the effect of closing the acceleration loop on the submerged-foil reference craft at 50 knots in a calm sea and is based on the mathematical model of Figure C-3. The c.g. normal acceleration-to-flap transfer functions ($-a_z/\delta_f$ and $-a_z/\delta_a$) are obtained by digital computation. Critical open-loop poles and zeros appear below.

Type of Root	Real Part	Imaginary Part
zeros*	0	0
zero	-.0645	-.0418
zero	-.0645	+.0418
zero	-24.18	0
pole	-.0586	-.0718
pole	-.0586	+.0718
pole	-.206	0
pole	-1.54	0
pole	-10	0
pole	-10.65	0
pole	-24.17	0

Variable Autopilot Parameter Settings

The variable autopilot parameter settings (K_h, K_θ, and K_{a_z}) used in the sea state simulation of the submerged-foil reference craft at 50 knots are tabulated in Table C-2.

* Triple zeros located at origin.

CANARD SUBMERGED-FOIL REFERENCE CRAFT AT 50 KNOTS

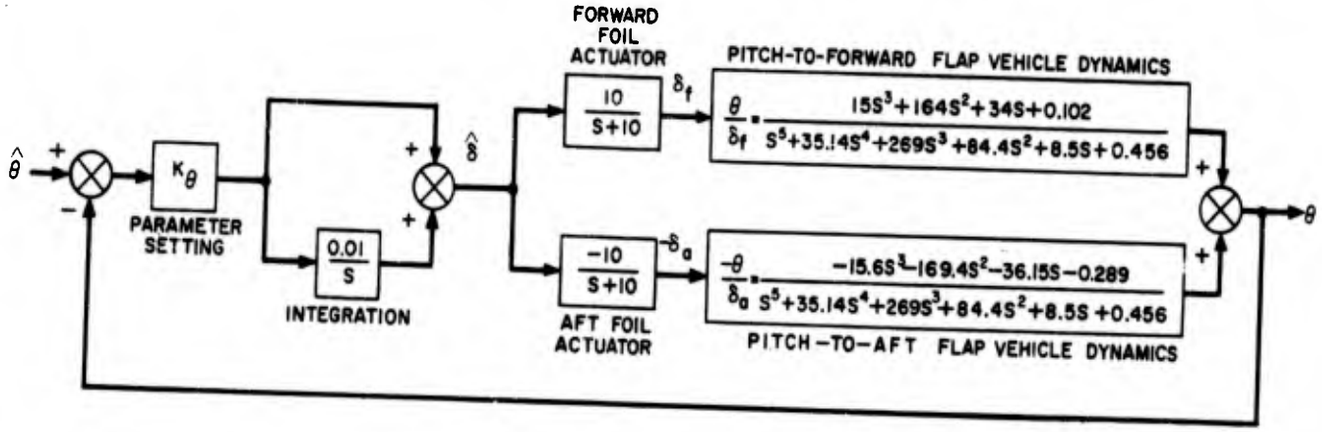

FIGURE C-1 BLOCK REPRESENTATION OF PITCH STABILIZATION LOOP

CANARD SUBMERGED-FOIL REFERENCE CRAFT AT 50 KNOTS

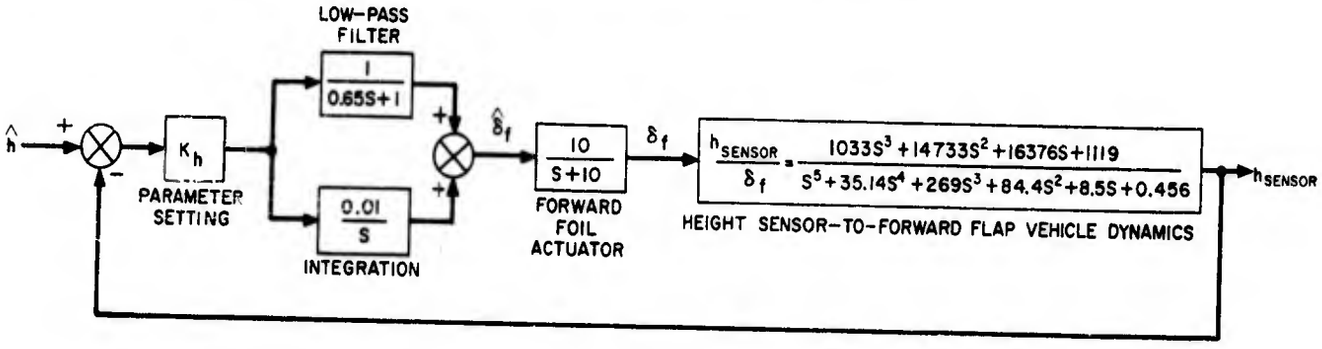

FIGURE C-2 BLOCK REPRESENTATION OF VERTICAL STABILIZATION LOOP

CANARD SUBMERGED-FOIL REFERENCE CRAFT AT 50 KNOTS

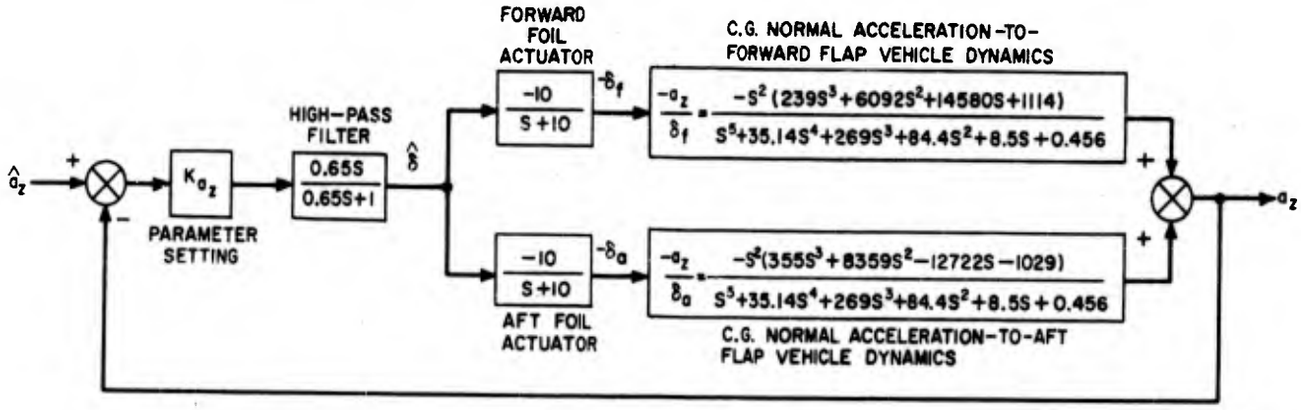

FIGURE C-3 BLOCK REPRESENTATION OF ACCELERATION LOOP

Table C-1

CRAFT AND FIXED AUTOPILOT PARAMETERS

QUANTITY	Submerged-Foil Reference Craft		Surface-Piercing-Foil Reference Craft		UNITS
	Fwd. Foil	Aft Foil	Fwd. Foil	Aft Foil	
x	52.8	-35.2	52.8	-35.2	ft.
z	18.08	19	16.23	16.73	ft.
h	4.08*	5*	2.23*	2.73*	ft.
$\bar{c}$	4.08	5	4.08	5	ft.
AR	6	6	6*	6*	dimension-less
S	100	150	106.4*	159.64*	ft^2
A	100	150	100*	150*	ft^2
Γ	0	0	20	20	deg.
σ	.336	.336	.502	.502	dimension-less
ζ_o	—	—	-.005	-.005	dimension-less
K_E	1	1	.747	.747	dimension-less
K_D	.0831	.0850	**	**	dimension-less
C'_{D_o}	.0127	.0147	.0121	.0103	dimension-less
C_{D_h}	.000525	.00047	—	—	per ft.
C_D	.0165*	.0186*	.01361*	.01551*	dimension-less
C_{L_α}	3.92*	3.88*	3.56*	3.51*	per rad.
δ_{trim}	3.09*	3.11*	3.40*	3.44*	deg.
τ_1	.65	—	—	—	sec.
τ_2	.65	.65	—	—	sec.
τ_3	.65	.65	—	—	sec.
K_p/K_h	.01	—	—	—	per sec.
K_{θ_p}/K_θ	.01	.01	—	—	per sec.

* Indicates value in calm sea only.

** Function of foil depth submergence.

Table C-2

VARIABLE AUTOPILOT PARAMETER SETTINGS

Sea State	Head Sea				Following Sea			
	Wave Steepness Ratio	K_θ	K_h	K_{a_z}	Wave Steepness Ratio	K_θ	K_h	K_{a_z}
4-Ft. Waves	11	14	.16	.006	11	5.7	.12	.007
	16.5	2.7	.16	.006	16.5	16.5	.09	.008
	22	8	.10	.009	22	19	.03	.026
	33	15.7	.09	.004	33	20	.02	.026
	44	20	.06	.017	44	16	.006	.025
	88	15	.003	.029	88	20	0	0
10-Ft. Waves	4.4	12.3	.07	.003	4.4	4.7	.08	.010
	6.6	.7	.10	.001	6.6	.34	.07	.019
	8.8	2.3	.07	.002	8.8	.83	.009	.007
	13.2	2.6	.01	.007	13.2	13	.005	0
	17.6	8.4	.001	.003	17.6	20	.02	0
	35.2	20	0	0	35.2	20	.16	0

Notes: 1. Wave height is crest-to-trough.
2. Wave steepness ratio = wave length/wave height.

DISTRIBUTION LIST

Chief, Bureau of Ships (46)
Navy Department
Washington 25, D. C.
Attn: Code 106 (1)
Code 335 (3)
Code 410 (1)
Code 420 (39)
Code 442 (1)
Code 449 (1)

Chief, Office of Naval Research
Navy Department
Washingron 25, D. C.
Attn: Code 438 (2)

Commanding Officer and Director (6)
David Taylor Model Basin
Carderock, Maryland
Attn: Code 500 (1)
Code 513 (1)
Code 520 (1)
Code 526 (1)
Code 530 (1)
Code 580 (1)

Chief, Bureau of Naval Weapons (2)
Navy Department
Washington 25, D.C.
Attn: Code RAAD-334 (1)
Code RRSY-1 (1)

Commander
Armed Services Technical Information Agency
Arlington Hall Station
Arlington 12, Virginia
Attn: TIPDR (10)

Mr. John B. Parkinson (1)
Langley Aeronautical Laboratory
National Aeronautics and Space Administration
Langley Field, Virginia

Boeing Airplane Company (1)
Aero-Space Division
Box 3707
Seattle 24, Washington

California Institute of Technology (1)
Pasadena, California
Attn: Professor T.Y. Wu
Hydrodynamics Laboratory

Hydrodynamic Research Laboratory (1)
Convair Division
General Dynamics Corporation
San Diego 12, California

Director, Stevens Institute of Technology (1)
Davidson Laboratory
Castle Point Station
Hoboken, New Jersey

Grumman Aircraft Engineering Corporation (1)
Marine Engineering Section
Bethpage, Long Island, New York

Hughes Aircraft Company (1)
Systems Development Laboratories
Culver City, California
Attn: Mr. W. N. Turner

Hydronautics, Incorporated (1)
200 Monroe Street
Rockville, Maryland

Sperry Piedmont Company (1)
Charlottesville, Virginia
Attn: Mr. V. E. Williams

Massachusetts Institute of Technology (1)
Department of Naval Architecture and Marine Engineering
Cambridge 39, Massachusetts

Director (1)
University of Minnesota
St. Anthony Falls Hydraulic Laboratory
Hennepin Island,
Minneapolis 14, Minnesota

Southwest Research Institute (1)
8500 Culebra Road
San Antonio 6, Texas
Attn: H. N. Abramson, Director of Mechanical Sciences

Technical Research Group, Inc. (1)
2 Aerial Way
Syosset, New York

Chief of Naval Operations (1)
Navy Department
Washington 25, D. C.
Attn: Capt. N. H. Fisher, OP-712

State University of Iowa (1)
Iowa Institute of Hydraulic Research
Iowa City, Iowa

Aerojet General Corporation (1)
Azusa, California
Attn: Mr. J. Levy

David Taylor Model Basin (1)
High Speed Phenomena Division
Langley Field, Va.
Attn: Mr. R. E. Olsen

Stanford University (1)
Stanford, California
Attn: Dr. B. Perry

Dynamic Developments, Inc. (1)
Midway Ave., Babylon, Long Island, New York

U. S. Naval Ordnance Test Station (1)
Oceanic Research Group
3202 E. Foothill Blvd.
Pasadena, California

University of California (1)
Institute of Engineering Research
Berkeley, California
Attn: Prof. R. Paulling

Lockheed Aircraft Corporation (1)
Hydrodynamic Group
Sunnyvale, California
Attn: Mr. R. W. Kermeen

Radio Corporation of America (1)
Aerospace Communications and Controls Division
Burlington, Massachusetts
Attn: Mr. D. Wellinger

Autonetics (1)
9150 E. Imperial Highway
Downey, California
Attn: Mr. J. M. Johnson, Jr.
Dept. 3441-12

UNCLASSIFIED